UNIVERSIDADE FEDERAL DE MINAS GERAIS
PROGRAMA DE PÓS-GRADUAÇÃO EM FÍSICA

Arthur Castro Cardoso

Simulation of quantum jump in qutrit photonic path system

BELO HORIZONTE
2021

Arthur Castro Cardoso

Simulation of quantum jump in qutrit photonic path system

Tese apresentada ao Programa de Pós-Graduação em Física do Instituto de Ciências Exatas da Universidade Federal de Minas Gerais como requisito parcial para obtenção do título de Doutor em Ciências.

Orientador: Sebastião José Nascimento de Pádua

Belo Horizonte

2021

Dados Internacionais de Catalogação na Publicação (CIP)

C268s Cardoso, Arthur Castro.
Simulation of quantum jump in photonic path system / Arthur Castro Cardoso. – 2021.
97f., enc. : il.

Orientador: Sebastião José Nascimento de Pádua.
Tese (doutorado) – Universidade Federal de Minas Gerais, Departamento de Física.
Bibliografia: f. 81-97.

1. Simulação quântica. 2. Sistemas quânticos. 3. Fótons.
I. Título. II. Pádua, Sebastião José Nascimento de. III. Universidade Federal de Minas Gerais, Departamento de Física.

CDU – 530.145 (043)

Ficha catalográfica elaborada por Romário Martins – CRB6 3595
Biblioteca Professor Manoel Lopes de Siqueira – Departamento de Física - UFMG

UNIVERSIDADE FEDERAL DE MINAS GERAIS
INSTITUTO DE CIÊNCIAS EXATAS
PROGRAMA DE PÓS-GRADUAÇÃO EM FÍSICA

FOLHA DE APROVAÇÃO

A presente tese, intitulada **"Simulation of quantum jump in qutrit photonic path system"** de autoria de **ARTHUR CASTRO CARDOSO** submetida à Comissão Examinadora, abaixo-assinada, foi aprovada para obtenção do grau de **DOUTOR EM CIÊNCIAS**, em dezenove de março de 2021.

Belo Horizonte, 19 de Março de 2021.

Prof. Sebastião José Nascimento de Pádua
Orientador do estudante
Departamento de Física/UFMG

Profa. Gabriela Barreto Lemos
Instituto de Física/UFRJ

Prof. Pedro Ernesto Schiavinatti Tavares
Departamento de Física/UFMG

Profa. Sandra Sampaio Vianna
Departamento de Física/UFPE

Prof. Raphael Campos Drumond
Departamento de Matemática/UFMG

Documento assinado eletronicamente por **Pedro Ernesto Schiavinatti Tavares**, **Professor do Magistério Superior**, em 24/03/2021, às 12:43, conforme horário oficial de Brasília, com fundamento no art. 5º do Decreto nº 10.543, de 13 de novembro de 2020.

Documento assinado eletronicamente por **Sebastião Jose Nascimento de Padua**, **Membro de comissão**, em 24/03/2021, às 14:33, conforme horário oficial de Brasília, com fundamento no art. 5º do Decreto nº 10.543, de 13 de novembro de 2020.

Documento assinado eletronicamente por **Sandra Sampaio Vianna**, **Usuário Externo**, em 24/03/2021, às 15:11, conforme horário oficial de Brasília, com fundamento no art. 5º do Decreto nº 10.543, de 13 de novembro de 2020.

Documento assinado eletronicamente por **Gabriela Barreto Lemos**, **Usuário Externo**, em 24/03/2021, às 15:40, conforme horário oficial de Brasília, com fundamento no art. 5º do Decreto nº 10.543, de 13 de novembro de 2020.

Documento assinado eletronicamente por **Raphael Campos Drumond**, **Professor do Magistério Superior**, em 25/03/2021, às 09:21, conforme horário oficial de Brasília, com fundamento no art. 5º do Decreto nº 10.543, de 13 de novembro de 2020.

A autenticidade deste documento pode ser conferida no site https://sei.ufmg.br/sei/controlador_externo.php?acao=documento_conferir&id_orgao_acesso_externo=0, informando o código verificador **0640002** e o código CRC **B348CAF6**.

Referência: Processo nº 23072.215643/2021-41 SEI nº 0640002

Dedico este trabalho à minha esposa, minha família
e a todos os defensores da ciência no Brasil.

Agradecimentos

Aos meus pais Humberto e Vera, ao meu irmão Eduardo e à minha esposa Samira, pelo apoio incondicional e pelo estímulo que foram essenciais para que este trabalho fosse realizado.

Ao meu orientador, o professor Sebastião José Nascimento de Pádua, pela orientação com paciência, dedicação e atenção.

Ao professor Breno Marques, por propor a realização do experimento de simulação de decaimento e me ajudar com a parte teórica.

Ao meu colega Artur Matoso, pelas dicas de alinhamento e por me ajudar com o LaTeX.

Ao professor Jader Cabral, por me ajudar na realização do experimento e no tratamento de dados.

Ao professor Pedro Tavares, pelo apoio e por me ajudar na proposta de implementação de portas lógicas quânticas.

Ao meu colega de laboratório João Guilherme Codé, por colaborar na realização do experimento da simulação de decaimento e pela ajuda na parte teórica.

Às secretárias da pós-graduação Ana Luiza e Marília, pela eficiência e profissionalismo.

Aos órgãos de fomento a pesquisa: CNPq, CAPES, INCT e FAPEMIG, pelo auxílio financeiro.

Resumo

Nesta tese, exploramos uma fonte de fótons atenuada ao nível de poucos fótons, cujo o estado quântico foi preparado em uma superposição de estados de caminhos transversais. Utilizando técnicas propostas por Baldijão *et. al.* [Phys. Rev. A. **97**, 032329 (2017)] e caracterizadas por Borges *et. al.* [Phys. Rev. A. **97**, 022301 (2018)], para realizar operações generalizadas nestes graus de liberdade, nós conseguimos gerar estados quânticos de três caminhos (qutrits) e implementar as operações necessárias para simular o decaimento espontâneo em um átomo de três níveis com saltos quânticos.

Utilizando grades de difração periódicas em um modulador espacial de luz, nós implementamos as operações quânticas para a simulação das dinâmicas de decaimento em sistemas de três níveis com salto quântico em termos da decomposição de Kraus, para cada um dos tipos de decaimento no sistema de três níveis: cascata, Λ e V. Nesta simulação experimental, a quantidade de fótons em cada estado de caminho faz o papel da população em cada um dos níveis de energia do átomo. As coerências entre os auto-estados de energia estão relacionadas com as visibilidades dos padrões de interferência entre os pares de feixes que formam a base dos estados de caminhos dos fótons. Os estados de caminho são caracterizados a partir de medidas de imagem dos feixes de fótons com perfil transversal Gaussianos e pelos padrões de interferência entre pares destes modos espaciais.

Também propomos teoricamente, utilizando a mesma metodologia, a realização experimental de portas lógicas quânticas e portas lógicas quânticas controladas em estados fotônicos de caminhos. Com a montagem experimental proposta, mostramos que é possível implementar em qubits de caminhos Gaussianos todas as portas lógicas descritas pelas matrizes de Pauli (σ_x, σ_y e σ_z), além de portas lógicas de fase. O mesmo método pode ser explorado para qutrits, ou ainda, sistemas multi-caminho de dimensões maiores.

Na simulação das dinâmicas de decaimento, obtivemos resultados satisfatórios para os termos da diagonal e para os módulo dos termos de fora da diagonal, isto é, apesar de um pequeno desvio, eles estão de acordo com a previsão teórica. Esta simulação nos fornece uma melhor compreensão de como os saltos quânticos podem afetar a coerência de um estado de três níveis. Além disso, esta implementação poder ser usada para entender como os saltos quânticos, em sistemas de grandes dimensões, afetam protocolos quânticos devido à decoerência.

Palavras-chave: Decaimento atômico, Operações quânticas, Portas lógicas quânticas, Salto quântico, Simulação quântica, Sistemas de três níveis.

Abstract

In this thesis, we use as an experimental platform laser beams in Gaussian modes attenuated to the level of a few photons. The quantum state is prepared in a superposition of transverse Gaussian paths states. By making use o the techniques proposed by Baldijão *et. al.* [Phys. Rev. A. **97**, 032329 (2017)] and characterized by Borges *et. al.* [Phys. Rev. A. **97**, 022301 (2018)], to perform generalized quantum operations in this degree of freedom. We are able to generate three-path (qutrits) quantum states and implement the necessary operations to simulate spontaneous decay in an tree-level atom with quantum jumps.

By using periodical diffraction phase gratings in a spatial light modulator, we implement the quantum operations for the simulation of the decay dynamics in three-level systems with quantum jumps in terms of the Kraus decomposition, for each one of the configurations: cascade, Λ and V. In this experimental simulation, the average number of photons in each path state plays the role of the population in each one of the energy levels of the atom. The coherences between the energy eigenstates are related to the visibilities of the interference patterns between the pair of beams that form the base of the photonic path states. The states are characterized by image measurements of the beams with transversal Gaussian profile an by the interference patterns between the pairs of these spatial modes.

Also we propose theoretically, making use of the same methodology, the experimental realization of quantum logic gates and controlled quantum logic gates in photonic path states. With the proposed experimental setup, we show that it is possible to implement in qubits paths states, all the logic gates described by the Pauli matrices (σ_x, σ_y e σ_z), beyond the phase logic gates. The same method can be explored for qutrits, or even multi-path systems of higher dimensions.

In the simulation of the decay dynamics, we obtained satisfactory results for the diagonal terms and for the modulus of the off-diagonal terms, that is, despite of a small deviation, they are in agreement with the theoretical predictions. This simulation provide us a better comprehension of how the quantum jumps can affect the coherence of a three-level state. Moreover, this implementation may be used to understand how the quantum jumps, in high dimension systems, affect the quantum protocols due to decoherence.

Keywords: Atomic decay, Quantum jump, Quantum logic gates, Quantum operations, Quantum simulation, Three-level systems.

Sumário

1 Introduction

Quantum optical systems have been widely used for fundamental tests of quantum mechanics and implementation of quantum information and quantum computation protocols [1–10]. The transverse profile of optical beams at photon count level has been a quick-rising platform for preparing discrete quantum states and for investigating quantum information theories and protocols [11]. Photon beams have been prepared in high dimension entangled states of their optical angular momenta in Hermite and Laguerre-Gauss modes [12–14]. Some useful optical systems explore photon transverse momentum, which can be discretized by slits [15–17] or in different photon paths with the aid of interferometers [18, 19] for preparing one-, two- or four-photon quantum states in slits modes or Gaussian modes [15, 20–23].

Quantum systems are in general not isolated systems and are most of the time subjected to uncontrolled interactions to an external quantum system and/or to its surrounds (environment) [24–26]. The system interactions with the environment cannot be described by unitary operations acting on the system and lead to dissipation (loss of energy to the environment) and decoherence [27–30] (loss of state coherence), consequently to a degradation in quantum protocols [31–34]. Different uncontrolled interactions, referred here as noise, that affect the coherence of the quantum system state or entanglement in bipartite or multipartite state systems have been simulated quantically, more specifically, dephasing, amplitude damping and Pauli noise [31, 35–43]. Quantum simulation means using a controlled quantum system to simulate complex dynamics.

Another important source of noise is the fundamental process called quantum jump, where a quantum system evolves stochastically in an abrupt unpredictable operation. An excited atomic system may undergo spontaneous decay through the interaction with the vacuum state of the electromagnetic field. Quantum jumps are an essential topic in the interpretation of quantum dynamics [44–47] and has been part of the historical debates about the foundations of quantum mechanics [48]. his stochastic process, first proposed by Bohr [49], had its existence contested by Schroedinger [50, 51] and was quantitatively described by Einstein through the calculation of the A and B coefficients [52]. This kind of system typically experiences a time-dependent exponential decay, in which the probability of an excited state $|i\rangle$ decaying to $|j\rangle$ in a time interval t, is given by $p_{ij} = 1 - e^{-\gamma_{ij}t}$, where γ_{ij} is the spontaneous decay rate between levels i and j. This process causes a reduction in the population of the excited state and also decoherence. The spontaneous decay of the state may spoil the implementation of quantum information protocols in atomic systems [53].

Over the last years, quantum jumps have been explored in protocols for quantum feedback control [54, 55] and quantum error correction, for detecting and correcting errors due to decoherence [56–58]. Observing quantum jumps is not an easy task as it requires non-demolition measurements [59]where after the measurement, the system is in an eigenstate of the measured observable, thus allowing repeated measurements. It is also required to realize measurements in a time scale much faster than the lifetime of the excited state. Despite of this, quantum jumps were observed in several quantum systems, for instance, in a single ion [60–63], molecule [64], electron in a trap [65], in superconductors [56], in photons in a cavity [54, 55, 58, 66, 67], and in artificial atoms [59, 68–72]. Present in the photoelectric effect [73] and in the spontaneous decay of an atom, this process has an important role in laser cooling [74–78]. Although in free atoms the jump occurs on the lifetime of the excited state this time can be increased or shortened by surrounding the atoms with a cavity [79–81]. More recently quantum jump was tracked in time by following the population of an auxiliary level coupled to the ground state of an artificial atom [72, 82]. This approach allowed the authors to perform an experiment "to catch in mid-flight"a quantum jump and to conclude that is possible to know if a quantum jump is about to occur.

This thesis reports an experimental simulation of decay dynamics of a three-level system by preparing a photonic qutrit path state and letting the photon beam in the qutrit state be modified by periodical phase modulation produced by a spatial light modulator (SLM). The use of the spatial light modulator (SLM) in these optical systems allows the photon state to be manipulated in different ways and can be used to implement a wide range of quantum operations [8, 12, 16, 18, 83, 84]. One crucial advantage of these physical quantum systems is that they are able to simulate much more complex quantum systems [85, 86]. Several experiments explore this fact to study different kinds of quantum system dynamics [31, 32]. The objective is to implement the spontaneous decay dynamics of a three-level atomic system in different configurations: cascade decay, Λ decay and V decay.

For making quantum computation, we need to prepare quantum states to encode information, manipulate it and perform measurements [87, 88]. Similarly to the classical computation, a quantum computer is based on blocks of quantum circuits composed by wires and quantum gates (QGs) which carries and transfer the information. Thus, implementing QG with high fidelity is crucial for the engineering of an efficient quantum computer. In classical computers, the logic gates are implemented by transistors and others electronic devices, usually, in a irreversible fashion. On the other hand, QGs are characterized by reversible quantum operations, since the inverse of an unitary matrix is also unitary [87, 89]. They are represented in terms of unitary operations which corresponds to a rotation of the generalized Bloch vector, that is, they do not change the state purity. This allow us to inverse quantum algorithms and functions as long as they contain only

QGs. Furthermore, as the product of unitary operators is also unitary, operations which are composed by a set of QGs are also reversible. For instance, a quantum addition algorithm can be exploited to perform subtraction, by running it reverse [90].

QGs are explored to manipulate quantum states and can be used to generate superposition states and entangled ones. In classical computation, the classical logic gates manipulates classical bit states which can be "0"or "1". On the other hand, for quantum computation we can have as input a superposition of the computational basis states, which are frequently entangled when we have more than one Qubit state as input. So, QGs are much more varied than the classical ones.

Over the last years, they were exploited to implement quantum communication protocols and algorithms as in generation of entangled states [91, 92], purification and concentration of entanglement [93], quantum error correction [94–96], quantum Fourier transform [97], quantum teleportation [98], quantum random walk [99], Shor's quantum factoring algorithm [100], quantum search algorithms [101] and Deutsch algorithm [102–104]. Therefore, the implementation of QG has a crucial role in the development of quantum computation [87,88]. The experimental implementation of QGs has been realized in several physical quantum systems, such as, trapped ions [103, 105], superconducting charges [106,107], nuclear spin in vacancy centres [108,109], Rydberg atoms [110], nuclear magnetic resonance (NMR) [95, 97, 100, 101, 104, 111–113] and optical systems [94, 98, 114, 115]. In his thesis, we propose the experimental implementation of quantum gates and controlled quantum gates in qubits and qutrits path systems.

This thesis is divided in two parts, in Part I there is a theoretical revision about the subjects that is are necessary for discussing the experimental applications. In Chapter 2, we studied the diffraction of a laser bean in periodical phase gratings. In Chapter 3, we made a quick review on the theory of quantum open systems and deduced the Kraus decomposition of the maps that represent the decay dynamics for the cascade, Λ and V configurations. In chapter 4, we studied some quantum gates and controlled quantum gates that we propose to implement in photonic path systems.

In Part II, we approach the experimental applications. In Chapter 5, we report the simulation of a quantum jump in photonic path system. By exploring the periodical phase modulation in an spatial light modulator we are able to simulate the decay dynamics for the cascade, Λ and V configurations. In Chapter 6, we propose an experimental implementation of quantum logic gates and controlled quantum logic gates in photonic path systems, also, by making use of periodical phase modulation in an spatial light modulator.

Parte I

Theoretical revision

2 Diffraction in periodical phase gratings and manipulation of photonic path states

Studying theory of diffraction of light is crucial for the comprehension of many phenomena in optics like the propagation of light and imaging formation process [116–118]. In this section we will approach the interaction of Gaussian beams with periodical phase diffraction gratings (PPG). A diffraction grating is a periodical phase or amplitude distribution imprinted in some material such that light transmitted or reflected by this material is diffracted in different beams referred as diffraction orders. We will also review some methods to generate and manipulate photonic Gaussian path states by exploring diffraction in PPG's [18,20,119]. In the experiment that we performed [120], it was necessary to expand the Hilbert space in order to realize quantum operation in the three-level systems. The expansion of the Hilbert space was obtained by reflecting incident Gaussian laser beam by phase diffraction gratings. In Section 2.1.1 we calculate the response of a linear phase grating (LPG) and in Section 2.1.2 we studied the response of a binary phase grating (BPG).

2.1 Diffraction in periodical phase gratings

A light source is situated in a very far position, $z \to -\infty$, so that the electromagnetic field in the plane $z = 0$ can be considered a plane wave, $E(x', y')$. In the Fraunhofer approximation, the scalar electric field in a distant plane $E(x, y)$ in z, Fig.1, is related to the field in $z = 0$ by [116]

$$E(x,y) = \frac{e^{ikz} e^{\frac{ik}{2z}\left(x^2+y^2\right)}}{i\lambda z} \int_{-\infty}^{\infty}\int_{-\infty}^{\infty} E(x',y')\, e^{\left[i\frac{2\pi}{\lambda z}(xx'+yy')\right]} dx'dy', \tag{2.1}$$

where $k = 2\pi/\lambda$ is the modulus of the wave vector of the field, λ is it's the wavelength, $2\pi x'/\lambda z$ and $2\pi y'/\lambda z$ are the spatial frequencies in the direction x e y, respectively. As it is shown in Eq.2.1, the field in the plane (x, y) is the Fourier transform of the field in (x', y') multiplied by a phase factor. Suppose a generic object of phase and amplitude, usually called "aperture", located in the plane $z = 0$ and illuminated by the electric field $E(x', y')$. The field in a distant plane, (x, y), will be

$$E(x,y) = \frac{e^{ikz} e^{\frac{ik}{2z}\left(x^2+y^2\right)}}{i\lambda z} \int_{-\infty}^{\infty}\int_{-\infty}^{\infty} E(x',y')\, \mathcal{T}(x',y')\, e^{i\Phi(x',y')} e^{\left[i\frac{2\pi}{\lambda z}(xx'+yy')\right]} dx'dy', \tag{2.2}$$

where $\mathcal{T}$ and $\Phi \in \mathbb{R}$. $\mathcal{T}(x', y')$ and $\Phi(x', y')$ are the transmittance profile and the phase profile, respectively, of the aperture. An ideal PPG is an aperture of transmittance profile

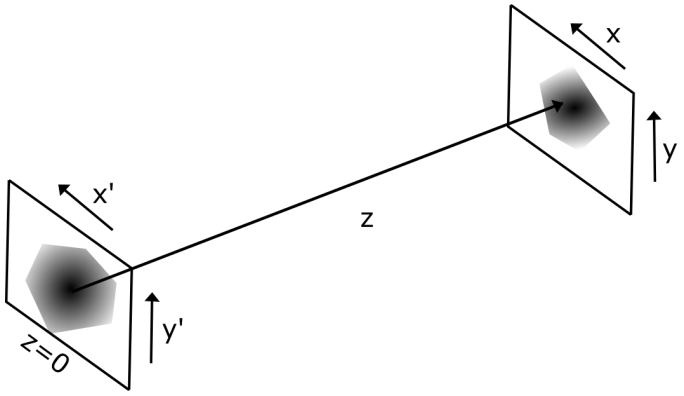

Figura 1 – Representation of the fields in the planes (x, y) and (x', y'), separated by a distance z.

$\mathcal{T}(x', y') = 1$, with a phase profile $\Phi(x', y')$, being described by a periodical function. When a Gaussian laser beam reaches a PPG it generates diffracted beams in different orders, that are multi-path Gaussian beams displaced equally in the direction of the phase variation [116]. Fig.2 represents a laser beam being diffracted by a PPG and generating diffraction orders.

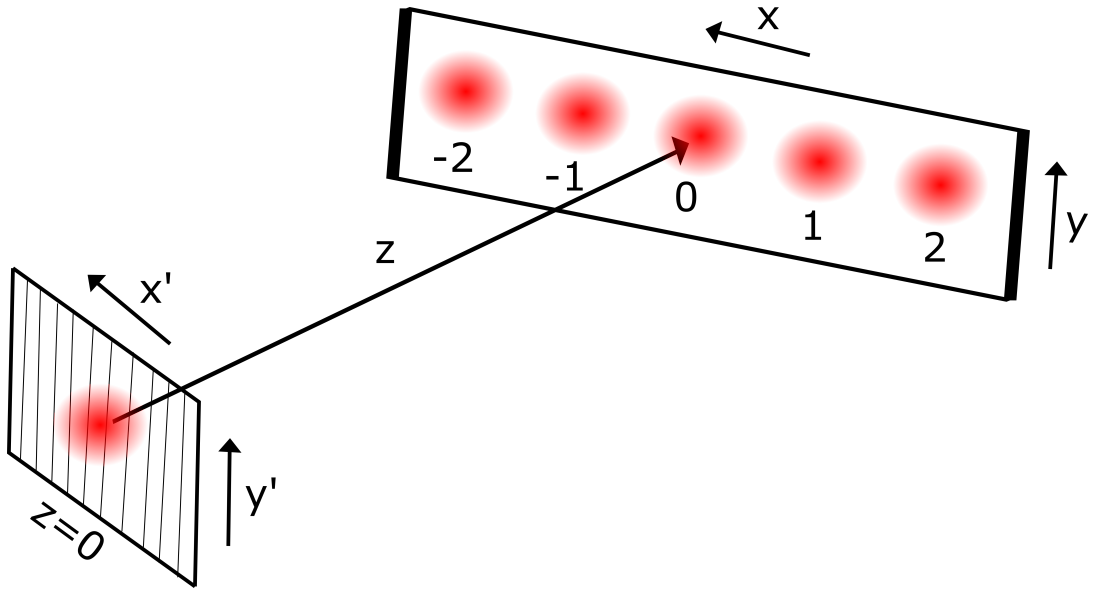

Figura 2 – Illustration of a Gaussian being diffracted by a PPG in the x'-direction at the plane $z = 0$ and giving rise to diffraction orders, labelled as $0, 1, -1, 2$ and -2, at the distant plane z.

Among the PPG's, we will analyse two phase grating in detail, the linear and the binary ones.

2.1.1 Linear diffraction grating

A linear phase diffraction grating (LPG) is a PPG in which the phase varies linearly with the position. The graph in Fig. 3 represents the phase variation of a LPG, $\Phi(x') = \frac{\phi x'}{T}$, as a function of the spatial variable x', in which ϕ is the maximum phase of the phase

spatial distribution and T is the period. The solution of the integral in the Eq.2.2 for

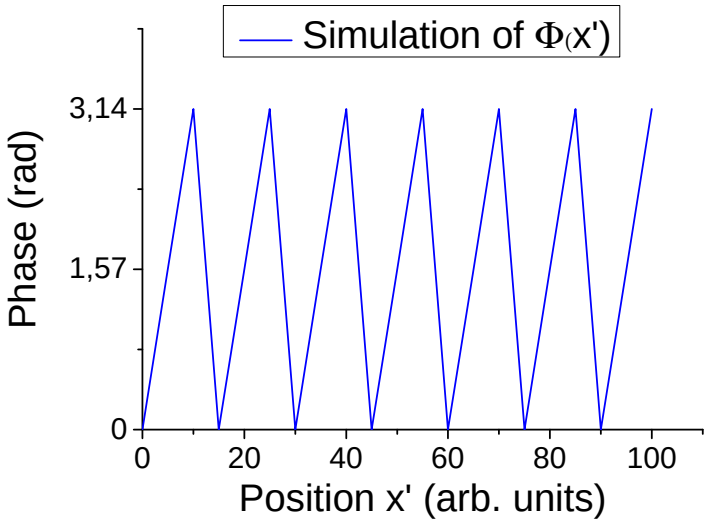

Figura 3 – Graph of the phase profile of a linear phase diffraction grating as function of the spatial variable x', with $\phi = 3,14$ rad and $T = 15$arb. units.

a Gaussian laser beam, with a linear phase function is well known and details of the calculation can be seen in the references [121, 122]. The exponential Function can be expanded as a Fourier series,

$$e^{i\Phi(x')} = \sum_{n=-\infty}^{\infty} c_n e^{-i\left(\frac{2\pi n x'}{T}\right)}. \tag{2.3}$$

We are able to calculate each coefficient, c_n, of the n Gaussian diffraction orders separated by a distance $\frac{2\pi n}{T}$,

$$c_n = e^{\frac{i(2\pi n+\phi)}{2}} \operatorname{sinc}\left[\frac{1}{2}(2\pi n + \phi)\right], \tag{2.4}$$

where the respective coefficients c_n of the diffracted orders n by the LPG at a distant plane z from the LPG, by substituting Eq. 2.3 in Eq. 2.2. From the c_n coefficients in Eq. 2.4, we are able to obtain the intensity of each diffraction order,

$$I_n = \left|c_n \mathcal{F}\left\{E_n\left(x', y'\right)\right\}\right|^2, \tag{2.5}$$

where $\mathcal{F}\left\{E^n\left(x', y'\right)\right\}$ is the Fourier transform of the incident electromagnetic field in the LPG at the plane x', y' (see Fig. 2). A graph with the theoretical predictions for the intensities of the three-first diffraction orders $n = 0, -1,$ and 1 as function of the maximum phase of the LPG is in Fig.4. For the maximum phase $\phi = 2\pi$, $I_{-1} = 1$, $I_0 = 0$ e $I_1 = 0$. So we can use this PPG to change the path mode of the incident light [18, 20, 119]. In this way, we are able to manipulate Gaussian photonic quantum path states and perform quantum operations.

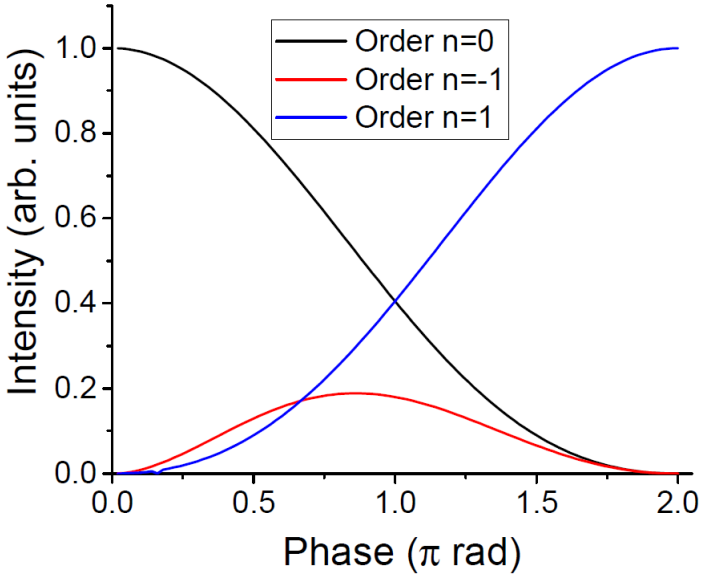

Figura 4 – Intensities values of the three first diffraction orders $n = 0, -1,$ and 1 as function of the maximum phase of the linear periodical diffraction grating, ϕ.

2.1.2 Binary diffraction grating

Another PPG we will make is the binary phase diffraction grating (BPG), in which the phase may assume two constant values. This PPG is composed of periodic step functions[1] of period T and a maximum phase ϕ. The phase profile of a BPG is shown in the graph in Fig. 5 and is written as

$$\Phi\left(x'\right) = \begin{cases} 0, & \text{if} \quad 0 \leq x' < \frac{T}{2}, \\ \phi, & \text{if} \quad \frac{T}{2} \leq x' < T. \end{cases} \tag{2.6}$$

By expanding the exponential of the phase function in Fourier series, as shown in Eq. 2.3, we are able to find the Fourier coefficients for the n diffraction orders [18, 119, 121, 122],

$$c_n = \begin{cases} e^{i\frac{\phi}{2}} cos\left(\frac{\phi}{2}\right), & \text{if} \quad n = 0, \\ 0, & \text{if} \quad n \quad \text{even}, \\ -\frac{2}{n\pi} e^{i\frac{\phi}{2}} sen\left(\frac{\phi}{2}\right), & \text{if} \quad n \quad \text{odd}, \end{cases} \tag{2.7}$$

with the related intensities given by Eq. 2.5. The relative intensities of the first three diffraction orders,$n = -1, 0, 1$, are plotted as function of the maximum phase in Fig.6. As the maximum phase grows from 0 to π, the intensity of the $n = 0$ order decreases from $I_{c_0} = 1$ to $I_{c_0} = 0$, while the the intensities of the orders $n = \pm 1$ go from $I_{c_{\pm 1}} = 0$ to a maximum value. We will use the BPG to generate qutrit path states of transversal Gaussian profiles.

[1] Also known as Heaviside function

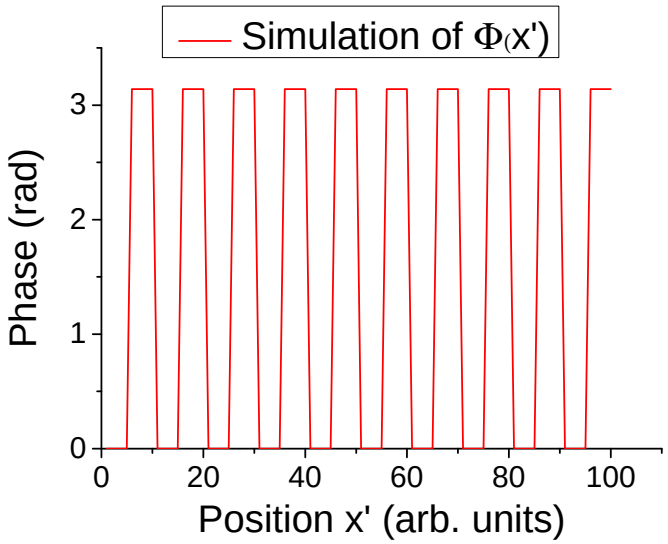

Figura 5 – Graph of the phase profile of a BPG as function of the transversal direction x' with: $\phi = 3,14$ rad. and $T = 10$arb.units.

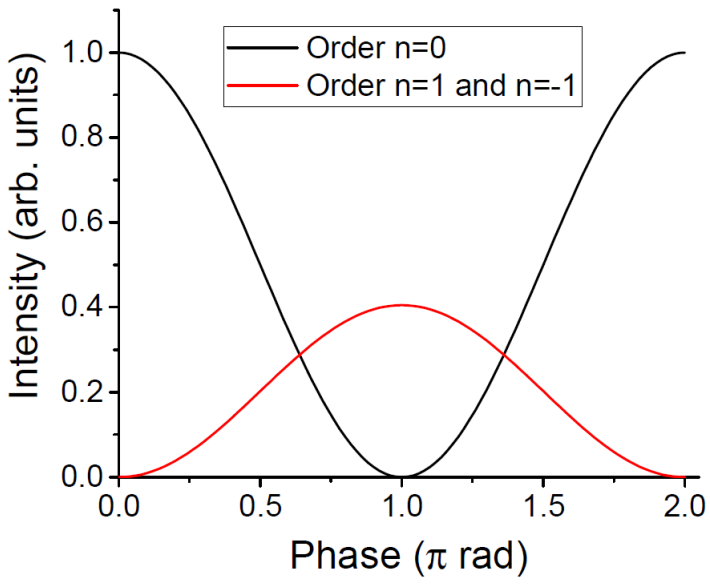

Figura 6 – Graph of the intensities of the diffraction orders, $n = -1; 0; 1$, generated by a binary phase diffraction grating, as function of the maximum phase ϕ.

2.2 The spatial light modulator, quantum states and quantum operations

PPG's are widely explored in quantum optics experiments and usually are generated by making use of a spatial light modulator (SLM) [18, 31, 123, 124]. With this device, we are able to construct a wide range of PPG's and implement a large amount of automated quantum operations in photonic path states [18, 119, 121, 122].

2.2.1 The Spatial Light Modulator

SLMs are divided in Amplitude e Phase SLMs. In this thesis, we used a Phase SLM and we will restrict our discussion about them. A Phase SLM is constituted of a grid of pixels in which we are able to adjust the phase acquired by the incident light in each pixel individually (Fig.7). In this thesis, we will make use of an liquid crystal on silicon spatial light modulator (LCOS-SLM). This device is formed by a liquid crystal layer between two electrodes on a silicon substrate, see Fig. 7. This way, we may adjust the difference of electric potential in each pixel [125]. Depending on the voltage applied

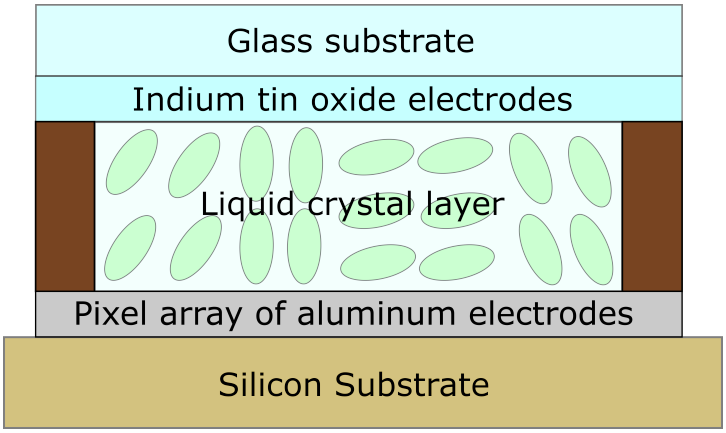

Figura 7 – Representation of the layers of a SLM of the type LCOS-SLM, which is an abbreviation of liquid crystal on silicon spatial light modulator. This device is composed by a glass substrate, over a grid of pixels of electrodes over a layer of liquid crystal. Under the liquid crystal layer there is another grid of pixel of electrodes, with all the other layers over a silicon substrate. Image adapted from [125].

by the electrodes in each pixel the liquid crystal birefringent molecules assume a certain orientation, changing the refraction index in each pixel. So, the total optical path travelled by the incoming light beam changes at an specific pixels, according to the orientation of the liquid crystal molecules. Selecting the right voltage in each pixel we are able to use the SLM to construct several PPG's to diffract an incident light beam. By programming the SLM we can construct and change the PPG's on it's screen quickly and automatically. We will make use of the SLM to generate PPG's and perform the quantum operations in the photonic Gaussian beam modes that define our photon path states [18, 119].

2.2.2 Quantum states and quantum operations

A pure quantum state in a Hilbert space of dimension D can be written as a state vector with the matrix representation in some orthonormal base as [126],

$$|\Psi\rangle = \begin{bmatrix} \psi_0 \\ \psi_1 \\ \psi_2 \\ \vdots \\ \psi_{D-1} \end{bmatrix} \tag{2.8}$$

with $\psi_i \in \mathbb{C}$, $\forall\ i$. Taking each matrix element in its polar form, $\psi_i = |\psi_i|\, e^{i\phi_i}$, we identify the term $|\psi_i|^2$ as the weight of the i-th base state in the state superposition, while phi_i is the associated phase of each state coefficient. A general quantum state in a Hilbert space of dimension D is described in terms of a DxD density matrix [117, 127, 128],

$$\rho = \begin{bmatrix} \rho_{0,0} & \rho_{0,1} & \rho_{0,2} & \cdots & \rho_{0,D-1} \\ \rho_{1,0} & \rho_{1,1} & \rho_{1,2} & \cdots & \rho_{1,D-1} \\ \rho_{2,0} & \rho_{2,1} & \rho_{2,2} & \cdots & \rho_{2,D-1} \\ \vdots & \vdots & \vdots & \ddots & \vdots \\ \rho_{D-1,0} & \rho_{D-1,1} & \rho_{D-1,2} & \cdots & \rho_{D-1,D-1} \end{bmatrix} \tag{2.9}$$

with the coefficients $\rho_{ij} \in \mathbb{C}$, $\sum_{i=0}^{D-1} \rho_{ii} = 1$ and $\rho_{ij} \in \mathbb{C}\ \forall\ i$ and j. Analysing the matrix elements in the polar representation, $\rho_{ij} = |\rho_{ij}|\, e^{i\phi_{ij}}$, we identify $|\rho_{ii}|$ as the relative population of a d-level system by representing each level as the i-th base state, ϕ_{ij} the phase of the complex off-diagonal matrix elements. The modulus of the off-diagonal terms $|\rho_{ij}|$ $(i \neq j)$ determines the coherence between the basis states $|i\rangle$ and $|j\rangle$. For a pure quantum state the density operator is $\rho = |\Psi\rangle\langle\Psi|$.

Like density matrix, a quantum operator is also represented in an orthonormal base in the Hilbert space of dimension D as a DxD matrix,

$$\mathbf{A} = \begin{bmatrix} A_{0,0} & A_{0,1} & A_{0,2} & \cdots & A_{0,D-1} \\ A_{1,0} & A_{1,1} & A_{1,2} & \cdots & A_{1,D-1} \\ A_{2,0} & A_{2,1} & A_{2,2} & \cdots & A_{2,D-1} \\ \vdots & \vdots & \vdots & \ddots & \vdots \\ A_{D-1,0} & A_{D-1,1} & A_{D-1,2} & \cdots & A_{D-1,D-1} \end{bmatrix} \tag{2.10}$$

A quantum state ρ, subject to the operation A gives rise to another quantum state $\rho\prime$, which is described the matrix product,

$$\rho' = \mathbf{A}\rho\mathbf{A}^{\dagger} \tag{2.11}$$

where $\mathbf{A}^{\dagger}$ denotes the Hermitian conjugated of the operator A. By programming a SLM with LPG's and BPG's we are able to implement a large number of quantum operations

like the one shown in Eq.2.10. We can use a BPG to diffract a single mode laser beam in other two paths to prepare qutrit path states of the type [18, 119, 121, 122].

$$|\Psi\rangle = \begin{bmatrix} a \\ be^{i\phi_2} \\ ae^{i\phi_3} \end{bmatrix} \tag{2.12}$$

with a, b and $\phi_i \in \mathbb{R}$. We are also able to realize non-diagonal operations. By using a LPG we are able to transfer a certain amount of light from a mode to another mode and therefore to change the relative weight of a basis state $|i\rangle$ with respect to the basis state $|j\rangle$. In Chapter 5 we will show the implementation of a simulation of a quantum jump in three-level systems (qutrits) encoded in photonic Gaussian path modes, by exploring light diffraction by phase modulation in PPGs. In Chapter 6 we propose how to construct quantum logic gates and controlled quantum logic gates in qubits and qutrits encoded in photonic paths by exploiting the same techniques.

3 Introduction to open quantum systems

In some cases the quantum systems are not perfectly isolated from their neighbourhood, they interact with the external environment. This interaction leads to energy dissipation and loss of coherence [27–30, 129]. A open quantum open system (OQS) is a quantum system constituted by two parts: a system of interest, which we will call S, coupled to another system E, called environment. In most of the cases, S is a small system[2] in comparison with E. The interactions between them results in a change of the state of the system and generates correlations with the environment [24, 26]. The derivations approached in this chapter until the Section 3.2.2 were adapted from the reference [24].

3.1 The Liouville-Von Neumann equation and the interaction picture

3.1.1 The Liouville-Von Neumman equation

The Schroedinger equation describes the unitary evolution, $U(t, t_0)$, of a quantum state as function of the Hamiltonian, $H(t)$ which acts over the system between the time t_0 and t [127, 128],

$$\frac{\partial}{\partial t}U(t, t_0) = -\frac{i}{\hbar}H(t)U(t, t_0), \tag{3.1}$$

The unitary operation transform,

$$U(t, t_0) = exp\left[-\frac{i}{\hbar}\int_{t_0}^{t} dt' H(t')\right], \tag{3.2}$$

is a solution of Eq.3.5. We classify the quantum system in terms of the Hamiltoniam which describes its dynamics [24]:

- If $H(t)$ is a function of time, the system is **closed**;
- If H is time independent, $U(t, t_0) = e^{-\frac{i}{\hbar}H(t-t_0)}$, the system is **isolated**.

A general quantum state like the one in Eq.2.9, can be represented by the density operator [24, 127]

$$\rho(t_0) = \sum_{\alpha} \omega_\alpha |\psi_\alpha(t_0)\rangle \langle\psi_\alpha(t_0)|, \tag{3.3}$$

where the coefficients $\omega_\alpha \in \mathbb{R}$. The temporal evolution of the state is represented by

$$\rho(t) = \sum_{\alpha} \omega_\alpha U(t, t_0) |\psi_\alpha(t_0)\rangle \langle\psi_\alpha(t_0)| U^\dagger(t, t_0) = U(t, t_0)\rho(t_0)U^\dagger(t, t_0). \tag{3.4}$$

[2] In number of degrees of freedom.

By differentiating both sides of Eq.3.4 in relation with the time we have,

$$\frac{d}{dt}\rho\left(t\right) = -\frac{i}{\hbar}\left[H(t), \rho\left(t\right)\right]. \tag{3.5}$$

Eq.3.5 is called Liouville-Von Neumann equation. It describes the time evolution of the density operator [24, 26] and can be rewritten as,

$$\frac{d}{dt}\rho\left(t\right) = \mathcal{L}(t)\rho(t), \tag{3.6}$$

where $\mathcal{L}(t)$ is called the Liouville operator: $\mathcal{L}(t)A = -\frac{i}{\hbar}\left[H(t), A\right]$, A is an generic operator, like the one shown in Eq.2.10.

3.1.2 The interaction picture

According to the dynamics of the quantum system we can choose a different picture for the operators. The Schrödinger picture is a formulation of quantum mechanics in which the state operators evolve in time, but the operators that represent observables are constant with respect to time. In the Heisenberg picture, the operators that represent observables incorporate a dependency on time, but the state operators are time-independent. In the interaction picture we divide the Hamiltonian in two terms: $H = H_0 + H_I(t)$, where H_0 is the total Hamiltonian of the whole free system and $H_I(t)$ is the Hamiltonian of the interaction between the subsystems S e E. By the Born rule, in the Schroedinger picture, the expected value of an operator is [127, 128]

$$\langle A(t)\rangle = tr\left[A(t)\rho(t)\right] = tr\left[A(t)U\left(t,t_0\right)\rho(t_0)U^{\dagger}\left(t,t_0\right)\right]. \tag{3.7}$$

In the interaction picture, we define:

$$U_0\left(t,t_0\right) \equiv e^{-iH_0(t-t_0)} \quad \text{e} \quad U_I\left(t,t_0\right) \equiv U_0^{\dagger}\left(t,t_0\right)U\left(t,t_0\right), \tag{3.8}$$

so the expected value of the same operator in this picture is

$$\langle A(t)\rangle = tr\left[U_0^{\dagger}\left(t,t_0\right)A(t_0)U_0\left(t,t_0\right)U_I\left(t,t_0\right)\rho(t_0)U_I^{\dagger}\left(t,t_0\right)\right] = tr\left[A_I(t)\rho_I(t)\right], \tag{3.9}$$

where the operators in the interaction picture are

$$A_I(t) = U_0^{\dagger}\left(t,t_0\right)A(t_0)U_0\left(t,t_0\right) \quad \text{e} \quad \rho_I(t) = U_I\left(t,t_0\right)\rho(t_0)U_I^{\dagger}\left(t,t_0\right). \tag{3.10}$$

In the interaction picture the operator that describes the quantum system and the operators that represent the observables are time dependent. Differently from the Heisenberg picture, the time evolution of the observables operators is not determined by the whole Hamiltonian, but by the free Hamiltonian H_0. Let's analyse two cases:

- If the interaction Hamiltonian is null, $\hat{H}_I(t) = 0$, we have: $U_0\left(t,t_0\right) = U\left(t,t_0\right)$ and $U_I\left(t,t_0\right) = \mathbb{I}$, i. e., the interaction picture reduces to the Heisenberg picture.

- If the free Hamiltonian vanishes, $H_0 = 0$, we have: $U_0(t, t_0) = \mathbb{I}$ and $U_I(t, t_0) = U(t, t_0)$, we are back to the Schroedinger picture.

The Liouville-Von Neumann equation in the interaction picture is

$$\frac{d}{dt}\rho_I(t) = -\frac{i}{\hbar}\left[H_I(t), \rho_I(t)\right], \tag{3.11}$$

and by integrating Eq.3.11, we obtain the final state

$$\rho_I(t) = \rho_I(t_0) - \frac{i}{\hbar}\int_{t_0}^{t} dt' \left[H_I(t'), \rho_I(t')\right], \tag{3.12}$$

where $H_I(t') = U_0^{\dagger}(t, t_0)\,\hat{H}_I U_0(t, t_0)$, is the interaction Hamiltonian in the interaction picture. Those equations are exact and describe the dynamics of a general close system. The treatment of an OQS below will be done in the interaction picture.

3.2 Dynamics of open quantum systems

An OQS is quantum system composed of the system of interest, S coupled to another system, E, which we usually call environment, where the global system, $S + E$, is a closed quantum system, as shown in Fig.8. The Hamiltonian which describes the

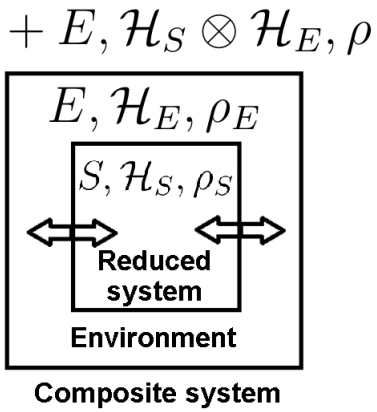

Figura 8 – Representation of an open quantum system, with the reduced system, S and the environment, E. Figure adapted from [24].

temporal evolution of this kind of system may be written as

$$H(t) = H_E \otimes \mathbb{I}_S + H_S \otimes \mathbb{I}_E + H_I(t), \tag{3.13}$$

where H_E is the free Hamiltonian of the environment, H_S is the free Hamiltonian of the reduced system (see Figure 8) and $H_I(t)$ is the interaction Hamiltonian between the systems S and E. We usually refer to E as environment, the term reservoir is used for an environment with infinite degrees of freedom, such that its frequency modes has a continuous spectrum. The term bath is used for a reservoir in a quantum state in thermal

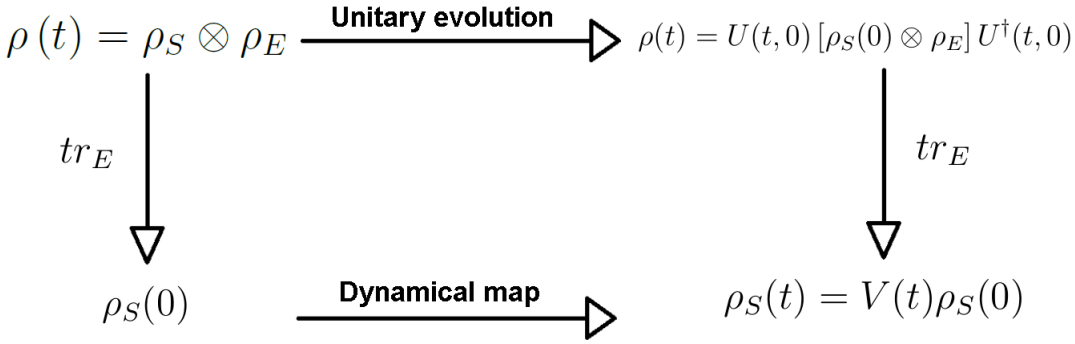

Figura 9 – Representation of the two different approaches of an open quantum system, composed by a reduced system, S and the environment E. tr_E represents the trace over the environment, $U(t)$ is the unitary transformation that gives the temporal evolution of the composite system and $V(t)$ represents the dynamical map that provides the time evolution of the reduced system. Figure adapted from [24].

equilibrium. The approach of OQS is very useful when we deal with a composed system for which the dynamics is very complicated and we are particularly interested only in the reduced system. This can be done in two ways (see Fig. 9). In the first one we take the time evolution of the whole density operator that represents the composed system, which is given by an unitary operation, and take the partial trace over the environment. In the second one we take the partial trace over the initial density operator of the composed system and make the time evolution of the state of the reduced system through the application of a dynamical map [24, 26]. The dynamical map depends on the type of interaction between S and E and describes the time evolution of the reduced system. It is completely characterized in terms of quantum operators of $\mathcal{H}_S$ Hilbert space.

In the initial time, $t_0 = 0$, the state of S and E are separable, that is, $\rho(0) = \rho_S(0) \otimes \rho_E$. As $tr_E\rho(0) = \rho_S(0)$, the Eq.3.4 and Eq.3.11 for the reduced system assume the following form

$$\rho_S(t) = tr_E\left[U(t,t_0)\,\rho(0)U^\dagger(t,t_0)\right], \tag{3.14}$$

$$\frac{d}{dt}\rho_S(t) = -itr_E\left[H(t),\rho(t)\right], \tag{3.15}$$

according the dynamics described in Fig.8. The final state for S in both approaches is the same, that is,

$$\rho_S(t) = V(t)\rho_S(0) = tr_E\left\{U(t,0)\left[\rho_S(0)\otimes\rho_E\right]U^\dagger(t,0)\right\}, \tag{3.16}$$

where $V(t)$ is a completely positive trace preserving dynamical map of the Hilbert subspace $\mathcal{S}(\mathcal{H}_S)$, of ρ_S on itself and $U(t,0)$ is the unitary operation shown in Eq.3.2.

3.2.1 Master equation in the Born-Markov approximation

According to the dynamics, the interaction between the system and the environment changes the reservoir state, leading to memory effects of S in E. But if the environment,

for instance, is a big thermal reservoir at constant temperature, those small changes will not be preserved for a long time and will not influence the future evolutions of S. For these types of system with a short correlation time, called as Markovian systems, we can dismember the dynamical map as following [24, 26],

$$V\left(t_1+t_2\right)=V\left(t_1\right)V\left(t_2\right). \tag{3.17}$$

A dynamical map can be represented in terms of the operators of the reduced system Hilbert space $\mathcal{S}(\mathcal{H}_{\mathcal{S}})$. The spectral decomposition of the density matrix ρ_E, which represents the environment is

$$\rho_E=\sum_{\alpha}\lambda_{\alpha}\left|\phi_{\alpha}\right\rangle\left\langle\phi_{\alpha}\right|, \tag{3.18}$$

where $\{|\phi_{\alpha}\rangle\}$ is an orthonormal basis of $\mathcal{S}(\mathcal{H}_{\mathcal{E}})$ and λ_{α} are non-negative real numbers that satisfy $\sum_{\alpha}\lambda_{\alpha}=1$. From the Eq.3.16, we have the following representation for the map $V(t)$

$$V(t)\rho_S=\sum_{\alpha,\beta}W_{\alpha\beta}(t)\rho_S W_{\alpha\beta}^{\dagger}(t), \tag{3.19}$$

where $W_{\alpha\beta}(t)$ are operators from $\mathcal{S}(\mathcal{H}_{\mathcal{S}})$, which are defined as

$$W_{\alpha\beta}(t)=\sqrt{\lambda_E}\left\langle\phi_{\alpha}\right|U(t,0)\left|\phi_{\beta}\right\rangle. \tag{3.20}$$

Moreover, it satisfies the condition

$$\sum_{\alpha,\beta}W_{\alpha\beta}(t)W_{\alpha\beta}^{\dagger}(t)=\mathbb{I}_S, \tag{3.21}$$

from which we can deduce that

$$tr_S\left\{V(t)\rho_S\right\}=tr_S\rho_S=1. \tag{3.22}$$

So, the dynamical map $V(t)$, represents a convex-linear, completely positive and trace preserving quantum operation [130].$V(t)$ is a specific map for a fixed time $t\geq 0$. If we want to calculate the state in a time $t'\neq t$ we need a family of dynamical maps $\left\{V(t)\middle|t\geq 0\right\}$, where $V(0)$ is the identity. The family of maps $\left\{V(t)\middle|t\geq 0\right\}$ describes the whole time evolution of the state of the reduced system, ρ_S.

Under certain mathematical conditions, see reference [24], a linear map $\mathcal{L}$, the generator of a semigroup[1] can be represented in the exponential form

$$V(t)=exp\left(\mathcal{L}t\right), \tag{3.23}$$

which yields the first-order differential equation for density matrix of the reduced system

$$\frac{d}{dt}\rho_S=\mathcal{L}\rho_S, \tag{3.24}$$

[1] A semigroup is an algebraic structure which consists in a set with associative binary operations.

which is called the Markovian quantum master equation or Lindblad equation. The generator of the semigroup $\mathcal{L}$, represents a super-operator and can be considered as a generalization of the Liouville super-operator which was introduced in the subsection 3.1.1. To construct the most general generator $\mathcal{L}$ we consider a finite-dimensional Hilbert space $\mathcal{S}(\mathcal{H}_{\mathcal{S}})$, with $\dim\mathcal{S}(\mathcal{H}_{\mathcal{S}}) = N$. Thus, the corresponding complex Liouville space has dimension N^2. Now, we choose a complete orthonormal basis of operators F_i, $i = 1, 2, ..., N^2$, in this space, such that

$$(F_i, F_j) \equiv tr_S \left\{ F_i^\dagger F_j \right\} = \delta_{ij}. \tag{3.25}$$

One of the basis operators is chosen to be proportional to the identity $F_{N^2} = N^{-1/2}\mathcal{I}_S$, so that the other basis operators are traceless, $trF_i = 0$ for $i = 1, 2, ..., N^2 - 1$. Considering the completeness relation of each one of the operators of Eq.3.20 we have

$$W_{\alpha\beta}(t) = \sum_{i=1}^{N^2} F_i \left(F_i, W_{\alpha\beta}(t)\right). \tag{3.26}$$

From the representation of the dynamical map in Eq.3.19, we identify

$$V(t)\rho_S = \sum_{i,j=1}^{N^2} c_{ij}(t) F_i \rho_S F_j^\dagger, \tag{3.27}$$

where

$$c_{ij}(t) \equiv \left(F_i, W_{\alpha\beta}(t)\right) \left(F_j, W_{\alpha\beta}(t)\right)^*. \tag{3.28}$$

The coefficients matrix $C = [c_{ij}]$ is Hermitian and positive. By the definition of the generator $\mathcal{L}$, Eq.3.23, and considering Eq.3.27, we have the limit

$$\begin{aligned}
\mathcal{L}\rho_S &= \lim_{\epsilon\to 0} \frac{1}{\epsilon} \left\{ V(\epsilon)\rho_S - \rho_S \right\} \\
&= \lim_{\epsilon\to 0} \left\{ \frac{1}{N} \frac{c_{N^2N^2}(\epsilon) - N}{\epsilon} \rho_S + \frac{1}{\sqrt{N}} \sum_{i=1}^{N^2-1} \left(\frac{c_{iN^2}(\epsilon)}{\epsilon} F_i \rho_S + \frac{c_{N^2i}(\epsilon)}{\epsilon} \rho_S F_i^\dagger \right) \right. \\
&\quad \left. + \sum_{i,j=1}^{N^2-1} \frac{c_{ij}(\epsilon)}{\epsilon} F_i \rho_S F_i^\dagger \right\},
\end{aligned} \tag{3.29}$$

from which we define the following coefficients

$$a_{N^2N^2} = \lim_{\epsilon\to 0} \frac{c_{N^2N^2}(\epsilon) - N}{\epsilon}, \tag{3.30}$$

$$a_{iN^2} = \lim_{\epsilon\to 0} \frac{c_{iN^2}(\epsilon)}{\epsilon}, \; i = 1, 2, ..., N^2 - 1, \tag{3.31}$$

$$a_{ij} = \lim_{\epsilon\to 0} \frac{c_{ij}(\epsilon)}{\epsilon}, \; i; j = 1, 2, ..., N^2 - 1, \tag{3.32}$$

$$F = \frac{1}{\sqrt{N}} \sum_{i=1}^{N^2-1} a_{iN^2} F_i, \tag{3.33}$$

$$G = \frac{1}{2N} a_{N^2N^2} \mathcal{I}_S + \frac{1}{2}\left(F^\dagger + F\right), \tag{3.34}$$

also, the Hermitian operator

$$H = \frac{1}{2i}\left(F^\dagger - F\right). \tag{3.35}$$

Considering that the coefficients matrix C is positive and Hermitian, with these definitions, we have:

$$\mathcal{L}\rho_S = -i\left[H, \rho_S\right] + \{G, \rho_S\} + \sum_{i,j=1}^{N^2-1} a_{ij} F_i \rho_S F_j^\dagger. \tag{3.36}$$

Since the generator is trace preserving for any density matrix ρ_S

$$0 = tr_S\left\{\mathcal{L}\rho_S\right\} = tr_S\left\{\left(2G + \sum_{i,j=1}^{N^2-1} a_{ij} F_j^\dagger F_i\right)\rho_S\right\}, \tag{3.37}$$

we have

$$G = -\frac{1}{2}\sum_{i,j=1}^{N^2-1} a_{ij} F_j^\dagger F_i. \tag{3.38}$$

Thus, from Eq.3.36, we get the first standard form of the generator

$$\mathcal{L}\rho_S = -i\left[H, \rho_S\right] + \sum_{i,j=1}^{N^2-1} a_{ij}\left(F_i \rho_S F_j^\dagger - \frac{1}{2}\left\{F_j^\dagger F_i, \rho_S\right\}\right). \tag{3.39}$$

Since the coefficients matrix $A = [a_{ij}]$ is positive, it can be diagonalized with the right unitary transformation

$$UAU^\dagger = \begin{bmatrix} \gamma_1 & 0 & \cdots & 0 \\ 0 & \gamma_2 & \cdots & 0 \\ \vdots & \vdots & \ddots & \vdots \\ 0 & 0 & 0 & \gamma_{N^2-1} \end{bmatrix}, \tag{3.40}$$

where: U is the unitary matrix used to diagonalize A and the eigenvalues γ_i are non-negative. Defining a new set of operators Λ_k

$$F_i = \sum_{k=1}^{N^2-1} u_{ki} \Lambda_k, \tag{3.41}$$

we obtain the diagonal form of the generator

$$\mathcal{L}\rho_S = -i\left[H, \rho_S\right] + \sum_{k=1}^{N^2-1} \gamma_k \left(\Lambda_k \rho_S \Lambda_k^\dagger - \frac{1}{2}\Lambda_k^\dagger \Lambda_k \rho_S - \frac{1}{2}\rho_S \Lambda_k^\dagger \Lambda_k\right), \tag{3.42}$$

where: γ_k is a positive constant and Λ_k are the so called Lindblad operators [131]. Eq.3.42 is a general form to obtain the density operator evolved in time from the semigroup generator $\mathcal{L}$. The first term is the unitary part of the dynamics generated by the Hamiltonian. Eq.3.42 can also be written in terms of the so-called "dissipator"

$$\mathcal{D}\left(\rho_S\right)) = \sum_{k=1}^{N^2-1} \gamma_k \left(\Lambda_k \rho_S \Lambda_k^\dagger - \frac{1}{2}\Lambda_k^\dagger \Lambda_k \rho_S - \frac{1}{2}\rho_S \Lambda_k^\dagger \Lambda_k\right), \tag{3.43}$$

such that Eq. 3.42 becomes

$$\mathcal{L}\rho_S = -i\left[H, \rho_S\right] + \mathcal{D}\left(\rho_S\right). \tag{3.44}$$

3.2.2 Kraus decomposition of the decay dynamics

3.2.2.1 Kraus decomposition for the two-level decay dynamics

An atom interacting with the vacuum state of the electromagnetic field is an example of an OQS. This interaction causes a reduction in the population of the excited states and decoherence [27–30, 129].The deductions approached in this section was adapted from the reference [120]. Lets consider the decay in a two-level atomic system as shown in Figure 10.

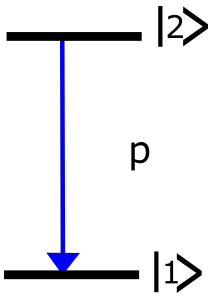

Figura 10 – Two level atomic system subject to decay.

The probability of decay is an exponential function of the time $p = 1 - e^{\gamma t}$, where γ is the decay rate of the atomic system, $|1\rangle$ and $|2\rangle$ are the ground and excited states, respectively. The graph in Figure 11 shows the exponential decay experienced by this kind of atomic system. Considering the environment (electromagnetic field) on its fundamental

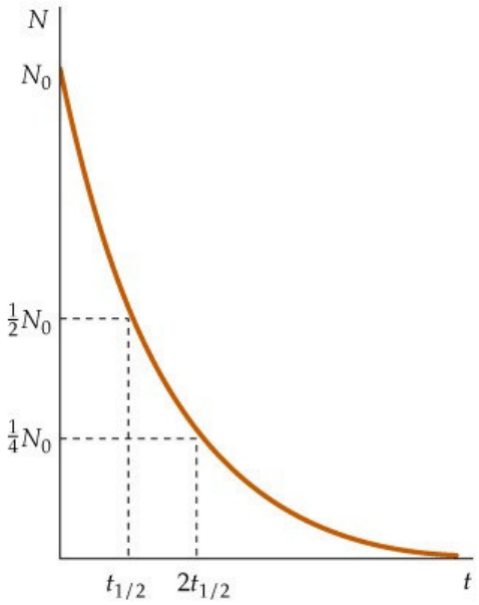

Figura 11 – Graph of the atomic population (N) in the excited state as function of the time (t) for a typical exponential decay, $p = 1 - e^{-\gamma t}$.

state, the initial state of the system can be written as:

$$\rho(0) = \rho_S(0) \otimes |0\rangle_E \langle 0|_E \,, \tag{3.45}$$

where ρ_S is the state of the atomic system and $|0\rangle_E \langle 0|_E$ is the vacuum state of the electromagnetic field. As the composite system is closed, its time evolution is always yielded by an unitary transformation:

$$\rho(t) = U_{SE}\rho_S(0) \otimes |0\rangle_E \langle 0|_E U_{SE}^\dagger, \tag{3.46}$$

where U_{SE} represents an unitary evolution which acts in $\mathcal{H}_S$ and $\mathcal{H}_E$. If we want to obtain the state of the atomic system evolved in time, $\rho_S(t)$, we must make the trace over the environment,

$$\rho_S(t) = \mathrm{Tr}\left[U_{SE}\rho_S(0) \otimes |0\rangle_E \langle 0|_E U_{SE}^\dagger\right], \tag{3.47}$$

or equivalently:

$$\rho_S(t) = \sum_i \langle i|_E U_{SE}\rho_S(0) \otimes |0\rangle_E \langle 0|_E U_{SE}^\dagger |i\rangle_E, \tag{3.48}$$

where: $\{|i\rangle_E\}$ is an orthonormal basis for $\mathcal{H}_E$. Evaluating $\langle i|_E U_{SE} |0\rangle_E$, we obtain an operator which acts only over $\mathcal{H}_S$. This way, we obtain the following representation for the decay map:

$$\rho_S(t) = V(t)\rho(0) = \sum_i K_i \rho_S(0) K_i^\dagger, \tag{3.49}$$

where K_i are the so called Kraus operators [132]. Notice that the Kraus decomposition of a map $V(t)$ is not unique, as we can write the environment state in different basis, but all the Kraus decompositions must provide the same time evolution for the density operator [24,31,37]. The decay channels that describes the decaying system can be written as

$$\begin{aligned} |1\rangle_S |0\rangle_E &\rightarrow |1\rangle_S |0\rangle_E, \\ |2\rangle_S |0\rangle_E &\rightarrow \sqrt{p}\,|1\rangle_S |1\rangle_E + \sqrt{1-p}\,|2\rangle_S |0\rangle_E, \end{aligned} \tag{3.50}$$

where p is the probability of the atomic system be excited or system decay. $|1\rangle_S$ and $|2\rangle_S$ are the ground and excited states of the atomic system, respectively. $|0\rangle_E$ represents the vacuum state of the electromagnetic field and $|1\rangle_E$ the state of the field with one photon. Is this case we made a mono-modal approach, for simplicity, by considering only a single-mode in the polarization and wave-vector degrees of freedom. Thus, we have a two-level atomic system and a two-level electromagnetic field. In the map of Eq.3.50, we considered the initial state of the environment (electromagnetic field) in the ground state (vacuum). Also, we considered an unidirectional flow of energy, that is, the atomic system decays giving rise to a photon in the electromagnetic field, but the former never is excited by the environment. In this context, the quantum operation that describes the map in Eq.3.50 is not unitary. From the map in Eq.3.50, we are able to construct the quantum

operator O_{SE} that provides the time evolution of the composed system,

$$O_{SE} = \begin{array}{c} \\ |1\rangle_S|0\rangle_E \\ |2\rangle_S|0\rangle_E \\ |1\rangle_S|1\rangle_E \\ |2\rangle_S|1\rangle_E \end{array} \begin{array}{c} \begin{array}{cccc} \langle 1|_S\langle 0|_E & \langle 2|_S\langle 0|_E & \langle 1|_S\langle 1|_E & \langle 2|_S\langle 1|_E \end{array} \\ \begin{pmatrix} 1 & 0 & 0 & 0 \\ 0 & \sqrt{1-p} & 0 & 0 \\ 0 & \sqrt{p} & 1 & 0 \\ 0 & 0 & 0 & 1 \end{pmatrix} \end{array} \tag{3.51}$$

The time evolution of the atomic system is

$$\rho_S(t) = \sum_i \langle i|_E O_{SE}\rho_S(0) \otimes |0\rangle_E \langle 0|_E O_{SE}^\dagger |i\rangle_E . \tag{3.52}$$

By evaluating $K_i = \langle i|_E O_{SE}|0\rangle_E$, we are able to obtain the Kraus operators for the two-level decay dynamics:

$$K_0 = \langle 0|_E O_{SE}|0\rangle_E = \begin{pmatrix} 1 & 0 \\ 0 & \sqrt{1-p} \end{pmatrix} \text{ and } K_1 = \langle 1|_E O_{SE}|0\rangle_E = \begin{pmatrix} 0 & \sqrt{p} \\ 0 & 0 \end{pmatrix} \tag{3.53}$$

3.2.2.2 Kraus decomposition for the three-level decay dynamics

In a three-level system, we consider the three configurations of spontaneous decay dynamics: cascade decay, Λ decay and V decay, each one with a forbidden transition and without degeneracy [120] (Fig. 12).

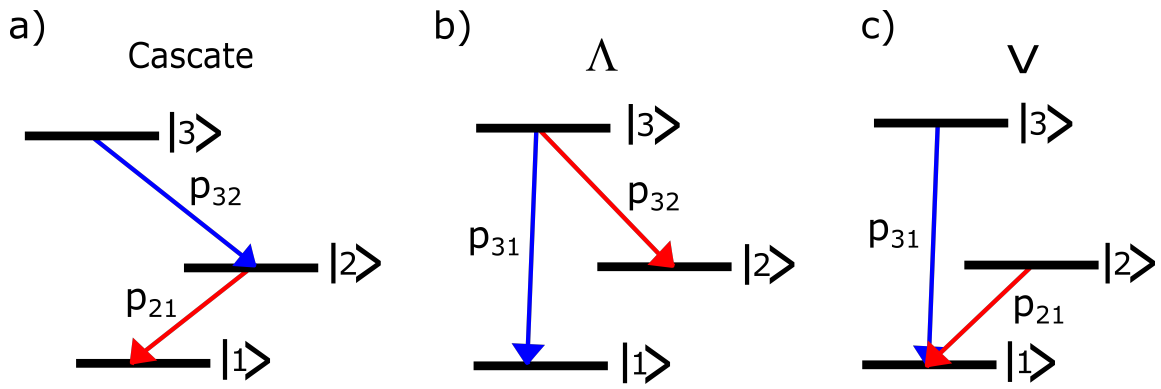

Figura 12 – Different configurations of spontaneous decay dynamic in a three-level system: a) cascade decay, b) Λ decay and c) V decay. Figure taken from reference [120].

The type of decay is regulated by the selection rules, which depends on the atomic levels involved in the transition. So, it depends specifically on the type of atomic system and its energy levels. This kind of system typically experiences a time-dependent exponential decay, in which the probability of an excited state $|i\rangle$ to decay to $|j\rangle$ is given by $p_{ij} = 1 - e^{-\gamma_{ij}t}$, where γ is the spontaneous decay rate between levels i and j.

The time evolution of the density matrix of the system is ruled by the master equation 3.42, where ρ_s is the density matrix of the system, $\Lambda_k = \sqrt{\gamma_{ij}}|j\rangle\langle i|$ is the Lindblad

operator and the decay channels are labelled by k. In the theory of quantum open system, for all these decay dynamics, the time evolution of the state $\rho(t)$ can be obtained by the application of a dynamical map, Eq.3.16. As an example, let's consider the decay channels, without excitations, for cascade configuration (Fig.12 a)):

$$\begin{aligned} |0,0\rangle_E |1\rangle_S &\rightarrow |0,0\rangle_E |1\rangle_S , \\ |0,0\rangle_E |2\rangle_S &\rightarrow \sqrt{p_{21}} |0,1\rangle_E |1\rangle_S + \sqrt{1-p_{21}} |0,0\rangle_E |2\rangle_S , \\ |0,0\rangle_E |3\rangle_S &\rightarrow \sqrt{p_{21}p_{32}} |1,1\rangle_E |1\rangle_S + \sqrt{p_{32}}\sqrt{1-p_{21}} |1,0\rangle_E |2\rangle_S + \sqrt{1-p_{32}} |0,0\rangle_E |3\rangle_S \end{aligned} \tag{3.54}$$

where our three-level atomic system system (environment) is represented by index S (E) with energy levels $|1\rangle$, $|2\rangle$ and $|3\rangle$ ($|i,j\rangle_E$ with $i,j = 0,1$). The environment is represented by two frequencies modes, to emphasize the non-degenerate decays, where the first (second) represent the number of photons in each frequency mode of the electromagnetic field, which was generated from the decay channel $|3\rangle_S \rightarrow |2\rangle_S$ ($|2\rangle_S \rightarrow |1\rangle_S$) with decay probability of p_{32} (p_{21}). The map of Eq.3.54 is represented by the following quantum operation

$$\begin{aligned} O_{SE} = \; & |1\rangle_S |00\rangle_E \langle 1|_S \langle 00|_E + \sqrt{p_{21}} |1\rangle_S |01\rangle_E \langle 2|_S \langle 00|_E + \sqrt{1-p_{21}} |2\rangle_S |00\rangle_E \langle 2|_S \langle 00|_E \\ & + \sqrt{p_{21}p_{32}} |1\rangle_S |11\rangle_E \langle 3|_S \langle 00|_E + \sqrt{p_{32}}\sqrt{1-p_{21}} |2\rangle_S |10\rangle_E \langle 3|_S \langle 00|_E \\ & + \sqrt{1-p_{32}} |3\rangle_S |00\rangle_E \langle 3|_S \langle 00|_E . \end{aligned} \tag{3.55}$$

By evaluating $K_i = \langle i|_E O_{SE} |0\rangle_E$ with the operator O_{SE} from Eq.3.55, we obtain the Kraus operators for the cascade decay dynamics in Table 1. This configuration has a peculiarity, in comparison with the Λ and V dynamics. Despite of the direct transition between the levels $|3\rangle \rightarrow |1\rangle$ is forbidden, we have an indirect transition $|3\rangle \rightarrow |2\rangle \rightarrow |1\rangle$, which involves both the channels $|3\rangle \rightarrow |2\rangle$ and $|2\rangle \rightarrow |1\rangle$. Because of this the cascade dynamics has one not null Kraus operator more than the others configurations (see Table1).

Analogously to the Kraus decomposition for the two-level decay system in Section 3.2.2.1, we can use the same approach to deduce the Kraus operators for all the three-level system decay dynamics. Tracing out the environment degrees of freedom, we can find the Kraus decomposition that represents this dynamical map. These operators are the solutions of Eq.3.42, for the reduced density matrix of the system. The decay channels for Λ (Fig.12 b)) configurations can be written as following,

$$\begin{aligned} |0,0\rangle_E |1\rangle_S &\rightarrow |0,0\rangle_E |1\rangle_S , \\ |0,0\rangle_E |2\rangle_S &\rightarrow |0,0\rangle_E |2\rangle_S , \\ |0,0\rangle_E |3\rangle_S &\rightarrow \sqrt{p_{32}} |1,0\rangle_E |2\rangle_S + \sqrt{p_{31}} |0,1\rangle_E |1\rangle_S + \sqrt{1-p_{32}-p_{31}} |0,0\rangle_E |3\rangle_S , \end{aligned} \tag{3.56}$$

where the environment is represented by two frequencies modes, to emphasize the non-degenerate decays. The first (second) represent the number of photons in each frequency mode of the electromagnetic field, which was generated from the decay channel $|3\rangle_S \rightarrow |2\rangle_S$

($|3\rangle_S \to |1\rangle_S$) with decay probability of p_{32} (p_{31}). Analogously, the decay channels for V (Fig.12 c)) decay are

$$\begin{aligned} |0,0\rangle_E |1\rangle_S &\to |0,0\rangle_E |1\rangle_S , \\ |0,0\rangle_E |2\rangle_S &\to \sqrt{p_{21}} |0,1\rangle_E |1\rangle_S + \sqrt{1-p_{21}} |0,0\rangle_E |2\rangle_S , \\ |0,0\rangle_E |3\rangle_S &\to \sqrt{p_{31}} |1,0\rangle_E |1\rangle_S + \sqrt{1-p_{31}} |0,0\rangle_E |3\rangle_S , \end{aligned} \tag{3.57}$$

where the environment is also represented by two frequencies modes, emphasizing the non-degenerate decays. The first (second) represent the number of photons in each frequency mode of the electromagnetic field, which was generated from the decay channel $|3\rangle_S \to |1\rangle_S$ ($|2\rangle_S \to |1\rangle_S$) with decay probability of p_{31} (p_{21}). All the not null Kraus operators for each configuration are presented in Table 1.

The Kraus operators satisfy the relation $\sum_i K_i K_i^\dagger = \mathbb{I}$ ($\mathbb{I}$ is the identity operator). The linear map $V(t)$, represented by the $\left\{K^\dagger\right\}$ is know as a completely positive trace preserving (CPTP) map, *i. e.*, it satisfies the following conditions:

1. It is linear: $V(t)\sum_i p_i\rho_i = \sum_i p_i V(t)\rho_i$.
2. It is trace preserving: $\mathrm{Tr}\{\rho\} = \mathrm{Tr}\{V(t)\rho\}$.
3. It is completely positive: if $\rho \geq 0$ then $V(t)\rho \geq 0$.

Indeed, the third property refers to a positive map, not a completely positive one. The completely positive condition means $V(t)\rho \geq 0$ even if ρ is in a Hilbert space of larger dimension than the one that $V(t)$ acts on. For instance, lets consider the case that the state ρ describes a two qubit state but the $V(t)$ acts in a single qubit, if $V(t)\rho \geq 0$ we say the map is completely positive[2]. To be more precise, $V(t) \otimes \mathbb{I}\rho \geq 0$

In Chapter 5 we will show the implementation of a simulation of a quantum open system [120]. More specifically, we will simulate quantum jumps in three-level system (qutrits) encoded in photonic Gaussian path modes, by exploring light diffraction by phase modulation in periodical phase gratings programmed in a spatial light modulator, as approached in Chapter 2.

[2] There are not a lot of examples of positive maps that are not completely positive. One of them is the transpose operation, see Box 8.2 of [87]

	Cascade	Λ	V
K_0	$\begin{pmatrix} 1 & 0 & 0 \\ 0 & \sqrt{1-p_{21}} & 0 \\ 0 & 0 & \sqrt{1-p_{32}} \end{pmatrix}$	$\begin{pmatrix} 1 & 0 & 0 \\ 0 & 1 & 0 \\ 0 & 0 & \sqrt{1-p_{32}-p_{31}} \end{pmatrix}$	$\begin{pmatrix} 1 & 0 & 0 \\ 0 & \sqrt{1-p_{21}} & 0 \\ 0 & 0 & \sqrt{1-p_{31}} \end{pmatrix}$
K_1	$\begin{pmatrix} 0 & \sqrt{p_{21}} & 0 \\ 0 & 0 & 0 \\ 0 & 0 & 0 \end{pmatrix}$	$\begin{pmatrix} 0 & 0 & 0 \\ 0 & 0 & \sqrt{p_{32}} \\ 0 & 0 & 0 \end{pmatrix}$	$\begin{pmatrix} 0 & \sqrt{p_{21}} & 0 \\ 0 & 0 & 0 \\ 0 & 0 & 0 \end{pmatrix}$
K_2	$\begin{pmatrix} 0 & 0 & 0 \\ 0 & 0 & \sqrt{p_{32}(1-p_{21})} \\ 0 & 0 & 0 \end{pmatrix}$	$\begin{pmatrix} 0 & 0 & \sqrt{p_{31}} \\ 0 & 0 & 0 \\ 0 & 0 & 0 \end{pmatrix}$	$\begin{pmatrix} 0 & 0 & \sqrt{p_{31}} \\ 0 & 0 & 0 \\ 0 & 0 & 0 \end{pmatrix}$
K_3	$\begin{pmatrix} 0 & 0 & \sqrt{p_{32}p_{21}} \\ 0 & 0 & 0 \\ 0 & 0 & 0 \end{pmatrix}$		

Tabela 1 – Kraus operators for cascade decay, Λ decay and V decay.

4 Quantum gates in qubit and qutrit systems

4.1 Quantum gates for qubits

4.1.1 Single qubit quantum gates

Analogous to classical computer, most of quantum computers approaches, explores a two-level system (qubits). The result of the implementation of a QG, represented by the unitary operator G, on a pure state $|\Psi\rangle$ is [87, 127]

$$|\Psi'\rangle = G\,|\Psi\rangle\,, \tag{4.1}$$

where $|\Psi'\rangle$ is the state after applying G. A Qubit pure state can be represented as a 2x1 matrix, with the matrix elements being the components of the qubit written in terms of the vector states of a basis

$$|\Psi\rangle = \frac{1}{\sqrt{2}}\begin{bmatrix} a \\ be^{i\phi} \end{bmatrix}, \tag{4.2}$$

with a, b, $\phi \in \mathbb{R}$ and $a^2 + b^2 = 1$. If the initial state is a mixed state it is represented by the density operator ρ, the output state of the quantum gate will be analogous to the one described in Eq.2.11 for general quantum transformations, *i. e.*:

$$\rho' = G\rho G^{\dagger}. \tag{4.3}$$

The Pauli matrices are examples of QGs for qubits [87, 88].

$$\sigma_x = \begin{bmatrix} 0 & 1 \\ 1 & 0 \end{bmatrix} \quad , \quad \sigma_y = \begin{bmatrix} 0 & -i \\ i & 0 \end{bmatrix} \quad \text{e} \quad \sigma_z = \begin{bmatrix} 1 & 0 \\ 0 & -1 \end{bmatrix}. \tag{4.4}$$

Figure 13 shows usual the illustration of Pauli gates on quantum circuits.

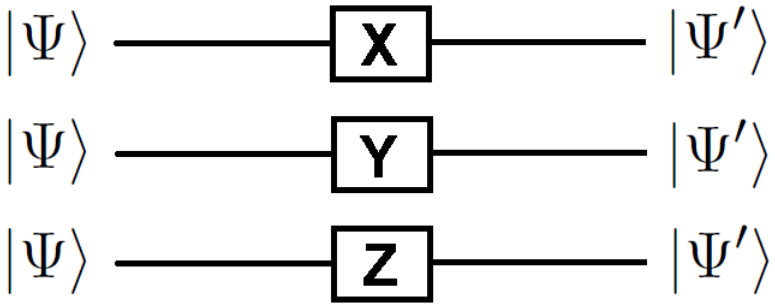

Figura 13 – Representation of the Pauli gates (σ_x, σ_y and σ_z) in quantum circuits with its input and output states.

The application of these QG in the state of Eq.4.2 provide us as output state:

$$|\Psi'\rangle = \sigma_x\,|\Psi\rangle = \begin{bmatrix} be^{i\phi} \\ a \end{bmatrix}, \tag{4.5}$$

$$|\Psi'\rangle = \sigma_y |\Psi\rangle = \begin{bmatrix} -ibe^{i\phi} \\ ia \end{bmatrix}, \tag{4.6}$$

$$|\Psi'\rangle = \sigma_z |\Psi\rangle = \begin{bmatrix} a \\ -be^{i\phi} \end{bmatrix}. \tag{4.7}$$

By comparing the states $|\Psi\rangle$ and $|\Psi'\rangle$ we observe that:

- σ_x inverts the components of the two computational basis states, $|0\rangle$ and $|1\rangle$;
- σ_y inverts the components of the two computational basis states, $|0\rangle$ and $|1\rangle$, adds a phase, $e^{i\pi}$ in $|0\rangle$ and a global phase $e^{i\frac{\pi}{2}}$ which does not yield observables effects;
- σ_z adds a phase, $e^{i\pi}$ in the computational basis state $|1\rangle$.

The σ_x QG could be thought as quantum NOT gate, the counterpart of classical NOT gate, since it transforms the computational basis states into orthogonal ones, $|0\rangle \rightarrow |1\rangle$ and $|1\rangle \rightarrow |0\rangle$. But if we have as input a superposition state, for instance, $|\psi\rangle = 1/\sqrt{2}\,(|0\rangle + |1\rangle)$, it will not provide as output an orthogonal state. Thus, σ_x does not always has as output an orthogonal state to the input one and, therefore, can not be called NOT gate [133].

There is another useful QG, called as phase-shift gate:

$$S = \begin{bmatrix} 1 & 0 \\ 0 & e^{i\theta} \end{bmatrix}, \tag{4.8}$$

which acting on the state 4.2, has the output

$$|\Psi'\rangle = S |\Psi\rangle = \begin{bmatrix} a \\ be^{i(\phi+\theta)} \end{bmatrix}. \tag{4.9}$$

The S gate inserts a relative phase ϕ in the computational basis state $|1\rangle$. Notice that, the σ_z gate is a particular case of a phase-shift gate for $\theta = \pi$.

4.1.2 Two qubits quantum gates

The two qubits QGs are called controlled quantum gates (CQGs), which act in a two-particle system Hilbert space. In this approach, we will make use of a two-dimensional system, we will explore a bipartite two-qubits state. One of them is used as control, C, and the other one as target, T. The way the QG acts on the target qubit depends on the state of the control qubit. The state of the qubit C indicates if the the CQG will be implemented or not, in the T qubit part. Assume the initial state,

$$|\Psi\rangle = (a\,|0\rangle_C + b\,|1\rangle_C) \otimes (c\,|0\rangle_T + d\,|1\rangle_T), \tag{4.10}$$

where, a, b, c and $d \in \mathbb{C}$. By considering that the state $|1\rangle_C$ means that the QG will be implemented and the state $|0\rangle_C$ that it will not be, we have, for example, the following transformation as result of the application of CNOT gate on each one of the basis states:

$$\begin{aligned} &|0\rangle_C \otimes |0\rangle_T \to |0\rangle_C \otimes |0\rangle_T\,, \quad |0\rangle_C \otimes |1\rangle_T \to |0\rangle_C \otimes |1\rangle_T\,, \\ &|1\rangle_C \otimes |0\rangle_T \to |1\rangle_C \otimes |1\rangle_T \quad \text{and} \quad |1\rangle_C \otimes |1\rangle_T \to |1\rangle_C \otimes |0\rangle_T\,. \end{aligned} \tag{4.11}$$

These transformations can be represented by the general formula:

$$|A\rangle_C \otimes |B\rangle_T \to |A\rangle_C \otimes |A \oplus B\rangle_T\,, \tag{4.12}$$

where $\oplus$ denotes addition modulo two. A representation of the CNOT gate on quantum circuits in shown in Figure14.

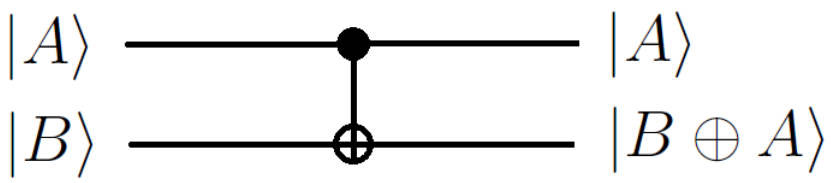

Figura 14 – Representation of a CNOT in quantum circuits with its input and output states. The top wire represents the input and output of the control qubit and the bottom wire represents the input and output target qubit.

From the basis states change described in Eq. 4.11, we have the matrix representation of the CNOT gate:

$$U_{CNOT} = \begin{bmatrix} 1 & 0 & 0 & 0 \\ 0 & 1 & 0 & 0 \\ 0 & 0 & 0 & 1 \\ 0 & 0 & 1 & 0 \end{bmatrix}. \tag{4.13}$$

The application of the CNOT gate in the state of the Eq.4.10 lead us to the final state,

$$|\Psi'\rangle = (ac\,|0\rangle_C + bd\,|1\rangle_C) \otimes |0\rangle_T + (ad\,|0\rangle_C + bc\,|1\rangle_C) \otimes |1\rangle_T\,. \tag{4.14}$$

By comparing the initial state, Eq.4.10, and the final one, Eq.4.14, we can see that the CQG, like a CNOT, can be used to generate entangled states [91, 92]. Notice that the input state is separable, while the output state is entangled and can not be written as $|\Psi'\rangle = |\Psi'\rangle_C \otimes |\Psi'\rangle_T$. Those types of CQG are widely used in quantum circuits to perform operations in quantum states.

4.2 Quantum gates for qutrits

4.2.1 Single qutrit quantum gates

Some reports indicate that there are many advantages on exploiting higher-dimensional systems (qudits) than two-level ones to implement quantum computation

and quantum information processing [134–137]. For instance, these advantages has been demonstrated in cryptographic schemes [138] and quantum key distribution protocols [139]. Also, it shows practical advantages for scaling up a quantum computer, improving the flexibility in the storage and processing information [140, 141]. A qudit quantum computer makes use of a string of qudits to manipulate and transfer information, as higher the qudits dimension the less the number of coupled information carriers it will need to perform a quantum information process. This is a crucial advantage when realizing experimental quantum computation based on trapped ions and spin system devices. So, implementing QG in qudit systems with dimension $d \geq 3$ can enhance the capability of quantum computers. In this section, we will show some QG for qutrit systems ($d = 3$), an analogous of Pauli Eq.4.4, and the phase-shift gates, Eq.4.8. The counterpart for qutrits of the Pauli operators are represented by [87, 142–145]

$$\sigma_x^{(01)} = \begin{bmatrix} 0 & 1 & 0 \\ 1 & 0 & 0 \\ 0 & 0 & 1 \end{bmatrix}, \quad \sigma_y^{(01)} = \begin{bmatrix} 0 & -i & 0 \\ i & 0 & 0 \\ 0 & 0 & i \end{bmatrix}, \quad \sigma_z^{(01)} = \begin{bmatrix} 1 & 0 & 0 \\ 0 & -1 & 0 \\ 0 & 0 & 1 \end{bmatrix}, \quad \sigma_x^{(02)} = \begin{bmatrix} 0 & 0 & 1 \\ 0 & 1 & 0 \\ 1 & 0 & 0 \end{bmatrix},$$

$$\sigma_y^{(02)} = \begin{bmatrix} 0 & 0 & -i \\ 0 & i & 0 \\ i & 0 & 0 \end{bmatrix}, \quad \sigma_z^{(02)} = \begin{bmatrix} 1 & 0 & 0 \\ 0 & 1 & 0 \\ 0 & 0 & -1 \end{bmatrix}, \quad \sigma_x^{(12)} = \begin{bmatrix} 1 & 0 & 0 \\ 0 & 0 & 1 \\ 0 & 1 & 0 \end{bmatrix}, \quad \sigma_y^{(12)} = \begin{bmatrix} i & 0 & 0 \\ 0 & 0 & -i \\ 0 & i & 0 \end{bmatrix},$$

$$\text{and } \sigma_z^{(12)} = \begin{bmatrix} 1 & 0 & 0 \\ 0 & 1 & 0 \\ 0 & 0 & -1 \end{bmatrix}. \tag{4.15}$$

Those operators change the initial state in an analogous way to the Pauli matrices, Eq.4.4. As effect of their application we have:

- $\sigma_x^{(ij)}$ inverts the components of the basis states, $|i\rangle$ and $|j\rangle$;
- $\sigma_y^{(ij)}$ inverts the components of the basis states, $|i\rangle$ and $|j\rangle$, adds a relative phase, $e^{i\pi}$ between the basis states $|i\rangle$ and $|j\rangle$ and a global phase $e^{i\frac{\pi}{2}}$;
- $\sigma_z^{(ij)}$ adds a relative phase, $e^{i\pi}$ between the basis states $|i\rangle$ and $|j\rangle$.

We have also the following phase-shift gates for qutrit systems

$$S^{(0)} = \begin{bmatrix} e^{i\theta} & 0 & 0 \\ 0 & 1 & 0 \\ 0 & 0 & 1 \end{bmatrix}, \quad S^{(1)} = \begin{bmatrix} 1 & 0 & 0 \\ 0 & e^{i\theta} & 0 \\ 0 & 0 & 1 \end{bmatrix} \quad \text{and} \quad S^{(2)} = \begin{bmatrix} 1 & 0 & 0 \\ 0 & 1 & 0 \\ 0 & 0 & e^{i\theta} \end{bmatrix}. \tag{4.16}$$

The application of QGs, $S^{(i)}$ adds a relative phase, θ to the basis state $|i\rangle$. As the qubit gates, the $\sigma_z^{(ij)}$ qutrit gates are particular cases for the $S^{(i)}$, for $\theta = \pi$.

4.3 Controlled quantum gates for hybrid-dimension systems

Controlled quantum gates can also be applied to hybrid-dimension systems. In this case, the target and the control qudits have different dimensions, for instance, one can have a qubit as C and a qutrit as T. This kind of hybrid-dimension approach can also be explored to quantum computation improving its flexibility in the storage and processing of quantum information. Also, it can helps to scale up quantum computers [136,141,146,147]. Let us build up a hybrid controlled-$\sigma_x^{(01)}$ gate, analogous to the one described in Eq.4.15, remembering that if the control input is in the basis state $|0\rangle$ the QG will not be applied, if it is in the basis state $|1\rangle$ it will be applied. The implementation of such gate provide us the following transformations:

$$\begin{aligned} |0\rangle_C \otimes |0\rangle_T \to |0\rangle_C \otimes |0\rangle_T\,, \quad |0\rangle_C \otimes |1\rangle_T \to |0\rangle_C \otimes |1\rangle_T\,, \\ |0\rangle_C \otimes |2\rangle_T \to |0\rangle_C \otimes |2\rangle_T\,, \quad |1\rangle_C \otimes |0\rangle_T \to |1\rangle_C \otimes |1\rangle_T\,, \\ |1\rangle_C \otimes |1\rangle_T \to |1\rangle_C \otimes |0\rangle_T \quad \text{and} \quad |1\rangle_C \otimes |2\rangle_T \to |1\rangle_C \otimes |2\rangle_T\,. \end{aligned} \tag{4.17}$$

From which we have the matrix representation for the hybrid controlled-$\sigma_x^{(01)}$ gate

$$U_{C\sigma_x^{(01)}} = \begin{bmatrix} 1 & 0 & 0 & 0 & 0 & 0 \\ 0 & 1 & 0 & 0 & 0 & 0 \\ 0 & 0 & 1 & 0 & 0 & 0 \\ 0 & 0 & 0 & 0 & 1 & 0 \\ 0 & 0 & 0 & 1 & 0 & 0 \\ 0 & 0 & 0 & 0 & 0 & 1 \end{bmatrix}. \tag{4.18}$$

In a similar manner as shown in Eq.4.18 for hybrid CQG for σ_x^{01}, we can do the same for all the other QG that was approached in Section 4.2.1.

In Chapter 6 we show a proposal to perform all QGs and CQGs reviewed in Chapter 4. For this purpose, we will make use of qubit and qutrit system encoded in photonic Gaussian path modes. This implementation can be realized by exploring light diffraction by phase modulation in PPGs presented in Chapter 2.

Parte II

Experimental applications

5 Simulation of a quantum jump in three-level system

In this chapter we will approach the simulation of quantum jump in a three-level system encoded in photonic Gaussian path modes [120], by exploiting periodical phase modulation in PPGs, studied in Chapter 2. Making use of a SLM, we will show how to generate and perform quantum operations in multi-path quantum systems to simulate the cascade, Λ and V dynamics (see Figure 12). The objective is to reproduce the time evolution of a state of decaying three-level atomic system in qutrit path modes, from $t = 0$ to $t \to \infty$. The methodology exploited in this implementation was based on techniques to perform general quantum operations on Gaussian paths systems proposed in [119, 122] and performed in [18, 121]. The use of the SLM in optical systems allows the photon state to be manipulated in different ways and can be used to implement a wide range of quantum operations [8, 12, 16, 18, 83, 84]. The text and the experimental results showed in this chapter were adapted from the publication of these results in reference [120].

5.1 Experimental setup, state preparation and state operation

5.1.1 Experimental setup and state preparation

The experimental setup used to realize the decay simulation is depicted in Figure 15. The first step for the simulation of atomic spontaneous decay in photonic qutrit path system is the state preparation. The initial state $|\psi_0\rangle$ is prepared in three parallel photon paths, which are displaced relatively to each other in the x-direction and have a transverse Gaussian electric field profile. The photon state preparation is realized by using a laser beam that passes through a half wave-plate (HWP), a polarizer beam-splitter (PBS) and a neutral-density filter (NDF). These three optical elements are used to attenuate the beam to single photon regime and to filter the polarization state to the horizontal one. After that, it reaches a phase-only reflection SLM in the region M4 as shown in Figure 15. A picture of the SLM used to prepare the state and realize the quantum operations is shown in Figure 16. This region is programmed with a BPG in x-direction that diffracts the incoming light in several diffraction orders, displaced in x-direction, as depicted in Figure 2. The three higher-intensities orders[1] are filtered and labelled as $|1\rangle_x \otimes |0\rangle_y$, $|2\rangle_x \otimes |0\rangle_y$ and $|3\rangle_x \otimes |0\rangle_y$. An illustration of the initial states generated by the SLM is shown in Figure 17. Proceeding in this way, we are able generate photonic path

[1] Orders -1, 0 and 1, see Figure 6.

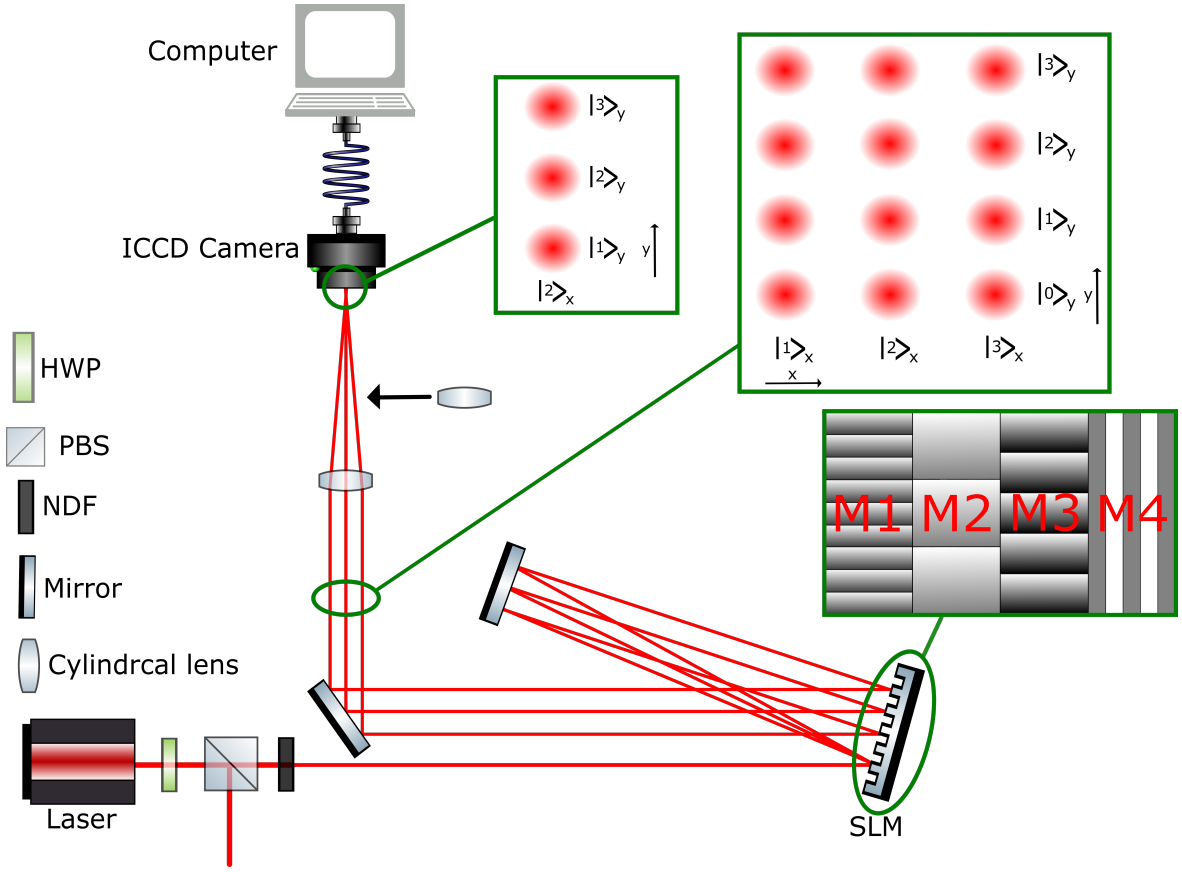

Figura 15 – Experimental setup used to prepare and to implement the operations on a qutrit parallel Gaussian beam state. A laser beam passes through a half wave-plate (HWP), a polarizer beam splitter (PBS) and a neutral density filter (NDF). This is necessary for filtering the polarization state and to attenuate it to the single photon regime. The laser beam reaches a SLM screen divided in four regions, each one with a periodical phase diffraction grating. The attenuated laser beam is initially diffracted by a periodical binary phase grating in the region M4 in three horizontal paths (x-direction). A state superposition of Gaussian modes paths, $|1\rangle_x \otimes |0\rangle_y$, $|2\rangle_x \otimes |0\rangle_y$ and $|3\rangle_x \otimes |0\rangle_y$, is considered to be our initial state. Each of the modes is reflected back in three different regions on the SLM: M1, M2 and M3. In the second incidence the beams are diffracted by linear phase gratings in which the first diffraction order propagates in three possible vertical directions, depending on the phase grating periodicity (mode paths: $|i\rangle_x \otimes |1\rangle_y$, $|i\rangle_x \otimes |2\rangle_y$ and $|i\rangle_x \otimes |3\rangle_y$, $i = 1, 2$ and 3). The multi-path system passes through a cylindrical lens which transforms all $|i\rangle_x \rightarrow |2\rangle_x$. After a spatial filtering, only the three possible first orders diffracted after the second incidence in the SLM reach the detection system. An intensified charged-coupled device (ICCD) camera records the photon counts in each position.

states of the type [18, 119, 121, 122]:

$$|\psi_0\rangle = \left(A_1 e^{i\phi_1} |1\rangle_x + A_2 e^{i\phi_2} |2\rangle_x + A_3 e^{i\phi_3} |3\rangle_x\right) \otimes |0\rangle_y , \tag{5.1}$$

where A_i and ϕ_i, $i = 1, 2$ and 3, are real numbers that depend on the maximum phase of the BPG. The A_i coefficient is equal to the modulus of the amplitude of the laser beam at the path i and ϕ_i is the phase of the state $|i\rangle_x \otimes |0\rangle_y$. The state generated was considered pure because it was prepared by selecting diffraction orders of a laser beam. We labelled

Figura 16 – Picture of the spatial light modulator used to prepare the state and realize the quantum operations in the experimental setup of Figure 15.

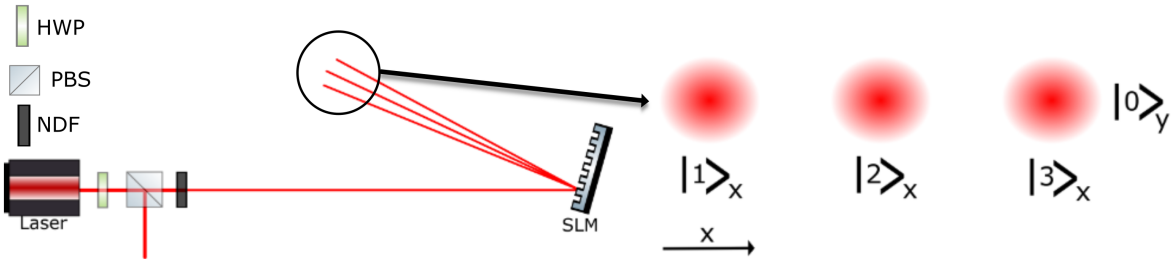

Figura 17 – Representation of the spatial light modulator generating the initial state $|\psi_0\rangle$ explored to simulate the decay dynamics.

as $|0\rangle_y$ the vertical spatial mode of the initial state field in the y-direction. The state $|l\rangle_y$ is given by:

$$|l\rangle_y = \int_{-\infty}^{+\infty} dy \exp\left[-\frac{(y-ld)^2}{2\sigma^2}\right] |1y\rangle\,, \tag{5.2}$$

where $l = 1, 2,$ and 3, ld is the centre position of each horizontal spatial mode that are displaced by d from its neighbour mode, σ is the Gaussian mode transverse width, $|1y\rangle = \frac{1}{2\pi^2}\int_{-\infty}^{\infty} dq \exp(-iqd)\,|1q\rangle$ is a representation of a coherence state of one photon, on average, in the transverse position and $|1q\rangle$ a coherence state of one photon, on average, in the transverse momentum variable in x-direction [117, 148]. We should emphasize that, with a BPG in region M4 of the SLM, we are able to prepare some states represented by Eq.5.1, not all of them. For instance, the states prepared by diffraction on a BPG usually have the coefficients $A_1 = A_3$.

5.1.2 Implementation of quantum operations

These three paths are retro-reflected by a mirror to the same SLM and each horizontal path mode is modulated by one of the three different LPGs, in which the phase increases linearly in the y-direction. Each of these Gaussian beams, at the path i, that defines the initial state components $|i\rangle_x \otimes |0\rangle_y$ strikes a specific region Mi ($i = 1, 2$ and 3), see Figure 18. To implement the quantum operations (Subsection 2.2.2) we need to simulate

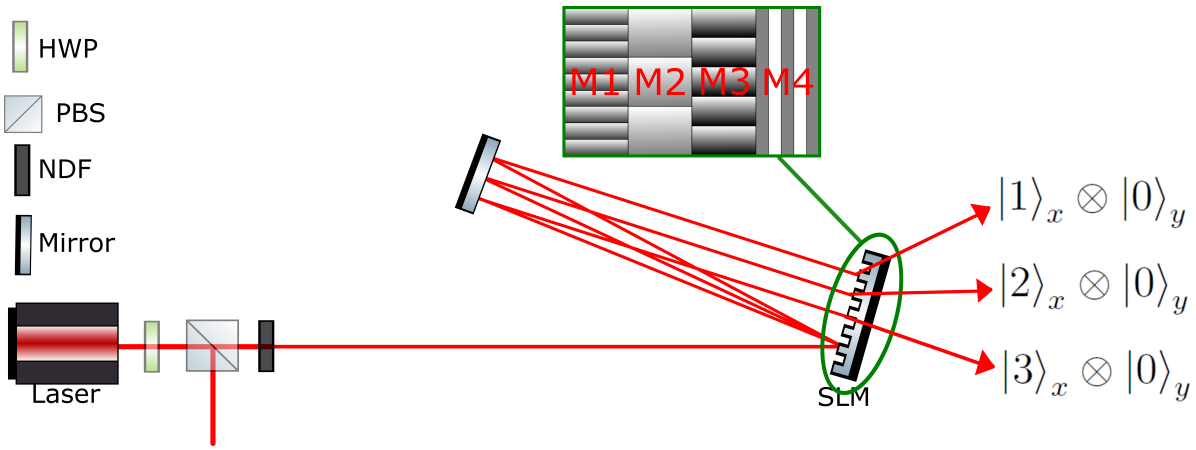

Figura 18 – Picture of three path modes generated at the first incidence at the spatial light modulator (SLM) in region M4, $|i\rangle_x \otimes |0\rangle_y$, being retro-reflected and striking a specified region Mi in the SLM ($i = 1, 2$ and 3).

the quantum jumps, we select only the first diffraction order[2] diffracted by LPG in the regions Mi ($i = 1, 2$ and 3). Our interferometer, Figure 15, has as input a three horizontal path modes and as output three vertical ones. The type of operation implemented by the SLM relies on two features of the LPG: periodicity and maximum phase.

5.1.2.1 Periodicity of the linear phase grating

The period of a PPG rules the separation between the diffracted orders (see Figure 19).

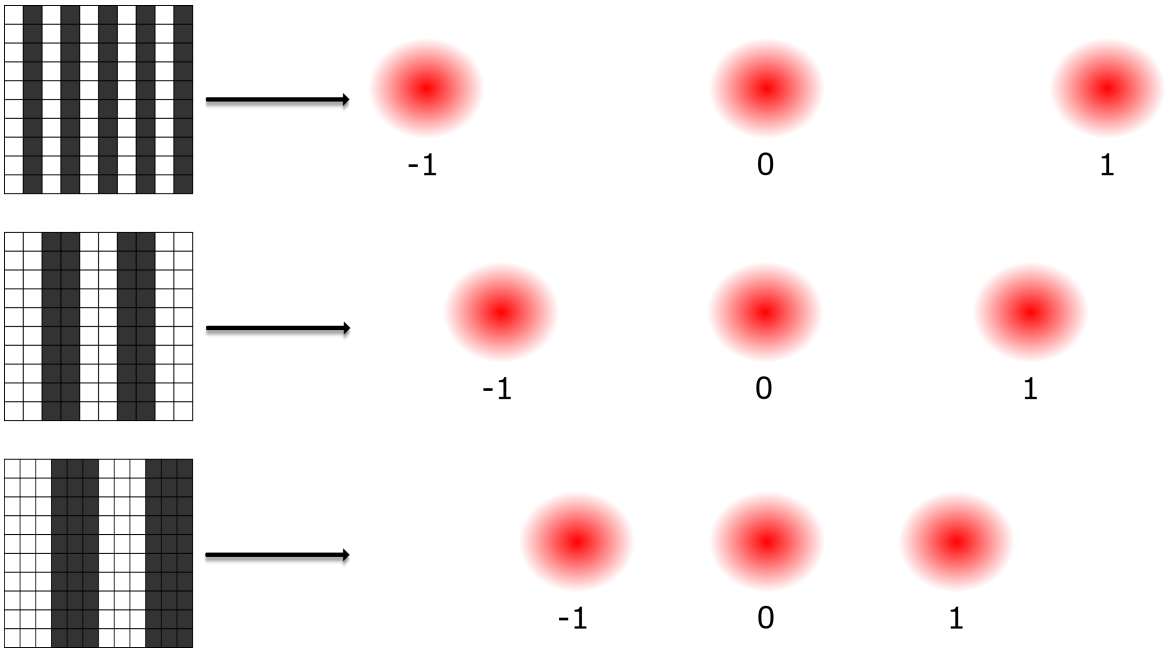

Figura 19 – Representation of the distance between diffracted orders (-1, 0 and 1) as function of the period of the periodical phase diffraction grating in the spatial light modulator.

[2] Order 1, see Figure 4

As higher the periodicity, the smaller the distance between the diffracted orders. So, the period of the LPGs will provide the type of transition between the path states that represents the energy levels. For instance, if we want to simulate a transition $|1\rangle_x \otimes |0\rangle_y \rightarrow |1\rangle_x \otimes |1\rangle_y$, will use a LPG of large period in the y-direction in the region M1. If the desired transition is $|1\rangle_x \otimes |0\rangle_y \rightarrow |1\rangle_x \otimes |2\rangle_y$ we will make use of a medium period LPG, for $|1\rangle_x \otimes |0\rangle_y \rightarrow |1\rangle_x \otimes |3\rangle_y$ we program the SLM with a small period one. The periods of the LPGs that were used in the simulation are 10 (small), 12 (medium) and 14 (large) in SLM pixel units (20μm x 20μm for each pixel).

5.1.2.2 Maximum phase of the linear phase grating

The intensity of light diffracted to the first diffraction order depends on the maximum phase of the LPG (see Figure 4). In the simulation of the decay dynamics, we make an analogy of the intensity in each vertical output path (Figure 15) and the population of each atomic state (Figure12). So, as higher the probability of decay (p_{ij}), the more light should be diffracted to the order $n = 1$, representing the transition $|i\rangle_x \otimes |0\rangle_y \rightarrow |i\rangle_x \otimes |j\rangle_y$. The probabilities $p_{ij} = 1 - e^{-\gamma_{ij}t}$ are function of the decay rates and time. Since the decay rates are fixed, the whole time evolution of the system is mapped on the probability of decay, $p_{ij}(t = 0) = 0$ to $p_{ij}(t \rightarrow \infty) = 1$. In this way, each operation performed by the LPG in the region Mv ($v = 1$, 2 and 3) is given by:

$$O_{M_v} |v\rangle_x \otimes |0\rangle_y = |v\rangle_x \otimes \left(\alpha_v |\ell\rangle_y + \beta_v |0\rangle_y\right), \tag{5.3}$$

where the mode $|v\rangle_x \otimes |l\rangle_y$ represents the spatial mode of the diffraction order $n = 1$ of the LPG in the region Mv, $|v\rangle_x \otimes |0\rangle_y$ represents the spatial mode of the diffraction order $n = 0$ of the LPG in the region Mv, ($v = 1$, 2 and 3). As mentioned previously, the vertical position of the order $n = 1$ of the diffracted Gaussian mode, $|l\rangle_y$, relies on the periodicity of the LPG while the coefficients α and β depends on its maximum phase. ϕ_v and θ_v are the phases acquired by the modes $|v\rangle_x \otimes |l\rangle_y$ and $|v\rangle_x \otimes |0\rangle_y$ after the diffraction, respectively. We would like to mention that we can program different LPGs[3] in each region Mv of the SLM, see Figure 18. In this way, we are able to implement different quantum operations on each horizontal path reaching the SLM, $|v\rangle_x \otimes |0\rangle_y$.

5.1.2.3 Pixelation effects on programming linear phase grating in the spatial light modulator

An interesting but complicating aspect of programming LPGs on the SLM is that we are not able to realize an ideal LPG, like the one depicted in Figure 3, on the SLM. This fact occurs because the SLM is constituted by an array of discrete pixels. In this context, we program the SLM with a sequence of step functions[4], as shown in Figure 20. This yields a loss of efficiency on the modulation, that is, it reduces the intensity of light diffracted to

[3] LPGs with different periodicity and maximum phase.
[4] Also known as Heaviside function.

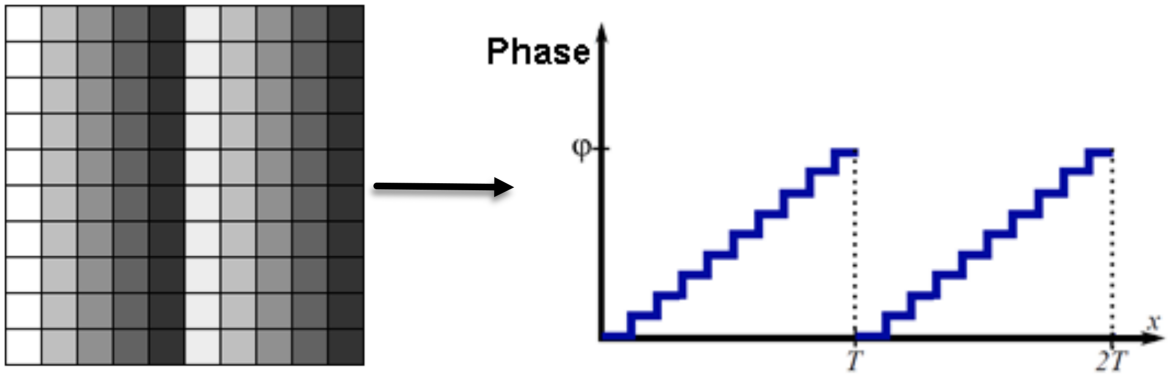

Figura 20 – Representation of the "linear"diffraction phase grating that can be programmed in the screen of a spatial light modulator.

the order $n = 1$. This effect was studied by Baldijão *et. al.* in [119, 122] and Borges *et. al.* in [18, 121], which they called as "pixelation effect". The loss of efficiency on the modulation relies on the periodicity of the LPG (number of pixels per period). Figure 21 shows the intensity of the first diffraction order of two LPGs with different periodicities. The LPG

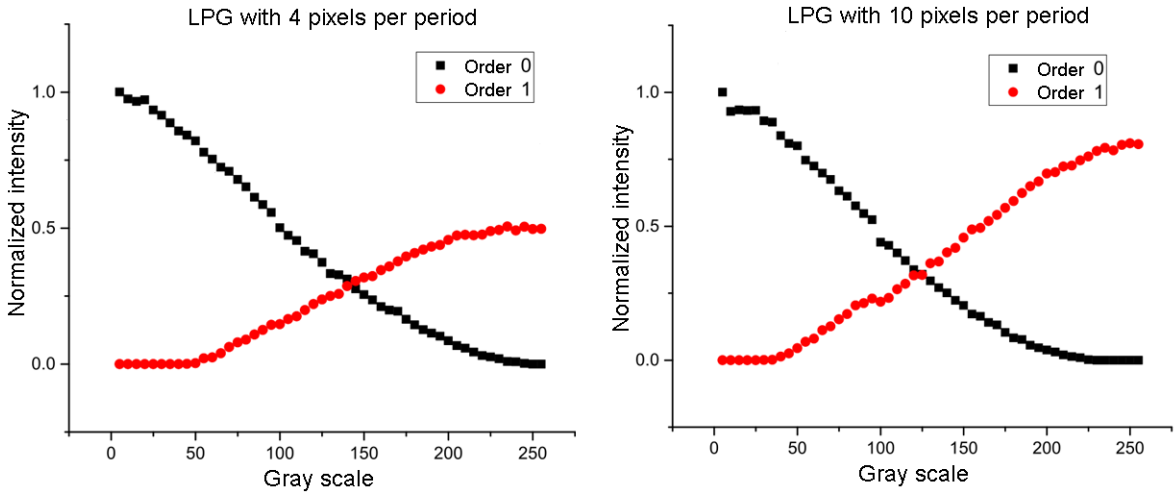

Figura 21 – Representation of the normalized intensities of the diffraction orders $n = 0$ and $n = 1$ for two "linear" phase gratings, as function of the grey scale in the spatial light modulator. One of them has 4 pixels per period and the other 10 pixels per period. The first one has approximately 50% of maximum efficiency while the second one has approximately 78% of maximum efficiency.

with 4 pixels per period has approximately 50% of maximum efficiency, *i. e.*, it transfers about 50% of the intensity of the incoming light to the $n = 1$ diffraction order. On the other hand, the LPG with 10 pixels per period has approximately the maximum efficiency of 78%. Therefore, the pixelation effect must be taken into account when simulating the decay dynamics.

5.2 Simulation of the decay dynamics

5.2.1 Implementation of the Kraus operators

We can implement a quantum operation, like the one described by Eq.5.3, in each individual path mode. So, that after the SLM, we have a quantum state represented by:

$$\begin{aligned} |\psi\rangle \;=\; & A_1 |1\rangle_x \otimes \left(\alpha_1 e^{i\phi_1} |\ell_1\rangle_y + \beta_1 e^{i\theta_v} |0\rangle_y\right) + A_2 |2\rangle_x \otimes \left(\alpha_2 e^{i\phi_2} |\ell_2\rangle_y + \beta_2 e^{i\theta_2} |0\rangle_y\right) \\ & + A_3 |3\rangle_x \otimes \left(\alpha_3 e^{i\phi_3} |\ell_3\rangle_y + \beta_3 e^{i\theta_3} |0\rangle_y\right), \end{aligned} \tag{5.4}$$

where A_i are parameters from the initial state; α_i, β_i, ϕ_i and θ_i depend on the maximum phase of the LPG in region Mi ($i = 1$, 2 and 3), while the vertical mode $|l_1\rangle$ ($l_i = 1$, 2 and 3) relies on the periodicity of the LPG in region Mi. As it is shown in Figure 15, we use a cylindrical lens to merge all the the horizontal paths in a single one on its focus, $|i\rangle_x \rightarrow |2\rangle_x$. By selecting only the $|1\rangle_y$, $|2\rangle_y$ and $|3\rangle_y$ modes, the intensified charged couple device camera (ICCD), which is in the focal plane of the cylindrical lens, will detect the following state:

$$|\psi\rangle = |2\rangle_x \otimes \left(A_1\alpha_1 e^{i\phi_1} |\ell_1\rangle_y + A_2\alpha_2 e^{i\phi_2} |\ell_2\rangle_y + A_3\alpha_3 e^{i\phi_3} |\ell_3\rangle_y\right). \tag{5.5}$$

Figure 22 shows a picture of the ICCD camera used to perform the measurements

Figura 22 – Image of the intensified charged-coupled device (ICCD) camera used to perform the measurements at the experimental setup, Figure 15.

The three decay dynamics in three-level systems: cascade, Λ and V were implemented in terms of their Kraus decomposition (Table 1). In this section, we will clarify how each Kraus operator were simulated by the diffraction grating in the SLM. First, let's consider the identity operation. As our experimental setup has a three-path horizontal modes as input state and a three-path vertical modes as output state, the identity is performed by inserting LPGs in the regions M1, M2 and M3 on the SLM. Figure 23 represents the

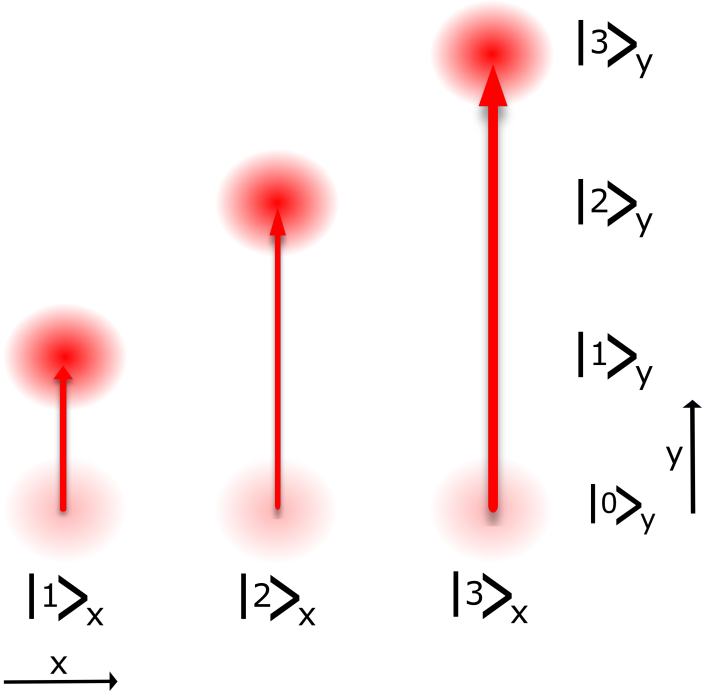

Figura 23 – Representation of the implementation of the identity operation in the experimental setup (Figure 15).

implementation of the identity operation on the SLM. By using a LPG of high period in region M1, we get the transition $|1\rangle_x \rightarrow |1\rangle_y$, with a medium period one in region M2, we have $|2\rangle_x \rightarrow |2\rangle_y$, while a small period in region M3, we reach $|3\rangle_x \rightarrow |3\rangle_y$. In this way, we can diffract the light as shown in Figure 23. In summary, the regions illuminated of the SLM where we insert the LPGs correspond to to the atomic eigenstates (photon path states) in which the atom (light beam) was before the atomic decay (diffraction). The periodicity of the LPGs rules the atomic eigenstate (photon path state) for which the atom (light beam) is decaying (diffracting). In the focal plane of the the cylindrical lens, the ICCD will record the three beams in the vertical direction with relative phases and intensities that correspond to the initial photon path state in the horizontal direction, in this way, the identity operation is implemented. To keep the ratio among the coefficients of the initial state A_i, Eq.5.1, we need to choose the maximum phase of the LPGs such that they have the same α_i coefficients.

The identity operation is present in the three decay dynamics: cascade, Λ and V. It is the K0 operator for $p_{ij} = 0$, *i. e.*, for $t = 0$ (see Table 1). For example, if we want to implement the K0 operator for the cascade dynamics for $p_{ij} \neq 0$, we just need to change the maximum phases of the LPGs in regions M2 and M3. The maximum phases of the LPGs are chosen based on calibrations of the intensity of the diffracted light to the $n = 1$ order, analogous to the ones performed in Figure 21. In this way, we diffract the amount of light corresponding to the level population at some fixed time.

In a similar way to the K0 operator, we can implement the K1 for the cascade

dynamics, as shown in Figure 24. In this implementation, we inserted a LPG of high

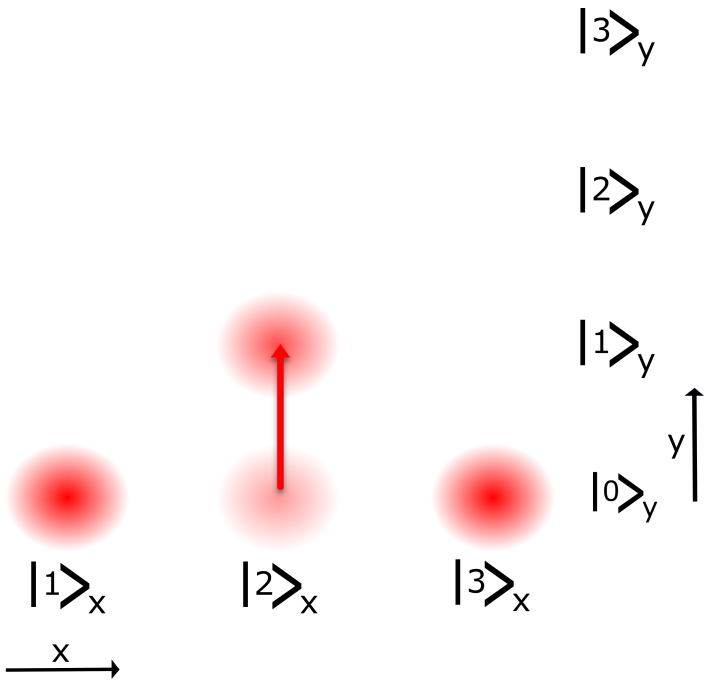

Figura 24 – Representation of the implementation K1 operator for the cascade dynamics.

periodicity in region M2 to diffract light from $|2\rangle_x \rightarrow |1\rangle_y$. The regions M1 and M3 were programmed to have no PPG. As for K0, if we want to simulate the K1 operator with a different probability of decay, we just need to change the maximum phase of the LPG in region M2. In an analogous manner, we can also implement the K2 (Figure 25) and K3 (Figure 26) operators for the cascade dynamics. For K2, we programmed a LPG of medium periodicity in region M3 to diffract light from $|3\rangle_x \rightarrow |2\rangle_y$, while the regions M1 and M2 were programmed to have no PPG. In the K3 implementation, we insert a LPG of high periodicity in region M3 to diffract light from $|3\rangle_x \rightarrow |1\rangle_y$, while the regions M1 and M2 were programmed to have no PPG. As for the other operations, if we want to simulate different probabilities of decay, we just need to change the maximum phase of the LPG.

All the Kraus operators were implemented by programming a frame sequence of different LPGs at the SLM, like a film (see Figure 15). Each frame contains PPG or constant phases in the tree M_i ($i = 1$, 2 and 3), as explained in the lasts paragraphs, such that a specific Kraus operator is implemented. Its time duration was set in 100 ms in the SLM screen. So, a complete SLM frame sequence lasts 300 ms for the Λ and V decay dynamics and 400 ms for the cascade decay. Single photon counts that allow us to characterize the output state were recorded by the ICCD. The camera exposure time was set to be equal to the SLM frame sequence duration in each measurement. Figure 27 illustrates the implementation of a sequence of all Kraus operators before the cylindrical lens for the cascade dynamics. Each one of the Kraus operators are detected in a different time at the ICCD. Between 0 and 100 ms it detects K0, between 100 and 200 ms it detects

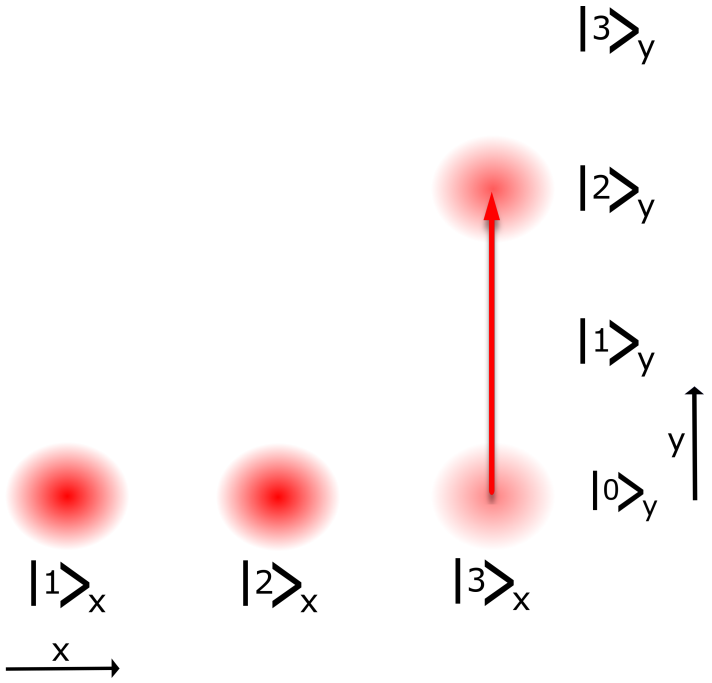

Figura 25 – Representation of the implementation K2 operator for the cascade dynamics.

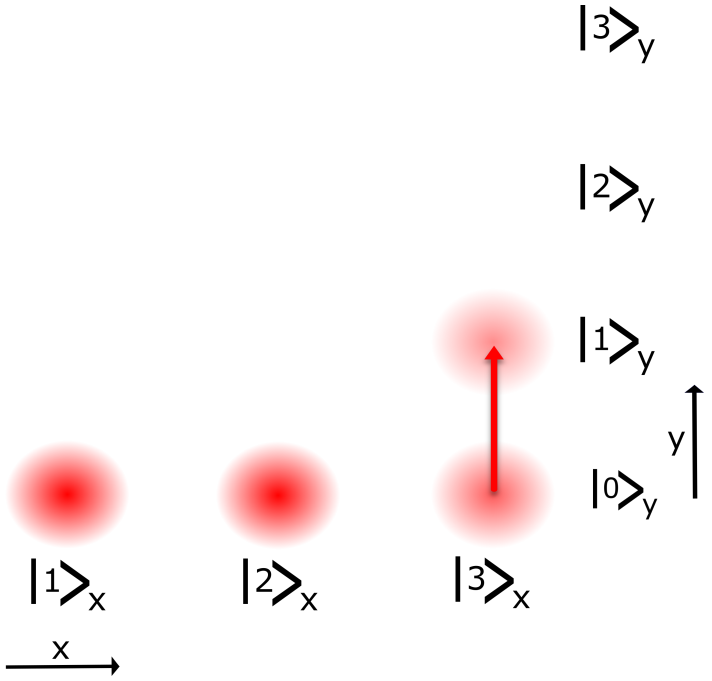

Figura 26 – Representation of the implementation K3 operator for the cascade dynamics.

K1, between 200 and 300 ms it detects K2 and between 300 and 400 ms it detects K3. So that, after a 400 ms measurement it provide us a sum of all images superposed.

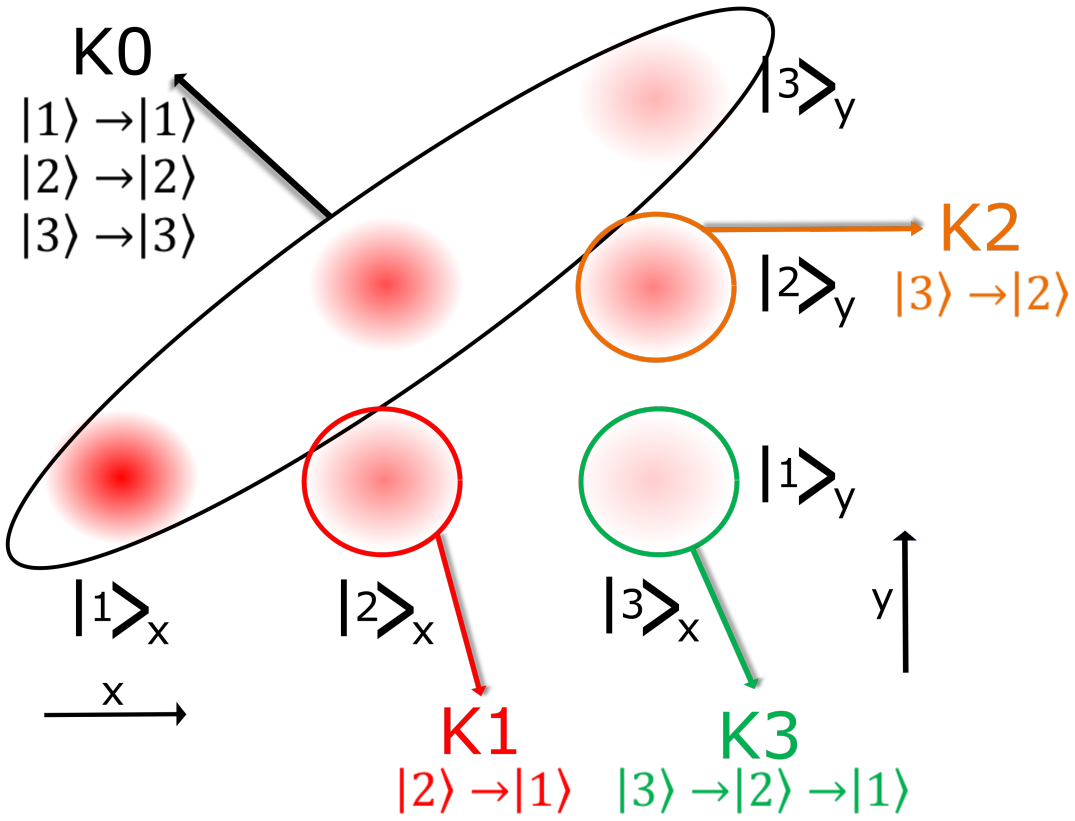

Figura 27 – Representation of the implementation of the sequence of all Kraus operators for the cascade dynamics. Each one of them are detected on a different time at the intensified charged couple device camera.

In all the Kraus operators sequence, the BPG that generates the initial photon path states in horizontal direction, in region M4 of the SLM was kept the same.

A clear correspondence between the parameters of the simulated atomic system and experimental optical interferometer, is shown in Table 2. The functions on the right column of Table 2 are the normalized intensities of the BPG orders $-1, 0, 1$ in the first, second and third lines, respectively. The function in the fourth line gives the normalized intensity of the first order of ideal LPG (for the pixelation effects in the modulation of LPGs, see [119, 122]).

An average of 64 measurements was taken for a $\{p_{32}, p_{31}, p_{21}\}$ set for characterizing the decay dynamics. By varying the p_{ij}-set we are able to simulate the time evolution for the dynamics of the three-level system decay, since the p_{ij} was parameterized by the evolution time t, as previously mentioned. Measurements at the image plane allow us to obtain the diagonal terms of the three-level density matrix, p_{ii}, which describes the relative population of level $|i\rangle$. For the complete decay dynamics characterization, we also

Atomic system	Optical system
I_1	$\frac{4}{\pi^2} sin^2\left(\frac{\phi_B}{2}\right)$
I_2	$cos^2\left(\frac{\phi_B}{2}\right)$
I_3	$\frac{4}{\pi^2} sin^2\left(\frac{\phi_B}{2}\right)$
p_{ij}	$sinc^2\left(\frac{\phi_j}{2} - \pi\right)$
Energy level $\|j\rangle$	Period $8 + 2j$ (pixel units) of the LPG

Tabela 2 – Correspondence between the experimental optical parameters and the atomic variables, where: ϕ_B is the maximum phase of the BPG in the region $M4$, ϕ_j is the maximum phase of the LPG in the region Mi with $i, j = 1, 2$ or 3 and $0 < \phi_j < \pi$. The functions on the right column are the non-normalized intensities of the BPG orders $-1, 0, 1$ in the first, second and third lines, respectively, and the intensity of the first order of the ideal LPG in the fourth line (for the pixelation effects in the modulation of LPGs, see [119, 122]).

have to measure the off-diagonal density matrix elements p_{ij} which give information about the state coherence.

5.2.2 Image measurements

5.2.2.1 The probability of detection

The probability of photon detection at the detection plane z is $P(\mathbf{r}, t) = \mathrm{Tr}(\Gamma\rho)$ [117], where ρ is the density matrix of the photonic qutrit and $\Gamma = \mathbb{E}^{(-)}(\mathbf{r}, t)\mathbb{E}^{(+)}(\mathbf{r}, t)$, with:

$$\mathbb{E}^{(-)}(\mathbf{r}, t) \propto \frac{1}{\sqrt{V}} \sum_{\mathbf{k}} \hat{a}^{\dagger}_{\mathbf{k}} e^{-i(\mathbf{k}.\mathbf{r}-\omega t)} \text{ and} \tag{5.6}$$

$$\mathbb{E}^{(+)}(\mathbf{r}, t) \propto \frac{1}{\sqrt{V}} \sum_{\mathbf{k}} \hat{a}_{\mathbf{k}} e^{i(\mathbf{k}.\mathbf{r}-\omega t)}, \tag{5.7}$$

where $\mathbb{E}^{(-)}(\mathbf{r}, t)$ and $\mathbb{E}^{(+)}(\mathbf{r}, t)$ are the negative-frequency and positive-frequency parts of the electric field operator at $\mathbf{r}$ and time t, $\mathbf{k}$ is the wave-vector of the filed, $\hat{a}_{\mathbf{k}}$ is the annihilation operator and $\hat{a}^{\dagger}_{\mathbf{k}}$ is the creation operator. Γ is the intensity operator, which propagates the electromagnetic field from the SLM to the image plane. For the image plane measurements, the probability of photon detection in a transverse position y is

$$P(y) = \sum_{j=1}^{3} \rho_{jj} e^{-\frac{(y-jd)}{\sigma^2}}, \tag{5.8}$$

where: d is the distance between the paths and σ is the width of the Gaussian modes. We used Eq.5.2 and ρ_{jj} are the diagonal terms of three-level system density operator. The diagonal terms are the relative populations in each energy eigenstate and in the optical

simulation $\rho_{jj} = \frac{I_j}{I_T}$, with I_j being the transverse profile of the j beam ($j = 1$, 2 and 3) detected at the image plane by the ICCD and $I_T = I_1 + I_2 + I_3$.

5.2.2.2 Cascade dynamics

In the cascade dynamics we have the initial state generated by the binary diffraction grating in the x-direction, shown in the Fig. 28 (a). With a MATLAB program we make a sum over the intensity in the columns and obtained a normalized integrated transverse optical profile (ITOP), plotted in Fig. 28 (b). With an image characterization of our

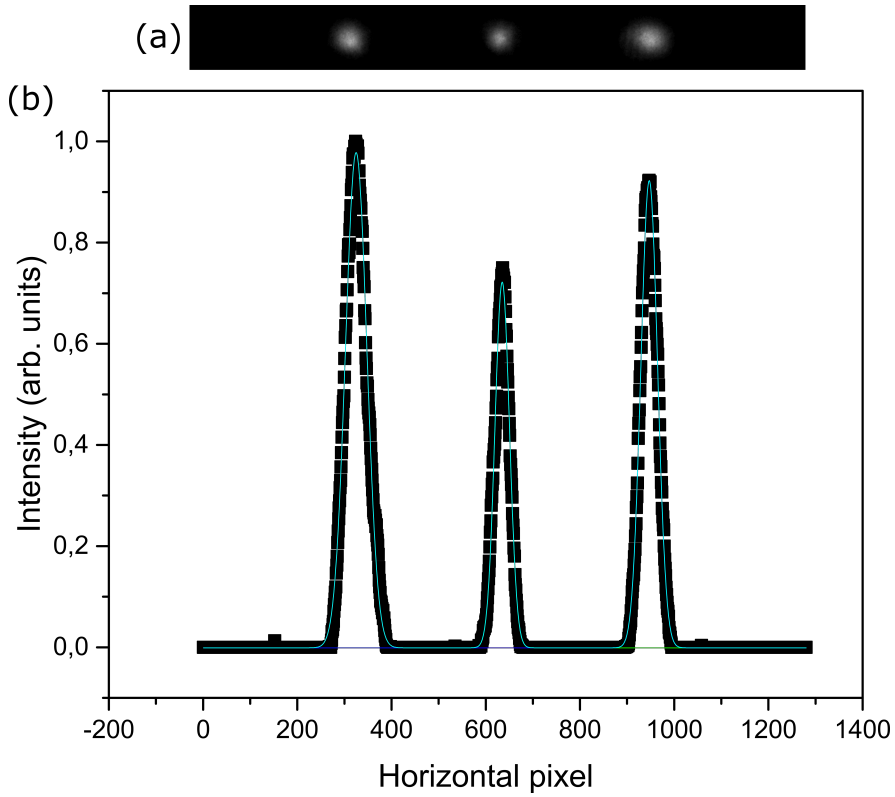

Figura 28 – (a) Image measurement of the initial state for the cascade dynamics. (b) Normalized integrated transversal optical profile (ITOP) of the initial state for the cascade dynamics fitted by a multi-peak Gaussian function.

initial state we may proceed to the implementation of the dynamics. By inserting all the diffraction gratings that simulate the Kraus operators in a film at the SLM, we measure the image of the three vertical path Gaussian states. Fig. 29 illustrates the image obtained by the implementation of the operator for some values of $p_{32} = p_{21} = p$, while its normalized integrated transversal optical profile (ITOPs) are shown in Fig. 30. We proceed with the image measurements for several values of p, from $p = 0$ to $p = 1$ with steps of 0.125. The theoretical prediction for the density matrix is obtained from Eq.3.49, with the Kraus operator from Table1. So, for the cascade dynamics, the density matrix that represents

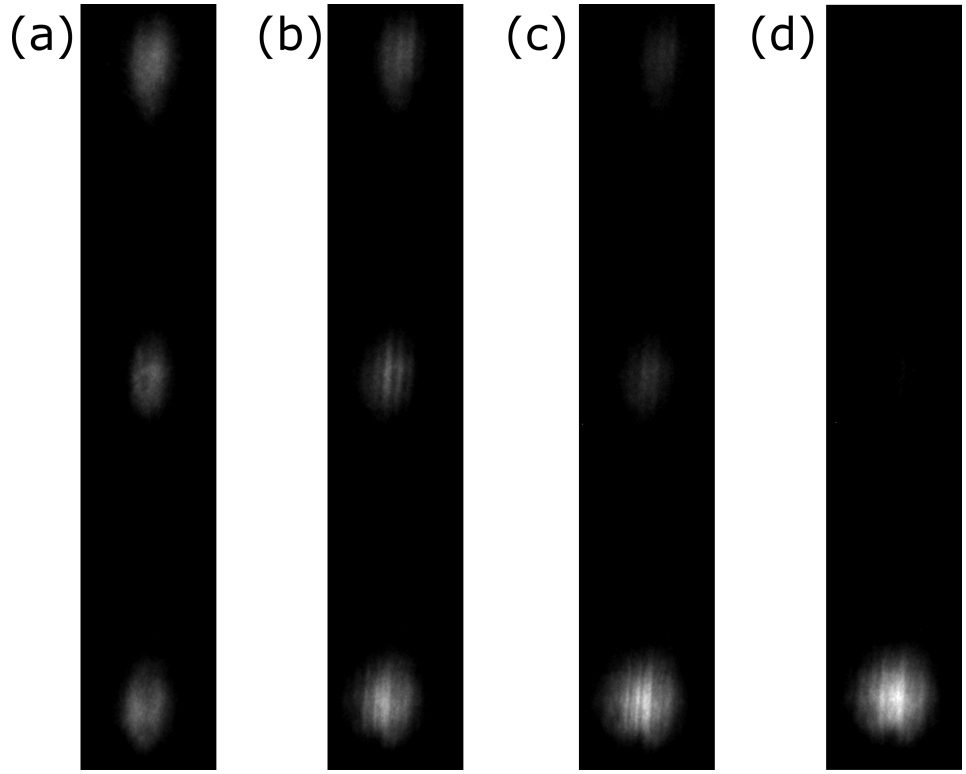

Figura 29 – Image measurements of the implementation of the cascade dynamics for different probabilities of decay ($p = 1 - e^{-\gamma t}$): (a) p=0, (b) p=0.5, (c) p=0.75 and (d) p=1.

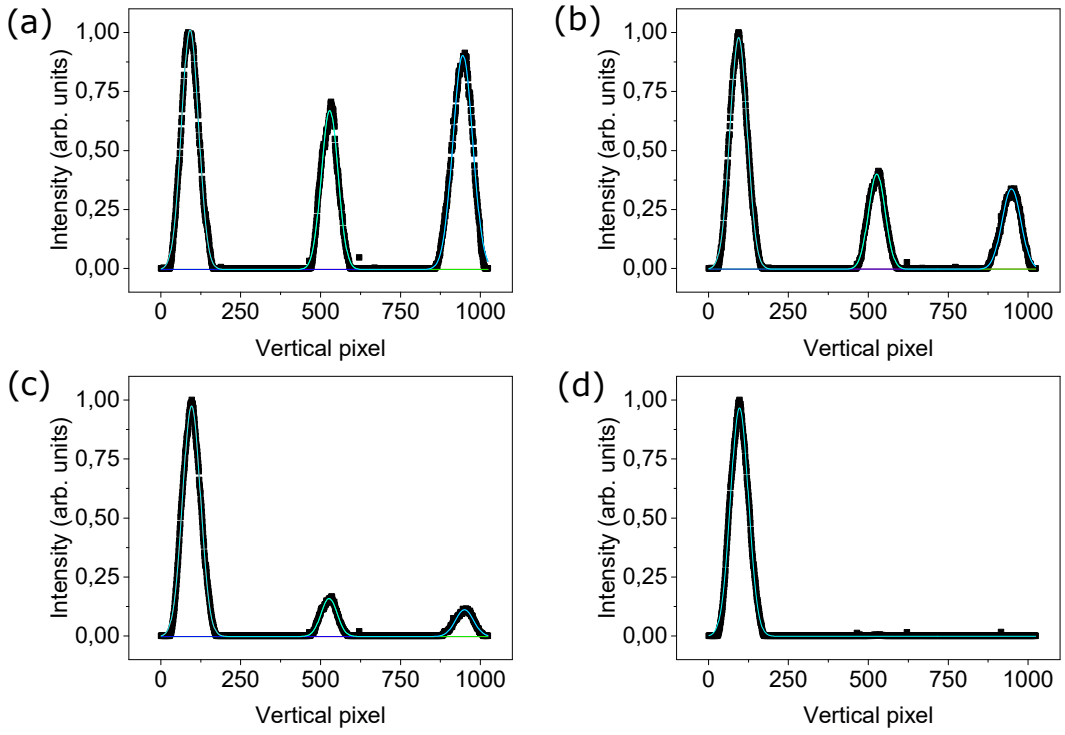

Figura 30 – Normalized integrated transverse optical profile of the image measurements of the implementation of the cascade dynamics for different probabilities of decay $p = 1 - e^{-\gamma t}$, where $\gamma_{32} = \gamma_{21} = \gamma$ for: (a) p=0, (b) p=0.5, (c) p=0.75 and (d) p=1, fitted by a multi-peak Gaussian.

the state evolved in time is:

$$\rho_C = \frac{1}{I_T}\begin{pmatrix} I_1 + I_2 p_{21} + I_3 p_{32} p_{21} & \sqrt{I_1 I_2}\sqrt{1-p_{21}} & \sqrt{I_1 I_3}\sqrt{1-p_{32}} \\ \sqrt{I_1 I_2}\sqrt{1-p_{21}} & I_2(1-p_{21}) + I_3 p_{32}(1-p_{21}) & \sqrt{I_2 I_3}\sqrt{1-p_{21}}\sqrt{1-p_{32}} \\ \sqrt{I_1 I_3}\sqrt{1-p_{32}} & \sqrt{I_2 I_3}\sqrt{1-p_{21}}\sqrt{1-p_{32}} & I_3(1-p_{32}) \end{pmatrix}. \tag{5.9}$$

As the initial state was generated by a laser beam, we assumed to be a pure state and equal to $|\psi_0\rangle = \frac{1}{I_T}\left(\sqrt{I_1}\,|1\rangle + \sqrt{I_2}\,|2\rangle + \sqrt{I_3}\,|3\rangle\right)$. With all the image measurements provided by the detections we get to reconstruct the time evolution of the diagonal elements of the density matrix. Figure 31 shows the time evolution of the diagonal elements for the cascade dynamics.

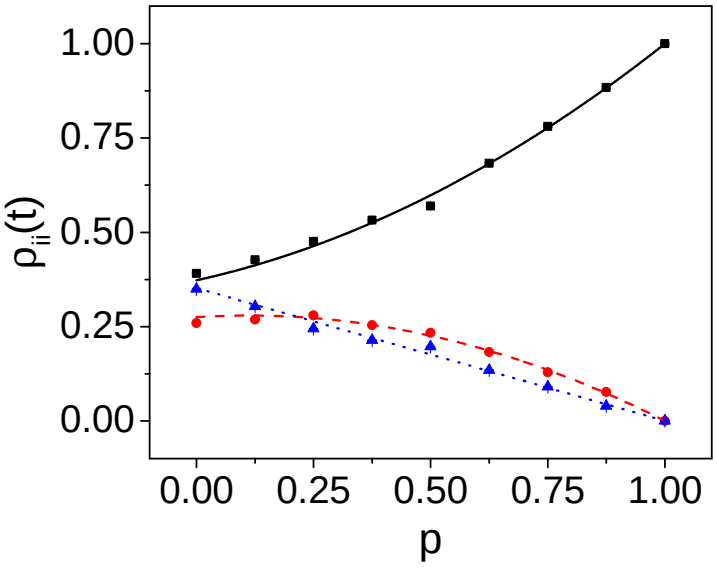

Figura 31 – Measured values (symbols) and theoretical prediction (lines) of the time evolution of the diagonal elements for the cascade dynamics, as function of the probability of decay $p = 1 - e^{-\gamma t}$. The black points and the black curve are the experimental and theoretical $\rho_{11}(t)$, the red points and the red curve are the experimental and theoretical $\rho_{22}(t)$ and the blue points and the blue curve are the experimental and theoretical $\rho_{33}(t)$.

5.2.2.3 Λ dynamics

For the Λ dynamics we proceeded in an analogous way to simulate the dynamics. After an image characterization of the three horizontal path initial pure state, we obtained the images of the three vertical output photon paths in Gaussian modes and the interference patterns between then, two by two. For this dynamics we made $\gamma_{31} = 2\gamma_{32}$, so that we have different values of p_{31} and p_{32} for $t \neq 0$. The theoretical prediction for the density

matrix is obtained from Eq.3.49, with the Kraus operator from Table 1, which yields:

$$\rho_{\Lambda}(t) = \frac{1}{I_T}\begin{pmatrix} I_1 + I_3 p_{31} & \sqrt{I_1 I_2} & \sqrt{I_1 I_3}\sqrt{1-p_{31}-p_{32}} \\ \sqrt{I_1 I_2} & I_1 + I_3 p_{32} & \sqrt{I_2 I_3}\sqrt{1-p_{31}-p_{32}} \\ \sqrt{I_1 I_3}\sqrt{1-p_{31}-p_{32}} & \sqrt{I_2 I_3}\sqrt{1-p_{31}-p_{32}} & I_3(1-p_{32}-p_{31}) \end{pmatrix}, \quad (5.10)$$

where we assumed the initial state to be pure and equal to $|\psi_0\rangle = \frac{1}{I_T}\left(\sqrt{I_1}\,|1\rangle + \sqrt{I_2}\,|2\rangle + \sqrt{I_3}\,|3\rangle\right)$. We characterized the state for $p_{31} = 0$ and $p_{32} = 0$ to the end of the dynamics, i. e., $p_{31} + p_{32} = 0$. The results for the time evolution of the diagonal terms for density state matrix for the Λ dynamics are depicted in Figure 32.

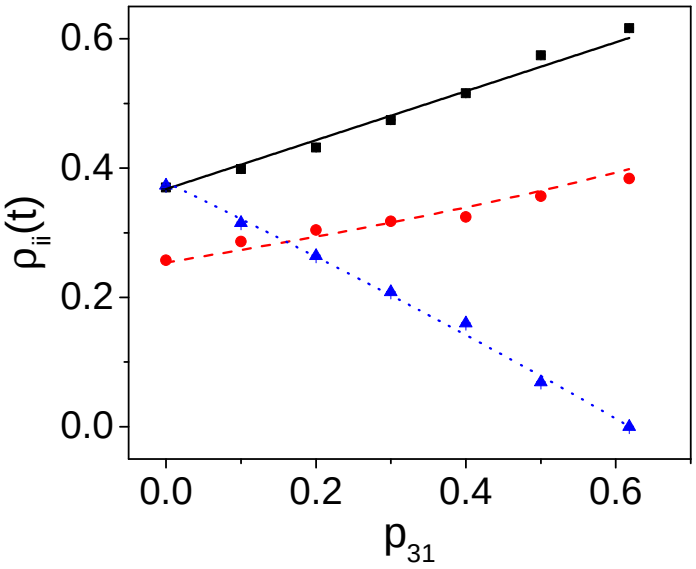

Figura 32 – Measured values (symbols) and theoretical prediction (lines) of the time evolution of the diagonal elements for the Λ dynamics as function of the probability if decay $p_{31} = 1 - e^{-\gamma_{31}t}$. The black points and the black curve are the experimental and theoretical $\rho_{11}(t)$, the red points and the red curve are the experimental and theoretical $\rho_{22}(t)$ and the blue points and the blue curve are the experimental and theoretical $\rho_{33}(t)$.

5.2.2.4 V dynamics

Finally for the V dynamics, we followed the same steps for the other two. We made an image characterization of the three horizontal path initial pure state, after we obtained the images of the three vertical output photon paths in Gaussian modes and the interference patterns between then, two by two. For this dynamics we made $\gamma_{21} = 2\gamma_{31}$, so that we also have different values of p_{21} and p_{31} for $t \neq 0$. We characterized the state from $t = 0$ to $t \to \infty$, with increments for p_{21} of 0.125. Like for the other dynamics, the theoretical prediction for density matrix that represents the time evolved state is calculated

from Eq.3.49, with the Kraus operator from Table 1, which provides:

$$\rho_V(t) = \frac{1}{I_T}\begin{pmatrix} I_1 + I_2 p_{21} + I_3 p_{31} & \sqrt{I_1 I_2}\sqrt{1-p_{21}} & \sqrt{I_1 I_3}\sqrt{1-p_{31}} \\ \sqrt{I_1 I_2}\sqrt{1-p_{21}} & I_2(1-p_{21}) & \sqrt{I_2 I_3}\sqrt{1-p_{21}}\sqrt{1-p_{31}} \\ \sqrt{I_1 I_3}\sqrt{1-p_{31}} & \sqrt{I_2 I_3}\sqrt{1-p_{21}}\sqrt{1-p_{31}} & I_3(1-p_{31}) \end{pmatrix}, \tag{5.11}$$

where we assumed the initial state to be pure and equal to $|\psi_0\rangle = \frac{1}{I_T}\left(\sqrt{I_1}\,|1\rangle + \sqrt{I_2}\,|2\rangle + \sqrt{I_3}\,|3\rangle\right)$. The results for the time evolution of the diagonal terms are shown in Figure 33

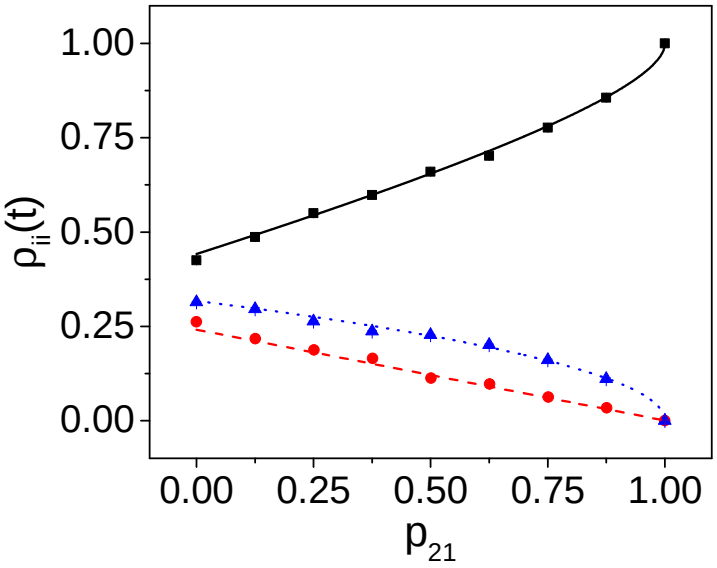

Figura 33 – Measured values (symbols) and theoretical prediction (lines) of the time evolution of the diagonal elements for the V dynamics as function of the probability of decay $p_{21} = 1 - e^{-\gamma_{21}t}$. The black points and the black curve are the experimental and theoretical $\rho_{11}(t)$, the red points and the red curve are the experimental and theoretical $\rho_{22}(t)$ and the blue points and the blue curve are the experimental and theoretical $\rho_{33}(t)$.

5.2.3 Interference measurements

5.2.3.1 The probability of detection

For a complete characterization of the state including the decoherence that occurs during the process of decay, we also measure the visibility of the interference patterns between the paths, two by two, for the same probabilities values. It was made by inserting another cylindrical lens that focus the beams in the vertical direction in the CCD plane (Figure 15). Blocking one of the three beams that represent the photon path qutrit state is equivalent to perform a projection on the unblocked path states. For instance, by blocking the $|3\rangle$ path from the cascade state of Eq.5.9, the resulting state will be the projection over $|1\rangle$ and $|2\rangle$, which will provide us the following renormalized density matrix that

represents the state:

$$\sigma(t) = \frac{1}{I_r}\begin{pmatrix} I_1 + I_2 p + I_3 p^2 & \sqrt{I_1 I_2}\sqrt{1-p} & 0 \\ \sqrt{I_1 I_2}\sqrt{1-p} & I_2(1-p) + I_3 p(1-p) & 0 \\ 0 & 0 & 0 \end{pmatrix}. \tag{5.12}$$

The probability of detection on the ICCD plane is $P(\mathbf{r}, t) = \mathrm{Tr}(\Gamma'\sigma(t))$, where Γ' is the Fourier transform of Γ operator and propagates the electromagnetic field from the SLM to the Fourier plane [15]. Thus, the interference patterns of the state 5.12 are:

$$Tr\left(\Gamma'_y \sigma\right) = e^{-\frac{-\sigma k^2 y^2}{f^2}}\left[1 + 2\left|\sigma_{ij}\right| cos\left(\frac{kyd}{f} + \phi_{ij}\right)\right], \tag{5.13}$$

where f is the focal length of the lens, k is the modulus of the wave vector and $\sigma_{ij} = |\sigma_{ij}|\, e^{i\phi_{ij}}$ is the off diagonal element ij of the density matrix shown in Eq.5.12. Thus the visibility of the interference pattern between the paths $|i\rangle$ and $|j\rangle$ becomes $\mathcal{V}_{ij} = 2\,|\sigma_{ij}(t)|$ [117,149,150].

5.2.3.2 Cascade dynamics

By performing all the interference pattern measurements for the same values of p that was performed the image measurements, we are able to obtain all the moduli of all the off-diagonal elements of the density matrix from the visibilities of the interference patterns. Some of the patterns measured are shown in Figure 34 and its ITOPs are in Figure 35

The theoretical predictions and the measured values of time evolution of the off-diagonal elements of the density matrix for the cascade dynamics are shown in Figure 36.

5.2.3.3 Λ dynamics

As shown for the cascade dynamics, we performed all the interference measurements for the same pair of values of p_{31} and p_{32} that were performed the image measurements. So, we obtained all the modulus of all the off-diagonal elements of the density matrix from the visibilities of the interference patterns. The theoretical predictions and the measured values of time evolution of the off-diagonal elements of the density matrix for the Λ dynamics are shown in Figure 37.

5.2.3.4 V dynamics

Finally, for the V dynamics, we performed all the interference measurements for the same pair of values of p_{31} and p_{21} that were performed the image measurements. So, we obtained all the modulus of all the off-diagonal elements of the density matrix from the visibilities of the interference patterns. The theoretical predictions and the measured values

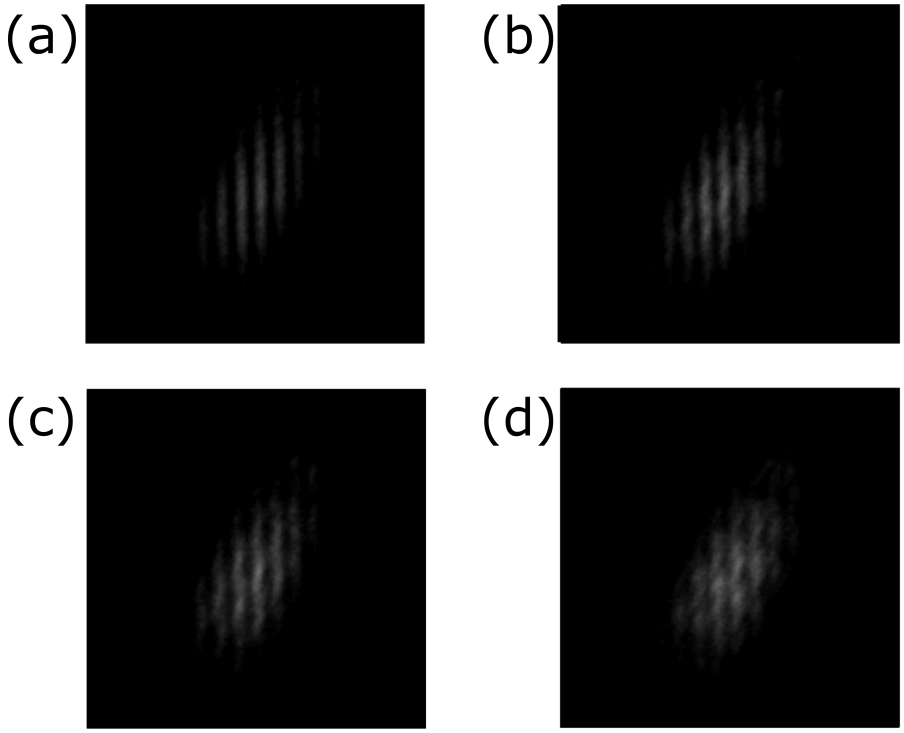

Figura 34 – Interference patterns between the path states $|1\rangle$ and $|2\rangle$, for the cascade dynamics for different probabilities of decay $p = 1 - e^{\gamma t}$. (a) $p = 0$, (b) $p = 0.25$, (c) $p = 0.5$ and (d) $p = 0,75$.

of time evolution of the off-diagonal elements of the density matrix for the V dynamics are shown Figure 38.

Although we have used an attenuated laser beam to the single photon regime, the same experimental results shown here can be obtained by using a high intensity light source given that all the operations used are based on linear optical interference. If the intense coherent light source replaces the single photon source, an CCD (Charge-Coupled Device) or CMOS (Complementary Metal Oxide Semiconductor) camera will substitute the single photon camera in the experiment we will obtain similar results. On the other hand, since we are simulating a three-level atomic system is convenient to use the quantum description.

In our simulation we are able to measure the time evolution of the diagonal and off-diagonal elements of the density matrix of a generic three-level system. We have the flexibility of changing the decay probabilities and then mimic different atomic systems with different decay dynamics (cascade, Λ and V). The procedure used to implement the simulations is general and it can be extended to multi-level systems with the number of levels higher than three. The only technical restrictions in our experimental setup, for this extension, are the sizes of the pixels arrays in the SLM and in the ICCD camera, which must fit all the Gaussian paths representing the higher dimension atomic system. For instance, we need to have a minimum number of periods of the PPGs inside the laser

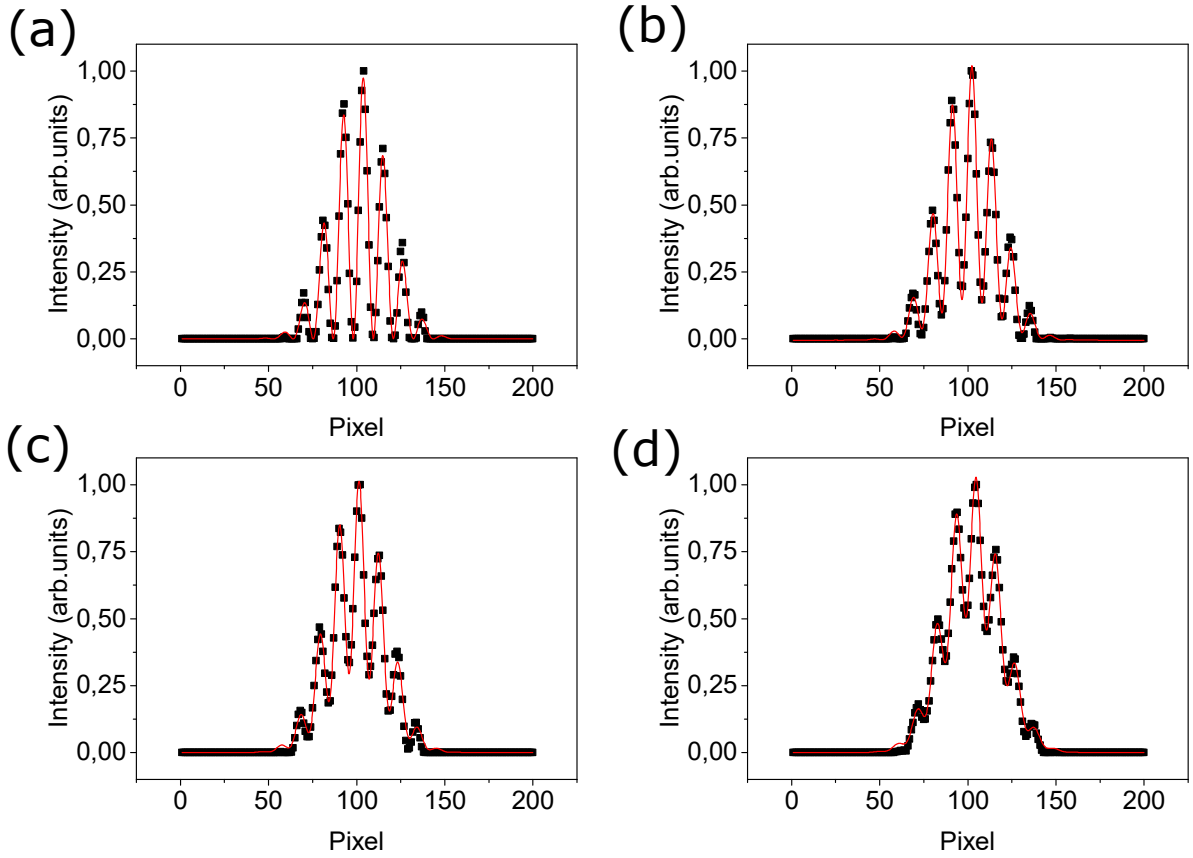

Figura 35 – ITOP of the interference pattern between the path states $|1\rangle$ and $|2\rangle$ for the cascade dynamics as function of the ICCD pixel for different probabilities of decay $p = 1-e^{-\gamma t}$. (a) $p = 0$, (b) $p = 0,25$, (c) $p = 0,5$ and (d) $p = 0,75$.

beam transverse profile so that it can be diffracted.

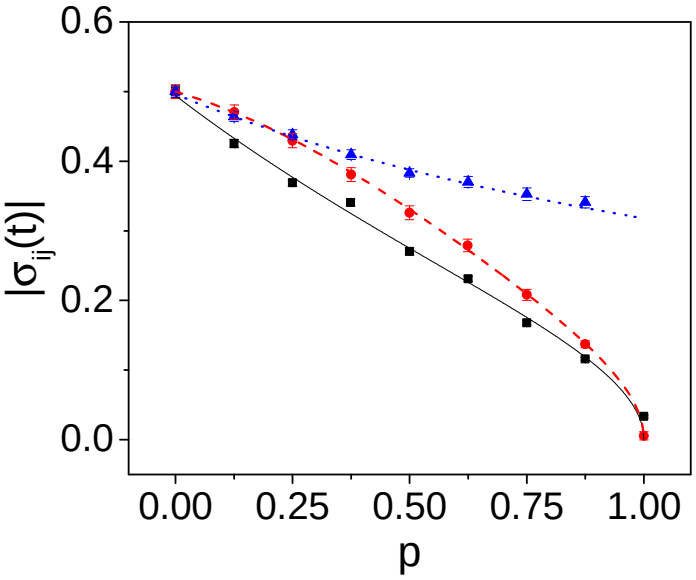

Figura 36 – Measured values (symbols) and theoretical prediction (lines) of the time evolution of the off-diagonal elements for the cascade dynamics as function of the probability of decay $p = 1 - e^{-\gamma t}$. The black points and the black curve are the experimental and theoretical $|\rho_{12}(t)|$, the red points and the red curve are the experimental and theoretical $|\rho_{13}(t)|$ and the blue points and the blue curve are the experimental and theoretical $|\rho_{23}(t)|$.

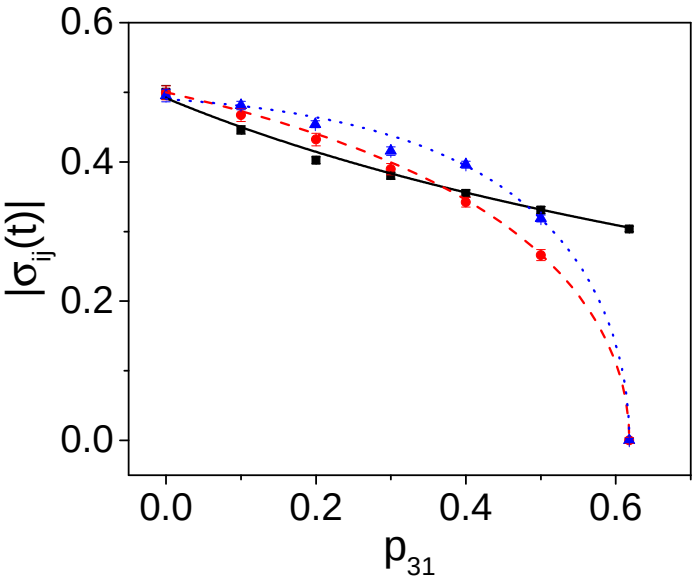

Figura 37 – Measured values (symbols) and theoretical prediction (lines) of the time evolution of the off-diagonal elements for the Λ dynamics as function of the probability of decay $p_{31} = 1 - e^{-\gamma_{31} t}$. The black points and the black curve are the experimental and theoretical $|\rho_{12}(t)|$, the red points and the red curve are the experimental and theoretical $|\rho_{13}(t)|$ and the blue points and the blue curve are the experimental and theoretical $|\rho_{23}(t)|$.

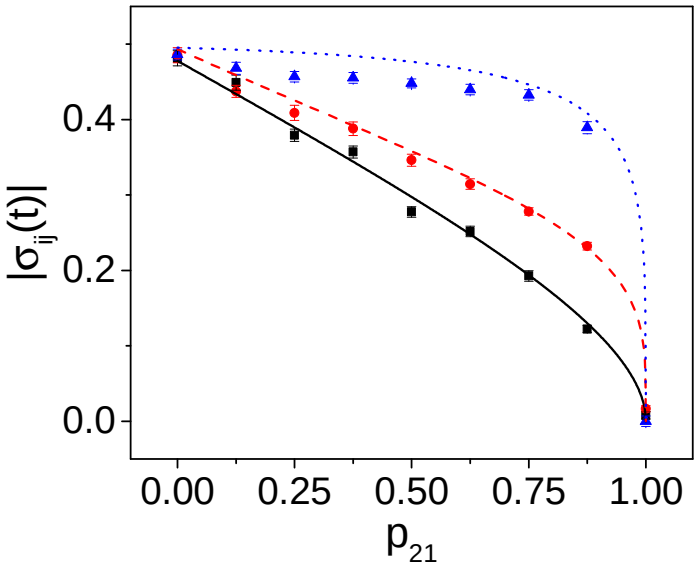

Figura 38 – Measured values (symbols) and theoretical prediction (lines) of the time evolution of the off-diagonal elements for the V dynamics as function of the probability of decay $p_{21} = 1 - e^{-\gamma_{21}t}$. The black points and the black curve are the experimental and theoretical $|\rho_{12}(t)|$, the red points and the red curve are the experimental and theoretical $|\rho_{13}(t)|$ and the blue points and the blue curve are the experimental and theoretical $|\rho_{23}(t)|$.

6 Proposal for implementation of quantum gates in photonic path system

6.1 Experimental setup, state preparation and operation

6.1.1 Experimental setup and state preparation

In this chapter, we propose the implementation of quantum gates (QG) and controlled quantum gates (CQG) in photonic path systems. As in the simulation of quantum jumps in three-level systems, Chapter 5, the methodology used for this proposal is inspired in the techniques used to perform general quantum operations on Gaussian paths systems proposed in [119, 122] and performed in [18, 121]. The state preparation and experimental setup are analogous to the simulation implementation, as shown in Figure 39. The initial state is prepared by diffraction of the laser beam in the BPG in region M4 is

$$|\psi_0\rangle = A_1 e^{i\phi_1} |1\rangle + A_2 e^{i\phi_2} |2\rangle + A_3 e^{i\phi_3} |3\rangle , \tag{6.1}$$

where A_i and ϕ_i are real numbers which relies on the maximum phase of the BPG in region M4, and $|i\rangle$ is the label of the path mode generated ($i = 1$, 2 and 3). The initial state was considered to be pure as it was produced by diffracting a laser beam. The three beams are reflected by a mirror back to the SLM 1. The SLM 1 screen is divided in four regions, each one with a periodical phase diffraction grating (LPG). The mode $|1\rangle$ reaches the region $M1$, $|2\rangle$ reaches region $M2$, $|3\rangle$ region $M3$, while region $M4$ was used to generate the three-path state, Eq.6.1.

6.1.2 Implementation of quantum operations

Each one of the beams that compose the three-path state is manipulated individually by programming a LPG on its region. By controlling the periodicities of the LPDG (see Figure 19), we can transfer light from a basis state to the other. For transitions to the nearest state, $|1\rangle \rightarrow |2\rangle$, $|2\rangle \rightarrow |1\rangle$, $|2\rangle \rightarrow |3\rangle$ and $|3\rangle \rightarrow |2\rangle$, we use a LPDG with high period. The diagram representing these transition are in Figure 40 and Figure 41. For the other transitions, $|1\rangle \rightarrow |3\rangle$ and $|3\rangle \rightarrow |1\rangle$ we will use a LPDG with low period. A depiction of these transition is in Figure 42. The maximum phase of the LPDGs are adjusted keep the relative intensities of the components of each state like the ones of the initial state, by taking into account the pixelation effect, approached in Section 5.1.2.3. Considering just the $n = 1$ diffraction order (Figure 4), all these permutation operations [18, 119, 121, 122] can be represented by:

$$O_{M_v} |v\rangle = \alpha_v |v\rangle + \alpha_\ell |\ell\rangle , \tag{6.2}$$

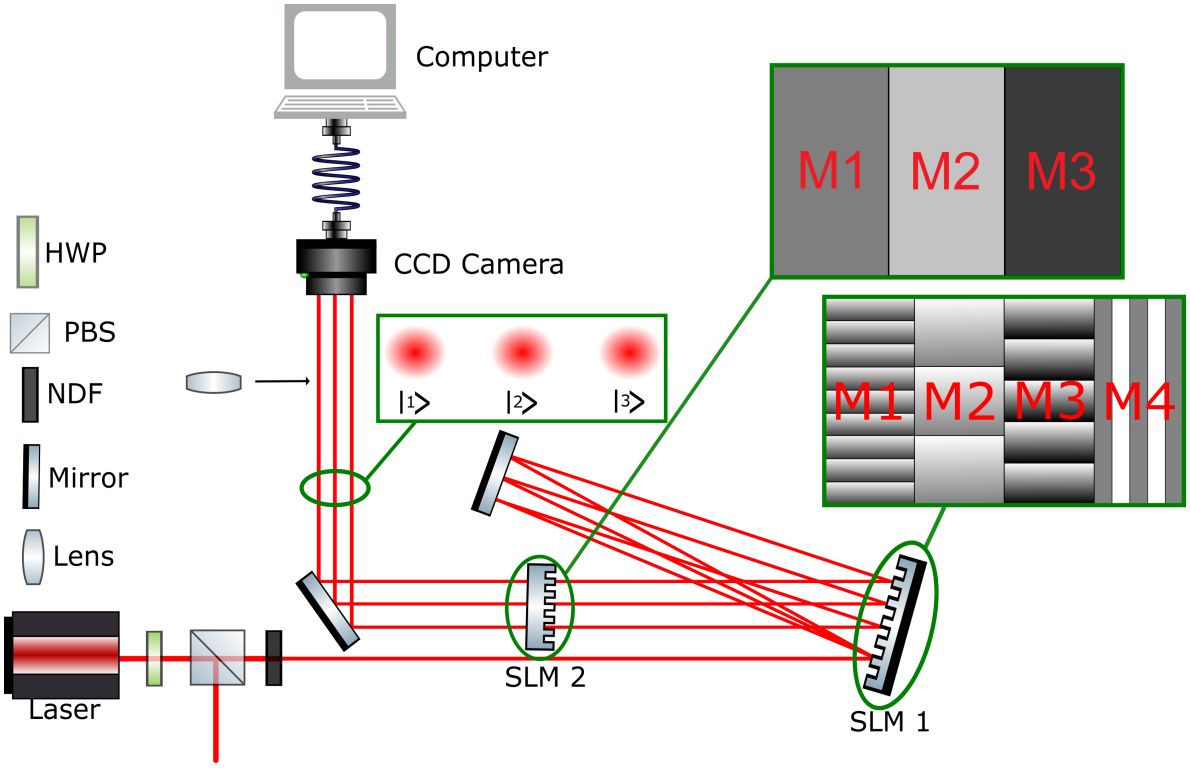

Figura 39 – Experimental setup used to prepare and to implement the operations on a qutrit parallel Gaussian beam state. A laser beam passes through a half wave-plate (HWP), a polarizer beam splitter (PBS) and a neutral density filter (NDF). This is necessary for filtering the polarization state and to attenuate it to the single photon regime. The laser beam reaches a SLM which the screen is divided in four regions, each one with a periodical phase diffraction grating. The attenuated laser beam is initially diffracted by a periodical binary phase grating in the region M4 in three horizontal paths (x-direction). A state superposition of Gaussian modes paths, $|1\rangle$, $|2\rangle$ and $|3\rangle$, is considered to be our initial state. Each of the modes is reflected back in three different regions on the SLM: M1, M2 and M3. In the second incidence the beams may be diffracted by linear phase gratings in SLM 1, which the first diffraction order propagates in the horizontal direction, depending on the phase grating periodicity. The SLM 2 is a transmission spatial light modulator which can insert a relative phase to each one of the paths $|1\rangle$, $|2\rangle$ and $|3\rangle$, that reach the regions M1, M2 and M3, respectively. An intensified charged-coupled device (ICCD) camera records the photon counts in each position.

where α_v and α_ℓ depends on the maximum phase of the LPG, and $|\ell\rangle$ is ruled by the periodicity of the LPG, with (v,$\ell = 1$, 2 and 3).

6.2 Proposal for implementation of quantum gates

6.2.1 Implementation of single qutrit quantum gates

The single qutrit QG will be implemented by exploring the permutation quantum operation approached in Section 6.1.2. With the experimental setup proposed for this purpose, Figure 39, we are able to implement all the qutrit QG discussed in Section 4.2.1.

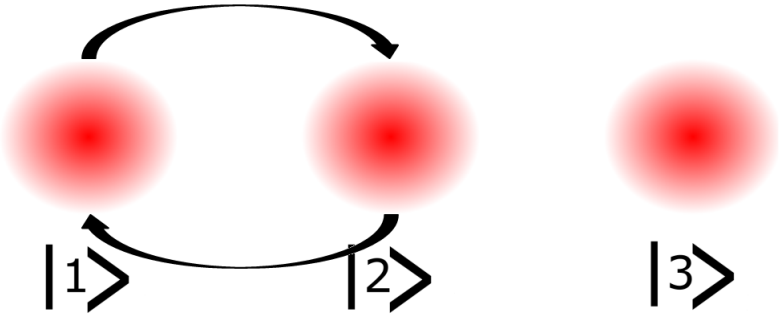

Figura 40 – Representation of transitions between the modes $|1\rangle$ and $|2\rangle$. To transfer light from $|1\rangle \rightarrow |2\rangle$, we program the region M1 of the SLM 1 with a LPG with phase increasing in the $+x$-direction and high periodicity. If we want transfer light from $|2\rangle \rightarrow |1\rangle$, we program the region M2 of the SLM 1 with a LPG with phase increasing in the $-x$-direction and high periodicity.

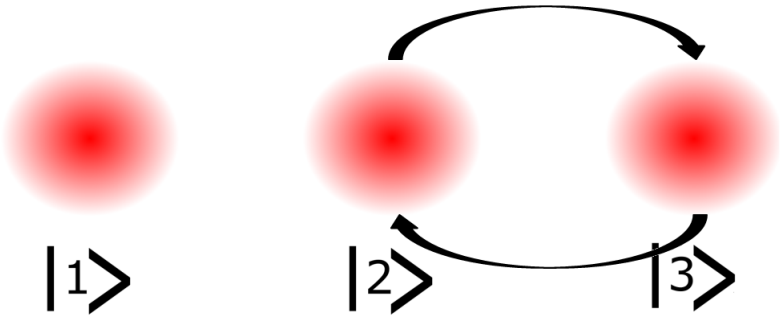

Figura 41 – Representation of transitions between the modes $|2\rangle$ and $|3\rangle$. To transfer light from $|2\rangle \rightarrow |3\rangle$, we program the region M2 of the SLM 1 with a LPG with phase increasing in the $+x$-direction and high periodicity. If we want transfer light from $|3\rangle \rightarrow |2\rangle$, we program the region M3 of the SLM 1 with a LPG with phase increasing in the $-x$-direction and high periodicity.

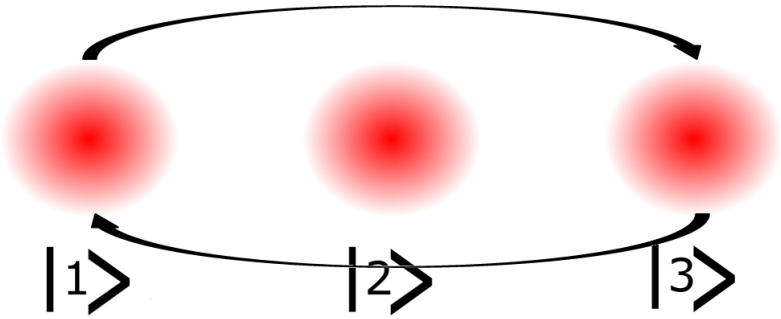

Figura 42 – Representation of transitions between the modes $|1\rangle$ and $|3\rangle$. To transfer light from $|1\rangle \rightarrow |3\rangle$, we program the region M1 of the SLM 1 with a LPG with phase increasing in the $+x$-direction and low periodicity. If we want transfer light from $|3\rangle \rightarrow |1\rangle$, we program the region M3 of the SLM 1 with a LPG with phase increasing in the $-x$-direction and low periodicity.

The initial state is generated by the first incidence at the SLM1 and the second incidence on it is used to implement the permutation operations. A second SLM, SLM2 in Figure 39, is placed at the path of the three reflected Gaussian beams by SLM1. The

screen of SLM2 is divided in three regions, M1, M2, and M3, which the three beams, represented by the states $|1\rangle$, $|2\rangle$ and $|3\rangle$passes through, respectively. Each one of these regions in programmed to add an individual phase to each one of the reflected beams by SLM1, if necessary. Notice that all QG operation are implemented in spatial modes in the horizontal direction only. It is not necessary to diffract the incident beams in the vertical direction as in the case of the simulation of quantum jump in three-level systems.

The $\sigma_x^{(ij)}$ will be implemented by performing the permutation operation between the path states $|i\rangle$ and $|j\rangle$. For $\sigma_y^{(ij)}$, we will need to perform the permutation operation between the path states $|i\rangle$ and $|j\rangle$ in the SLM 1 and insert a phase $e^{i\pi}$ on the state $|i\rangle$, by programming it in the region Mi on the SLM 2. Finally, $\sigma_z^{(ij)}$ and $S^{(i)}$ will be implemented by adding a phase factor $e^{i\pi}$ and $e^{i\theta}$, respectively, to the mode $|i\rangle$. For the case of these two operators, the phases can be added by SLM 1 or SLM 2. Due to the pixelation effects, we cannot transfer the incoming mode representing a component of the initial state to an outgoing mode representing the permuted state with the same initial mode amplitude modulus. We will use then a spatial filter to block unwanted remaining light which was not diffracted in the desired output mode. After SLM 2, the three-path is reflected by a mirror to an ICCD camera.

Like in the simulation performed in Chapter 5, the output state will be characterized by the image measurements by projecting the image of SLM2 at the ICCD plane and interference ones, by inserting a lens with focus on the detection plane (Figure 39). In this way, we have a complete characterization of the intensity in each mode, the coherence and relative phase between the path states. We are then able to construct the density matrix of the output state. By performing the same measurements for the initial state, we can compare the input and output states and verify the implementation of the QGs.

We would like to remark that this methodology can also be used for qubits, so with the same setup and techniques we can also implement all the quantum gates presented in Section 4.1.1. These operations can be generalized for higher-dimension systems with number of paths higher than three. As in the case of the simulation, the only technical restrictions in our experimental setup are the sizes of the pixels arrays in the SLM and in the ICCD.

6.2.2 Implementation of hybrid controlled quantum gates

To implement the CQG approached in Section 4.3, we will explore two degrees of freedom of a same particle instead of a two-particle system to implement the hybrid CQGs. The SLM only modulates the incoming light with horizontal polarization, so, the idea is to use the polarization as control qubit and the path modes as target qutrit. The experimental setup and the state preparation used for this purpose is almost the same one used for the implementation of a QG (Figure 39). After the first incidence, the state

produced by a BPG in region M4 is:

$$|\psi_0\rangle = \left(A_1 e^{i\phi_1}|1\rangle + A_2 e^{i\phi_2}|2\rangle + A_3 e^{i\phi_3}|3\rangle\right) \otimes |H\rangle\,, \tag{6.3}$$

where A_i and ϕ_i are real numbers which relies on the maximum phase of the BPG in region M4, $|i\rangle$ are the label of the path mode generated ($i = 1$, 2 and 3) and $|H\rangle$ represents the horizontal polarization state of the beams. The initial state was considered to be pure as it was produced by diffracting a laser beam. Between the first and second incidence on the SLM 1, we will insert a HWP, which will change the polarization of the generated state, Eq.6.3, according the orientation of it optical axis. For instance, if the optical axis of the HPW has a $22,5°$ orientation to the horizontal, after it we have the following state:

$$|\psi_0\rangle = \left(A_1 e^{i\phi_1}|1\rangle + A_2 e^{i\phi_2}|2\rangle + A_3 e^{i\phi_3}|3\rangle\right) \otimes \frac{1}{\sqrt{2}}\left(|H\rangle + |V\rangle\right), \tag{6.4}$$

where $|V\rangle$ represents the vertical polarization state.

In the implementation of the hybrid CQG, we will explore the same permutation operations that were studied in Section 6.1.2. But, because of the fact that the SLM only modulates the horizontal polarization, they will be implemented only in the $|H\rangle$ mode. After the HWP, the state is reflected back to the SLM 1, where the $|i\rangle$ mode reaches the Mi region ($i = 1$, 2 and 3), which are programmed to have LPG that can implement the permutation operations. Each one of these operations can be represented by:

$$O_{M_v}|v\rangle \otimes \left(|H\rangle + |V\rangle\right) = \left(\alpha_v|v\rangle + \alpha_\ell|\ell\rangle\right) \otimes |H\rangle + |v\rangle \otimes |V\rangle\,, \tag{6.5}$$

The control $\sigma_x^{(ij)}$ hybrid QG will be implemented by performing the permutation operation between the path states $|i\rangle$ and $|j\rangle$. For control hybrid $\sigma_y^{(ij)}$, we will need to perform the permutation operation between the path states $|i\rangle$ and $|j\rangle$ in the SLM 1. Also, we will insert a phase $e^{i\pi}$ on the state $|i\rangle$, by programming it in the region Mi on the SLM 2. Finally, control hybrid $\sigma_z^{(ij)}$ and $S^{(i)}$ will be implemented by adding a phase $e^{i\pi}$ and $e^{i\theta}$, respectively, to the mode $|i\rangle$. Due to the pixelation effects, we cannot transfer the whole incoming light from the initial mode representing the input state to the other mode representing the output state. Then, we will use a spatial filter to block the unwanted remaining light which was not diffracted, described by the first term of the state in Eq.6.5. After SLM 2, the three-path is reflected by a mirror to an ICCD camera.

As shown in the simulation performed in Chapter 5 and in the proposal in Section 6.2.1, the output state will be characterized by image measurements at the image plane by using a spherical lens between the SLM2 and the ICCD, and interference ones, by inserting a lens with focus on the detection plane (Figure 39). Also, with a polariser (which is not in Figure 39) near the ICCD camera, we will perform projection over the polarization state to characterize the $|H\rangle$ and $|V\rangle$ outputs. In this way, we have a complete characterization of the intensity in each mode, the coherence and relative phase between the path states.

We are able to construct the density matrix of the output state. By performing the same measurements for the initial state, we can compare the input and output states and verify the implementation of the hybrid CQGs.

We would like to emphasize that this methodology can also be used for qubit path states, thus, we can implement CQGs like the ones studied in Section 4.1.2. Also, it can be performed for higher-dimensions system with number of path higher than three. The only technical restrictions in our experimental setup are the sizes of the pixels arrays in the SLM and in the ICCD.

7 Conclusion

The main objective of this work is to implement a quantum simulation of quantum jump dynamics in three-level systems on photonic path systems by using attenuated laser beams as three-paths photonic states for mimic an atomic three-level state subject to quantum jump. By exploring periodical phase modulation in a spatial light modulator, we are able to prepare the qutrit Gaussian paths modes states and implement general operation on them. This enables us to implement the Kraus operators for each one of the decay configurations: cascade, Λ and V.

In Chapter 2, we reviewed light diffraction theory. We focused on the theory of diffraction by periodical phase gratings (PPGs), more precisely, in linear diffraction gratings (LPG) and binary diffraction gratings(BPG). We approached the relative intensities of the diffraction orders generated on the distant plane of the PPGs. These techniques allow us to perform quantum general operations on path Gaussian modes that define the photon path states. By using BPGs we can prepare a superposition of three-path states and exploring LPGs we can implement quantum operations on them. Also, we made a quick study about the SLM and how it works. In the final section of the chapter, we realized a quick review of quantum states and how the quantum operations modify a quantum state.

In Chapter 3, we made a basic review on the theory of quantum open systems. We started from Liouville-Von Neumann equation, and the interaction picture. After, we defined closed and quantum open systems and remarked their differences. We defined a dynamical map, which provide us the time evolution of an OQS and we reached the quantum master equation in the Born-Markov approximation in terms of the Lindblad operators. Finally, we deduced the Kraus decomposition of the maps that represent the spontaneous decay dynamics for a two-level system and deduced the same decomposition for the decay in three-level systems for the cascade, Λ and V configurations. Moreover, we emphasized that all the deduced Kraus decompositions represent a linear CPTP dynamical map.

In chapter 4, we introduced some quantum gates and controlled quantum gates that we propose to implement in photonic path systems. In the first section, we reviewed the Pauli QG and the phase QG for a single qubit, we studied the effects of the implementation of each one of the gates in an input state. Also, we proposed the same QG for two qubits, establishing the control and target one, and how they can be used to generate entangled states. A version Pauli QG for a single qutrit systems and Phase QG for a three-level systems are also described. In the last section of the chapter, we focused on the hybrid CQGs, these types of CQGs have target and control qudits of different dimensions.

In Chapter 5, we reported the simulation of quantum jump in atomic three-level systems by using photonic path state systems. We detailed how the initial three-beam modes were prepared by the BPGs as photonic three path states. We explained how the quantum jumps were simulated by the LPGs. Also, we approached how, each one of the Kraus operators are programmed at the SLM. We showed the results for the diagonal terms of the density matrix, which were obtained from the image measurements, with their theoretical predictions. Also, by the measuring the interference path of the beams two-by-two, we obtained the modulus of the off-diagonal terms of the density matrix. The results provided by the simulation of all the three-level decay dynamics, were compared with the theoretical predictions.

Finally, in Chapter 6, we proposed an experimental implementation of QG and CQG in photonic path state systems making use of periodical phase modulation in a spatial light modulator. With an experimental setup analogous to the one used in the simulation of quantum jump, we are able to implement all the QGs and CQGs approached in Chapter 4. For the implementation of the two qubits CQG and hybrids CQG, we proposed to explore the path degree of freedom as target and the polarization degree of freedom as control. We detailed how each one of the QGs and CQG can be implemented in terms of the permutation operations and phase change operations by using two SLMs. The first SLM will be programmed with a LPG to perform the permutation, while the second one will be programmed to add a relative phase to each one of the QGs.

We simulated the three-level atomic system dynamics by using photonic three-path state. By exploring periodical phase modulation in a SLM, we were able to implement the Kraus operators for all the three-level decay dynamics: cascade, Λ and V. The experimental characterizations of the density matrix for the output state are in agreement to the theoretical predictions despite a small deviation. With a precise periodical phase modulation of the photonic attenuated laser beams, we are able to implement a large number of operations and simulate the different dynamics of decay in a three-level system. This simulation gives us a better comprehension of how quantum jump affects the coherence of a three-level system. Moreover, this implementation can be used for understanding how quantum jumps in high dimension systems affect quantum protocols due to the state decoherence.

The quantity of achievable quantum operations with this apparatus makes it a good choice for other implementations. For instance, an atomic system being excited by an external electromagnetic field, not only the decaying, could be simulated. A large number of QG and CQG can also be realized, by using the same methodology, as proposed in Chapter 6. Also, we can test the behaviour of a quantum channel subjected to this kind of noise or even the behaviour of a quantum information protocol in a noisy quantum channel.

The procedure exploited in the simulation of decay dynamics and in the proposal of implementation of QGs is general and it can be extended to multilevel systems, with the number of levels higher than three. The only technical restrictions in our experimental setup, for this extension, are the sizes of the pixels arrays in the SLM and in the ICCD camera, which must fit all the Gaussian paths representing the higher dimension atomic system. For instance, we need to have a minimum number of periods of the diffraction periodical gratings inside the laser beam transverse profile so that it can be diffracted.

Referências

[1] Flamini, Fulvio, Nicolò Spagnolo e Fabio Sciarrino: *Photonic quantum information processing: a review*. Reports on Progress in Physics, 82(1):016001, nov 2018. https://doi.org/10.1088/1361-6633/aad5b2. Citado na página 17.

[2] Slussarenko, Sergei e Geoff J. Pryde: *Photonic quantum information processing: A concise review*. Applied Physics Reviews, 6(4):041303, 2019. https://doi.org/10.1063/1.5115814. Citado na página 17.

[3] Hensen, B., H. Bernien, A. E. Dréau, A. Reiserer, N. Kalb, M. S. Blok, J. Ruitenberg, R. F. L. Vermeulen, R. N. Schouten, C. Abellán, W. Amaya, V. Pruneri, M. W. Mitchell, M. Markham, D. J. Twitchen, D. Elkouss, S. Wehner, T. H. Taminiau e R. Hanson: *Loophole-free Bell inequality violation using electron spins separated by 1.3 kilometres*. Nature, 526(7575):682–686, 2015. https://doi.org/10.1038/nature15759. Citado na página 17.

[4] Giustina, Marissa, Marijn A. M. Versteegh, Sören Wengerowsky, Johannes Handsteiner, Armin Hochrainer, Kevin Phelan, Fabian Steinlechner, Johannes Kofler, Jan Åke Larsson, Carlos Abellán, Waldimar Amaya, Valerio Pruneri, Morgan W. Mitchell, Jörn Beyer, Thomas Gerrits, Adriana E. Lita, Lynden K. Shalm, Sae Woo Nam, Thomas Scheidl, Rupert Ursin, Bernhard Wittmann e Anton Zeilinger: *Significant-Loophole-Free Test of Bell's Theorem with Entangled Photons*. Phys. Rev. Lett., 115:250401, Dec 2015. https://link.aps.org/doi/10.1103/PhysRevLett.115.250401. Citado na página 17.

[5] Shalm, Lynden K., Evan Meyer-Scott, Bradley G. Christensen, Peter Bierhorst, Michael A. Wayne, Martin J. Stevens, Thomas Gerrits, Scott Glancy, Deny R. Hamel, Michael S. Allman, Kevin J. Coakley, Shellee D. Dyer, Carson Hodge, Adriana E. Lita, Varun B. Verma, Camilla Lambrocco, Edward Tortorici, Alan L. Migdall, Yanbao Zhang, Daniel R. Kumor, William H. Farr, Francesco Marsili, Matthew D. Shaw, Jeffrey A. Stern, Carlos Abellán, Waldimar Amaya, Valerio Pruneri, Thomas Jennewein, Morgan W. Mitchell, Paul G. Kwiat, Joshua C. Bienfang, Richard P. Mirin, Emanuel Knill e Sae Woo Nam: *Strong Loophole-Free Test of Local Realism*. Phys. Rev. Lett., 115:250402, Dec 2015. https://link.aps.org/doi/10.1103/PhysRevLett.115.250402. Citado na página 17.

[6] Ralph, Tim C. e Geoff J. Pryde: *Chapter 4 - Optical Quantum Computation*. Volume 54 de *Progress in Optics*, páginas 209–269. Elsevier, 2010. http://www.

sciencedirect.com/science/article/pii/S0079663810054090. Citado na página 17.

[7] Kok, Pieter, W. J. Munro, Kae Nemoto, T. C. Ralph, Jonathan P. Dowling e G. J. Milburn: *Linear optical quantum computing with photonic qubits*. Rev. Mod. Phys., 79:135–174, Jan 2007. https://link.aps.org/doi/10.1103/RevModPhys.79.135. Citado na página 17.

[8] Marques, B., M. R. Barros, W. M. Pimenta, M. A. D. Carvalho, J. Ferraz, R. C. Drumond, M. Terra Cunha e S. Pádua: *Double-slit implementation of the minimal Deutsch algorithm*. Phys. Rev. A, 86:032306, Sep 2012. https://link.aps.org/doi/10.1103/PhysRevA.86.032306. Citado 3 vezes nas páginas 17, 18 e 48.

[9] Kolenderski, Piotr, Urbasi Sinha, Li Youning, Tong Zhao, Matthew Volpini, Adán Cabello, Raymond Laflamme e Thomas Jennewein: *Aharon-Vaidman quantum game with a Young-type photonic qutrit*. Phys. Rev. A, 86:012321, Jul 2012. https://link.aps.org/doi/10.1103/PhysRevA.86.012321. Citado na página 17.

[10] Bouwmeester, Dik, Jian Wei Pan, Klaus Mattle, Manfred Eibl, Harald Weinfurter e Anton Zeilinger: *Experimental quantum teleportation*. Nature, 390:575–579, Dec 1997. https://doi.org/10.1038/37539. Citado na página 17.

[11] Leach, Jonathan, Miles J. Padgett, Stephen M. Barnett, Sonja Franke-Arnold e Johannes Courtial: *Measuring the Orbital Angular Momentum of a Single Photon*. Phys. Rev. Lett., 88:257901, Jun 2002. https://link.aps.org/doi/10.1103/PhysRevLett.88.257901. Citado na página 17.

[12] Dada, Adetunmise C., Jonathan Leach, Gerald S. Buller, Miles J. Padgett e Erika Andersson: *Experimental high-dimensional two-photon entanglement and violations of generalized Bell inequalities*. Nature Physics, 7:677–680, Sep 2011. https://doi.org/10.1038/nphys1996. Citado 3 vezes nas páginas 17, 18 e 48.

[13] Langford, N. K., R. B. Dalton, M. D. Harvey, J. L. O'Brien, G. J. Pryde, A. Gilchrist, S. D. Bartlett e A. G. withe: *Measuring Entangled Qutrits and Their Use for Quantum Bit Commitment*. Phys. Rev. Lett., 93:053601, Jul 2004. https://link.aps.org/doi/10.1103/PhysRevLett.93.053601. Citado na página 17.

[14] Mair, Alois, Alipasha Vaziri, Gregor Weihs e Anton Zeilinger: *Entanglement of the orbital angular momentum states of photons*. Nature, 412:313–316, Jul 2001. https://doi.org/10.1038/35085529. Citado na página 17.

[15] Neves, Leonardo, G. Lima, J. G. Aguirre Gómez, C. H. Monken, C. Saavedra e S. Pádua: *Generation of Entangled States of Qudits using Twin Photons*. Phys. Rev.

Lett., 94:100501, Mar 2005. https://link.aps.org/doi/10.1103/PhysRevLett.94.100501. Citado 2 vezes nas páginas 17 e 65.

[16] Lima, G., A. Vargas, L. Neves, R. Guzmán e C. Saavedra: *Manipulating spatial qudit states with programmable optical devices*. Opt. Express, 17(13):10688–10696, Jun 2009. http://www.opticsexpress.org/abstract.cfm?URI=oe-17-13-10688. Citado 3 vezes nas páginas 17, 18 e 48.

[17] Walborn, S.P., C.H. Monken, S. Pádua e P.H. Souto Ribeiro: *Spatial correlations in parametric down-conversion*. Physics Reports, 495:87–139, 2010. Citado na página 17.

[18] Borges, G. F., R. D. Baldijão, J. G. L. Condé, J. S. Cabral, B. Marques, M. Terra Cunha, A. Cabello e S. Pádua: *Automated quantum operations in photonic qutrits*. Phys. Rev. A, 97:022301, Feb 2018. https://link.aps.org/doi/10.1103/PhysRevA.97.022301. Citado 11 vezes nas páginas 17, 18, 21, 23, 24, 26, 28, 48, 49, 53 e 70.

[19] Hu, Xiao Min, Jiang Shan Chen, Bi Heng Liu, Yu Guo, Yun Feng Huang, Zong Quan Zhou, Yong Jian Han, Chuan Feng Li e Guang Can Guo: *Experimental Test of Compatibility-Loophole-Free Contextuality with Spatially Separated Entangled Qutrits*. Phys. Rev. Lett., 117:170403, Oct 2016. https://link.aps.org/doi/10.1103/PhysRevLett.117.170403. Citado na página 17.

[20] Solís-Prosser, M. A., A. Arias, J. J. M. Varga, L. Rebón, S. Ledesma, C. Iemmi e L. Neves: *Preparing arbitrary pure states of spatial qudits with a single phase-only spatial light modulator*. Opt. Lett., 38(22):4762–4765, Nov 2013. http://ol.osa.org/abstract.cfm?URI=ol-38-22-4762. Citado 3 vezes nas páginas 17, 21 e 23.

[21] Machado, P., A. A. Matoso, M. R. Barros, L. Neves e S. Pádua: *Engineering quantum correlations for $m \times n$ spatially encoded two-photons states*. Phys. Rev. A, 99:063839, Jun 2019. https://link.aps.org/doi/10.1103/PhysRevA.99.063839. Citado na página 17.

[22] Peeters, W. H., J. J. Renema e M. P. van Exter: *Engineering of two-photon spatial quantum correlations behind a double slit*. Phys. Rev. A, 79:043817, Apr 2009. https://link.aps.org/doi/10.1103/PhysRevA.79.043817. Citado na página 17.

[23] Assis, P. L. de, M. A. D. Carvalho, L. P. Berruezo, J. Ferraz, I. F. Santos, F. Sciarrino e S. Pádua: *Control of quantum transverse correlations on a four-photon system*. Opt. Express, 19(4):3715–3729, Feb 2011. http://www.opticsexpress.org/abstract.cfm?URI=oe-19-4-3715. Citado na página 17.

[24] Breuer, H. P. e F. Petruccione: *The theory of open quantum systems*. Oxford University Press, Great Clarendon Street, 2002. Citado 7 vezes nas páginas 17, 29, 30, 31, 32, 33 e 37.

[25] Alicki, Robert e K. Lendi: *Quantum Dynamical Semigroups and Applications*, volume 717. ISBN 978-3-540-70861-2. Citado na página 17.

[26] Carmichael, H. J.: *An open systems approach to quantum optics*. Springer-Verlag, Berlin Heidelberg, 1993. Citado 5 vezes nas páginas 17, 29, 30, 32 e 33.

[27] Zurek, Wojciech Hubert: *Decoherence, einselection, and the quantum origins of the classical*. Rev. Mod. Phys., 75:715–775, May 2003. https://link.aps.org/doi/10.1103/RevModPhys.75.715. Citado 3 vezes nas páginas 17, 29 e 36.

[28] Zurek, Wojciech Hubert: *Decoherence and the Transition from Quantum to Classical - Revisited*, páginas 1–31. Birkhäuser Basel, Basel, 2007, ISBN 978-3-7643-7808-0. https://doi.org/10.1007/978-3-7643-7808-0_1. Citado 3 vezes nas páginas 17, 29 e 36.

[29] Marquardt, Florian e Annett Püttmann: *Introduction to dissipation and decoherence in quantum systems*, 2008. Citado 3 vezes nas páginas 17, 29 e 36.

[30] Schlosshauer, Maximilian: *Quantum decoherence*. Physics Reports, 831:1–57, 2019, ISSN 0370-1573. http://www.sciencedirect.com/science/article/pii/S0370157319303084, Quantum decoherence. Citado 3 vezes nas páginas 17, 29 e 36.

[31] Marques B., Matoso A. A., Pimenta W. M. Gutiérrez Esparza A. J. Santos M. F. Pádua S.: *Experimental simulation of decoherence in photonics qudits*. Scientific Reports, 5(16049). Citado 4 vezes nas páginas 17, 18, 26 e 37.

[32] Almeida, M. P., F. de Melo, M. Hor-Meyll, A. Salles, S. P. Walborn, P. H. Souto Ribeiro e L. Davidovich: *Environment-Induced Sudden Death of Entanglement*. Science, 316(5824):579–582, 2007, ISSN 0036-8075. http://science.sciencemag.org/content/316/5824/579. Citado 2 vezes nas páginas 17 e 18.

[33] Jiménez Farías, O., C. Lombard Latune, S. P. Walborn, L. Davidovich e P. H. Souto Ribeiro: *Determining the Dynamics of Entanglement*. Science, 324(5933):1414–1417, 2009, ISSN 0036-8075. https://science.sciencemag.org/content/324/5933/1414. Citado na página 17.

[34] Unden, Thomas, Priya Balasubramanian, Daniel Louzon, Yuval Vinkler, Martin B. Plenio, Matthew Markham, Daniel Twitchen, Alastair Stacey, Igor Lovchinsky, Alexander O. Sushkov, Mikhail D. Lukin, Alex Retzker, Boris Naydenov, Liam P.

McGuinness e Fedor Jelezko: *Quantum Metrology Enhanced by Repetitive Quantum Error Correction*. Phys. Rev. Lett., 116:230502, Jun 2016. https://link.aps.org/doi/10.1103/PhysRevLett.116.230502. Citado na página 17.

[35] Chiuri, A., V. Rosati, G. Vallone, S. Pádua, H. Imai, S. Giacomini, C. Macchiavello e P. Mataloni: *Experimental Realization of Optimal Noise Estimation for a General Pauli Channel*. Phys. Rev. Lett., 107:253602, Dec 2011. https://link.aps.org/doi/10.1103/PhysRevLett.107.253602. Citado na página 17.

[36] Aolita, Leandro, Fernando de Melo e Luiz Davidovich: *Open-system dynamics of entanglement:a key issues review*. Reports on Progress in Physics, 78(4):042001, Mar 2015. https://doi.org/10.1088/0034-4885/78/4/042001. Citado na página 17.

[37] Salles, A., F. de Melo, M. P. Almeida, M. Hor-Meyll, S. P. Walborn, P. H. Souto Ribeiro e L. Davidovich: *Experimental investigation of the dynamics of entanglement: Sudden death, complementarity, and continuous monitoring of the environment*. Phys. Rev. A, 78:022322, Aug 2008. https://link.aps.org/doi/10.1103/PhysRevA.78.022322. Citado 2 vezes nas páginas 17 e 37.

[38] Laurat, J., K. S. Choi, H. Deng, C. W. Chou e H. J. Kimble: *Heralded Entanglement between Atomic Ensembles: Preparation, Decoherence, and Scaling*. Phys. Rev. Lett., 99:180504, Nov 2007. https://link.aps.org/doi/10.1103/PhysRevLett.99.180504. Citado na página 17.

[39] Barbosa, F. A. S., A. S. Coelho, A. J. de Faria, K. N. Cassemiro, A. S. Villar, P. Nussenzveig e M. Martinelli: *Robustness of bipartite Gaussian entangled beams propagating in lossy channels*. Nature Photonics, 4:858–861, Dec 2010. https://doi.org/10.1038/nphoton.2010.222. Citado na página 17.

[40] Xu, Jin Shi, Chuan Feng Li, Xiao Ye Xu, Cheng Hao Shi, Xu Bo Zou e Guang Can Guo: *Experimental Characterization of Entanglement Dynamics in Noisy Channels*. Phys. Rev. Lett., 103:240502, Dec 2009. https://link.aps.org/doi/10.1103/PhysRevLett.103.240502. Citado na página 17.

[41] Häffner, H., F. Schmidt-Kaler, W. Hänsel, C. F. Roos, T. Körber, M. Chwalla, M. Riebe, J. Benhelm, U. D. Rapol, C. Becher e R. Blatt: *Robust entanglement*. Applied Physics B, 81:151–153, 2005. https://doi.org/10.1007/s00340-005-1917-z. Citado na página 17.

[42] Farías, O. Jiménez, G. H. Aguilar, A. Valdés-Hernández, P. H. Souto Ribeiro, L. Davidovich e S. P. Walborn: *Observation of the Emergence of Multipartite Entanglement Between a Bipartite System and its Environment*. Phys. Rev. Lett., 109:150403, Oct 2012. https://link.aps.org/doi/10.1103/PhysRevLett.109.150403. Citado na página 17.

[43] Kwiat, Paul G., Andrew J. Berglund, Joseph B. Altepeter e Andrew G. White: *Experimental Verification of Decoherence-Free Subspaces*. Science, 290(5491):498–501, 2000, ISSN 0036-8075. https://science.sciencemag.org/content/290/5491/498. Citado na página 17.

[44] Cook, Richard J: *What are Quantum Jumps?* Physica Scripta, T21:49–51, jan 1988. https://iopscience.iop.org/article/10.1088/0031-8949/1988/T21/009. Citado na página 17.

[45] Dalibard, Jean, Yvan Castin e Klaus Mølmer: *Wave-function approach to dissipative processes in quantum optics*. Phys. Rev. Lett., 68:580–583, Feb 1992. https://link.aps.org/doi/10.1103/PhysRevLett.68.580. Citado na página 17.

[46] Gisin, Nicolas e Ian C. Percival: *Wave-function approach to dissipative processes: are there quantum jumps?* Physics Letters A, 167(4):315–318, 1992, ISSN 0375-9601. http://www.sciencedirect.com/science/article/pii/037596019290264M. Citado na página 17.

[47] Gisin, N., P. L. Knight, I. C. Percival, R. C. Thompson e D. C. Wilson: *Quantum State Diffusion Theory and a Quantum Jump Experiment*. Journal of Modern Optics, 40(9):1663–1671, 1993. https://doi.org/10.1080/09500349314551671. Citado na página 17.

[48] Dick, Rainer: *Quantum jumps, superpositions, and the continuous evolution of quantum states*. Studies in History and Philosophy of Science Part B: Studies in History and Philosophy of Modern Physics, 57:115–125, 2017, ISSN 1355-2198. http://www.sciencedirect.com/science/article/pii/S1355219816300673. Citado na página 17.

[49] N. Bohr, Dr. Phil.: *On the constitution of atoms and molecules*. The London, Edinburgh, and Dublin Philosophical Magazine and Journal of Science, 26(151):1–25, 1913. https://doi.org/10.1080/14786441308634955. Citado na página 17.

[50] SCHRÖDINGER, E.: *ARE THERE QUANTUM JUMPS?* The British Journal for the Philosophy of Science, 3(10):109–233, Aug 1952, ISSN 0007-0882. https://doi.org/10.1093/bjps/III.10.109. Citado na página 17.

[51] Bitbol, Michel: *Schrödinger Against Particles and Quantum Jumps*, páginas 81–106. Springer Berlin Heidelberg, Berlin, Heidelberg, 2007, ISBN 978-3-540-32665-6. https://doi.org/10.1007/978-3-540-32665-6_5. Citado na página 17.

[52] Einstein, Albert: *Strahlungs-Emission und Absorption nach der Quantentheorie*. Deutsche Physikalische Gesellschaft, 18:318–323, jan 1916. Citado na página 17.

[53] Lukin, M. D., M. Fleischhauer, R. Cote, L. M. Duan, D. Jaksch, J. I. Cirac e P. Zoller: *Dipole Blockade and Quantum Information Processing in Mesoscopic Atomic Ensembles*. Phys. Rev. Lett., 87:037901, Jun 2001. https://link.aps.org/doi/10.1103/PhysRevLett.87.037901. Citado na página 17.

[54] Deléglise, Samuel, Igor Dotsenko, Clément Sayrin, Julien Bernu, Michel Brune, Jean Michel Raimond e Serge Haroche: *Reconstruction of non-classical cavity field states with snapshots of their decoherence*. Nature, 455:510–514, Sep 2008. https://doi.org/10.1038/nature07288. Citado na página 18.

[55] Sayrin, Clément, Igor Dotsenko, Xingxing Zhou, Bruno Peaudecerf, Théo Rybarczyk, Sébastien Gleyzes, Pierre Rouchon, Mazyar Mirrahimi, Hadis Amini, Michel Brune, Jean Michel Raimond e Serge Haroche: *Real-time quantum feedback prepares and stabilizes photon number states*. Nature, 477:73–77, Sep 2011. https://doi.org/10.1038/nature10376. Citado na página 18.

[56] Ofek, Nissim, Andrei Petrenko, Reinier Heeres, Philip Reinhold, Zaki Leghtas, Brian Vlastakis, Yehan Liu, Luigi Frunzio, S. M. Girvin, L. Jiang, Mazyar Mirrahimi, M. H. Devoret e R. J. Schoelkopf: *Extending the lifetime of a quantum bit with error correction in superconducting circuits*. Nature, 536:441–445, Aug 2016. https://doi.org/10.1038/nature18949. Citado na página 18.

[57] Ofek, Nissim, Andrei Petrenko, Reinier Heeres, Philip Reinhold, Zaki Leghtas, Brian Vlastakis, Yehan Liu, Luigi Frunzio, S. M. Girvin, Liang Jiang, Mazyar Mirrahimi, M. H. Devoret e R. J. Schoelkopf: *Demonstrating Quantum Error Correction that Extends the Lifetime of Quantum Information*, 2016. Citado na página 18.

[58] Sun, L., A. Petrenko, Z. Leghtas, B. Vlastakis, G. Kirchmair, K. M. Sliwa, A. Narla, M. Hatridge, S. Shankar, J. Blumoff, L. Frunzio, M. Mirrahimi, M. H. Devoret e R. J. Schoelkopf: *Tracking photon jumps with repeated quantum non-demolition parity measurements*. Nature, 511:444–448, Jul 2014. https://doi.org/10.1038/nature13436. Citado na página 18.

[59] Vijay, R., D. H. Slichter e I. Siddiqi: *Observation of Quantum Jumps in a Superconducting Artificial Atom*. Phys. Rev. Lett., 106:110502, Mar 2011. https://link.aps.org/doi/10.1103/PhysRevLett.106.110502. Citado na página 18.

[60] Sauter, Th., W. Neuhauser, R. Blatt e P. E. Toschek: *Observation of Quantum Jumps*. Phys. Rev. Lett., 57:1696–1698, Oct 1986. https://link.aps.org/doi/10.1103/PhysRevLett.57.1696. Citado na página 18.

[61] Bergquist, J. C., Randall G. Hulet, Wayne M. Itano e D. J. Wineland: *Observation of Quantum Jumps in a Single Atom*. Phys. Rev. Lett., 57:1699–1702, Oct 1986.

https://link.aps.org/doi/10.1103/PhysRevLett.57.1699. Citado na página 18.

[62] Nagourney, Warren, Jon Sandberg e Hans Dehmelt: *Shelved optical electron amplifier: Observation of quantum jumps*. Phys. Rev. Lett., 56:2797–2799, Jun 1986. https://link.aps.org/doi/10.1103/PhysRevLett.56.2797. Citado na página 18.

[63] Hulet, Randall G., D. J. Wineland, J. C. Bergquist e Wayne M. Itano: *Precise test of quantum jump theory*. Phys. Rev. A, 37:4544–4547, Jun 1988. https://link.aps.org/doi/10.1103/PhysRevA.37.4544. Citado na página 18.

[64] Th. Basché, S. Kummer, C. Bräuchle: *Direct spectroscopic observation of quantum jumps of a single molecule*. Nature, 373:132–134, 1995, ISSN 1476-4687. https://doi.org/10.1038/373132a0. Citado na página 18.

[65] Peil, S. e G. Gabrielse: *Observing the Quantum Limit of an Electron Cyclotron: QND Measurements of Quantum Jumps between Fock States*. Phys. Rev. Lett., 83:1287–1290, Aug 1999. https://link.aps.org/doi/10.1103/PhysRevLett.83.1287. Citado na página 18.

[66] S. Gleyzes, S. Kuhr, C. Guerlin J. Bernu S. Deléglise U. Busk Hoff M. Brune J. Raimond S. Haroche: *Quantum jumps of light recording the birth and death of a photon in a cavity*. Nature, 446:297–300, 2007, ISSN 1476-4687. https://doi.org/10.1038/nature05589. Citado na página 18.

[67] Guerlin, Christine, Julien Bernu, Samuel Deléglise, Clément Sayrin, Sébastien Gleyzes, Stefan Kuhr, Michel Brune, Jean Michel Raimond e Serge Haroche: *Progressive field-state collapse and quantum non-demolition photon counting*. Nature, 448:889–893, Aug 2008. https://doi.org/10.1038/nature06057. Citado na página 18.

[68] Jelezko, F., I. Popa, A. Gruber, C. Tietz, J. Wrachtrup, A. Nizovtsev e S. Kilin: *Single spin states in a defect center resolved by optical spectroscopy*. Applied Physics Letters, 81(12):2160–2162, 2002. https://doi.org/10.1063/1.1507838. Citado na página 18.

[69] Neumann, Philipp, Johannes Beck, Matthias Steiner, Florian Rempp, Helmut Fedder, Philip R. Hemmer, Jörg Wrachtrup e Fedor Jelezko: *Single-Shot Readout of a Single Nuclear Spin*. Science, 329(5991):542–544, 2010, ISSN 0036-8075. https://science.sciencemag.org/content/329/5991/542. Citado na página 18.

[70] L. Robledo, L. Childress, H. Bernien B. Hensen P. F. A. Alkemade R. Hanson: *High-fidelity projective read-out of a solid-state spin quantum register*. Nature, 477:574–578, 2011, ISSN 1476-4687. https://doi.org/10.1038/nature10401. Citado na página 18.

[71] Hatridge, M., S. Shankar, M. Mirrahimi, F. Schackert, K. Geerlings, T. Brecht, K. M. Sliwa, B. Abdo, L. Frunzio, S. M. Girvin, R. J. Schoelkopf e M. H. Devoret: *Quantum Back-Action of an Individual Variable-Strength Measurement*. Science, 339(6116):178–181, 2013, ISSN 0036-8075. https://science.sciencemag.org/content/339/6116/178. Citado na página 18.

[72] Minev, Z. K., S. O. Mundhada, S. Shankar, P. Reinhold, R. Gutiérrez-Jáuregui, R. J. Schoelkopf, M. Mirrahimi, H. J. Carmichael e M. H. Devoret: *To catch and reverse a quantum jump mid-flight*. Nature, 570:200–204, Jun 2019. https://doi.org/10.1038/s41586-019-1287-z. Citado na página 18.

[73] M. Ossiander, J. Riemensberger, S. Neppl M. Mittermair M. Schäffer A. Duensing M. S. Wagner R. Heider M. Wurzer M. Gerl M. Schnitzenbaumer J. V. Barth F. Libisch C. Lemell J. Burgdörfer P. Feulner R. Kienberger: *Absolute timing of the photoelectric effect*. Nature, 561:374–377, 2018, ISSN 1476-4687. https://doi.org/10.1038/s41586-018-0503-6. Citado na página 18.

[74] Lett, Paul D., Richard N. Watts, Christoph I. Westbrook, William D. Phillips, Phillip L. Gould e Harold J. Metcalf: *Observation of Atoms Laser Cooled below the Doppler Limit*. Phys. Rev. Lett., 61:169–172, Jul 1988. https://link.aps.org/doi/10.1103/PhysRevLett.61.169. Citado na página 18.

[75] Aspect, A., E. Arimondo, R. Kaiser, N. Vansteenkiste e C. Cohen-Tannoudji: *Laser Cooling below the One-Photon Recoil Energy by Velocity-Selective Coherent Population Trapping*. Phys. Rev. Lett., 61:826–829, Aug 1988. https://link.aps.org/doi/10.1103/PhysRevLett.61.826. Citado na página 18.

[76] Dalibard, J. e C. Cohen-Tannoudji: *Laser cooling below the Doppler limit by polarization gradients: simple theoretical models*. J. Opt. Soc. Am. B, 6(11):2023–2045, Nov 1989. http://josab.osa.org/abstract.cfm?URI=josab-6-11-2023. Citado na página 18.

[77] Kasevich, Mark e Steven Chu: *Laser cooling below a photon recoil with three-level atoms*. Phys. Rev. Lett., 69:1741–1744, Sep 1992. https://link.aps.org/doi/10.1103/PhysRevLett.69.1741. Citado na página 18.

[78] Gupta, R., C. Xie, S. Padua, H. Batelaan e H. Metcalf: *Bichromatic laser cooling in a three-level system*. Phys. Rev. Lett., 71:3087–3090, Nov 1993. https://link.aps.org/doi/10.1103/PhysRevLett.71.3087. Citado na página 18.

[79] Goy, P., J. M. Raimond, M. Gross e S. Haroche: *Observation of Cavity-Enhanced Single-Atom Spontaneous Emission*. Phys. Rev. Lett., 50:1903–1906, Jun 1983. https://link.aps.org/doi/10.1103/PhysRevLett.50.1903. Citado na página 18.

[80] Jhe, W., A. Anderson, E. A. Hinds, D. Meschede, L. Moi e S. Haroche: *Suppression of spontaneous decay at optical frequencies: Test of vacuum-field anisotropy in confined space*. Phys. Rev. Lett., 58:666–669, Feb 1987. https://link.aps.org/doi/10.1103/PhysRevLett.58.666. Citado na página 18.

[81] Martini, F. De, G. Innocenti, G. R. Jacobovitz e P. Mataloni: *Anomalous Spontaneous Emission Time in a Microscopic Optical Cavity*. Phys. Rev. Lett., 59:2955–2958, Dec 1987. https://link.aps.org/doi/10.1103/PhysRevLett.59.2955. Citado na página 18.

[82] Minev, Zlatko Kristev: *Catching and Reversing a Quantum Jump Mid-Flight*. Tese de Doutoramento, Yale University, 2018. Citado na página 18.

[83] Solís-Prosser, M. A., M. F. Fernandes, O. Jiménez, A. Delgado e L. Neves: *Experimental Minimum-Error Quantum-State Discrimination in High Dimensions*. Phys. Rev. Lett., 118:100501, Mar 2017. https://link.aps.org/doi/10.1103/PhysRevLett.118.100501. Citado 2 vezes nas páginas 18 e 48.

[84] Larocque, Hugo, Jérémie Gagnon-Bischoff, Dominic Mortimer, Yingwen Zhang, Frédéric Bouchard, Jeremy Upham, Vincenzo Grillo, Robert W. Boyd e Ebrahim Karimi: *Generalized optical angular momentum sorter and its application to high-dimensional quantum cryptography*. Opt. Express, 25(17):19832–19843, Aug 2017. http://www.opticsexpress.org/abstract.cfm?URI=oe-25-17-19832. Citado 2 vezes nas páginas 18 e 48.

[85] Georgescu, I. M., S. Ashhab e Franco Nori: *Quantum simulation*. Rev. Mod. Phys., 86:153–185, Mar 2014. https://link.aps.org/doi/10.1103/RevModPhys.86.153. Citado na página 18.

[86] Barreiro, Julio T., Markus Müller, Philipp Schindler, Daniel Nigg, Thomas Monz, Michael Chwalla, Markus Hennrich, Christian F. Roos, Peter Zoller e Rainer Blatt: *An open-system quantum simulator with trapped ions*. Nature, 470:486–491, Feb 2011. https://doi.org/10.1038/nature09801. Citado na página 18.

[87] Nielsen, Michael A. e Isaac L. Chuang: *Quantum Computation and Quantum Information*. Cambridge University Press, 2010. Citado 5 vezes nas páginas 18, 19, 40, 42 e 45.

[88] Barnett, Stephen: *Quantum Information*. Oxford University Press, Inc., New York, NY, USA, 2009, ISBN 0198527632, 9780198527633. Citado 3 vezes nas páginas 18, 19 e 42.

[89] Feynman, Richard P.: *Quantum mechanical computers*. Foundations of Physics, 16:507–531, Jun 1986. https://doi.org/10.1007/BF01886518. Citado na página 18.

[90] Leggett, A.J., Artur Ekert, Juan Pablo Paz, Wojciech Hubert Zurek, Dik Bouwmeester, John C. Howell, Antia Lamas-Linares, Juan Ignacio Cirac, Guido Burkard, Hans Andreas Engel e Daniel Loss: *Fundamentals of Quantum Information*. Springer-Verlag Berlin Heidelberg, 2002, ISBN 978-3-540-45933-0. https://www.springer.com/gp/book/9783540433675. Citado na página 19.

[91] Wang, Xiaoguang e Paolo Zanardi: *Quantum entanglement of unitary operators on bipartite systems*. Phys. Rev. A, 66:044303, Oct 2002. https://link.aps.org/doi/10.1103/PhysRevA.66.044303. Citado 2 vezes nas páginas 19 e 44.

[92] Turchette, Q. A., C. S. Wood, B. E. King, C. J. Myatt, D. Leibfried, W. M. Itano, C. Monroe e D. J. Wineland: *Deterministic Entanglement of Two Trapped Ions*. Phys. Rev. Lett., 81:3631–3634, Oct 1998. https://link.aps.org/doi/10.1103/PhysRevLett.81.3631. Citado 2 vezes nas páginas 19 e 44.

[93] Alber, Gernot, Aldo Delgado, Nicolas Gisin e Igor Jex: *Efficient bipartite quantum state purification in arbitrary dimensional Hilbert spaces*. Journal of Physics A: Mathematical and General, 34(42):8821–8833, oct 2001. https://doi.org/10.1088/0305-4470/34/42/307. Citado na página 19.

[94] O'Brien, J. L., G. J. Pryde, A. G. withe e T. C. Ralph: *High-fidelity Z-measurement error encoding of optical qubits*. Phys. Rev. A, 71:060303, Jun 2005. https://link.aps.org/doi/10.1103/PhysRevA.71.060303. Citado na página 19.

[95] Cory, D. G., M. D. Price, W. Maas, E. Knill, R. Laflamme, W. H. Zurek, T. F. Havel e S. S. Somaroo: *Experimental Quantum Error Correction*. Phys. Rev. Lett., 81:2152–2155, Sep 1998. https://link.aps.org/doi/10.1103/PhysRevLett.81.2152. Citado na página 19.

[96] Zhang, Jingfu, Raymond Laflamme e Dieter Suter: *Experimental Implementation of Encoded Logical Qubit Operations in a Perfect Quantum Error Correcting Code*. Phys. Rev. Lett., 109:100503, Sep 2012. https://link.aps.org/doi/10.1103/PhysRevLett.109.100503. Citado na página 19.

[97] Weinstein, Y. S., M. A. Pravia, E. M. Fortunato, S. Lloyd e D. G. Cory: *Implementation of the Quantum Fourier Transform*. Phys. Rev. Lett., 86:1889–1891, Feb 2001. https://link.aps.org/doi/10.1103/PhysRevLett.86.1889. Citado na página 19.

[98] Boschi, D., S. Branca, F. De Martini, L. Hardy e S. Popescu: *Experimental Realization of Teleporting an Unknown Pure Quantum State via Dual Classical and Einstein-Podolsky-Rosen Channels*. Phys. Rev. Lett., 80:1121–1125, Feb 1998. https://link.aps.org/doi/10.1103/PhysRevLett.80.1121. Citado na página 19.

[99] Douglas, B. L. e J. B. Wang: *Efficient quantum circuit implementation of quantum walks*. Phys. Rev. A, 79:052335, May 2009. https://link.aps.org/doi/10.1103/PhysRevA.79.052335. Citado na página 19.

[100] Vandersypen, Lieven M. K.; Steffen, Matthias; Breyta Gregory; Yannoni Costantino S.; Sherwood Mark H.; Chuang Isaac L.: *Experimental realization of Shor's quantum factoring algorithm using nuclear magnetic resonance*. Nature, 414:883–887, 2001. https://doi.org/10.1038/414883a. Citado na página 19.

[101] Vandersypen, Lieven M. K., Matthias Steffen, Mark H. Sherwood, Costantino S. Yannoni, Gregory Breyta e Isaac L. Chuang: *Implementation of a three-quantum-bit search algorithm*. Applied Physics Letters, 76(5):646–648, 2000. https://doi.org/10.1063/1.125846. Citado na página 19.

[102] Jones, J. A. e M. Mosca: *Implementation of a quantum algorithm on a nuclear magnetic resonance quantum computer*. The Journal of Chemical Physics, 109(5):1648–1653, 1998. https://doi.org/10.1063/1.476739. Citado na página 19.

[103] Gulde, Stephan; Riebe, Mark; Lancaster Gavin P. T.; Becher Christoph; Eschner Jürgen; Häffner Hartmut; Schmidt Kaler Ferdinand; Chuang Isaac L.; Blatt Rainer: *Implementation of the Deutsch–Jozsa algorithm on an ion-trap quantum computer*. Nature, 421:48–50, 2003. https://doi.org/10.1038/nature01336. Citado na página 19.

[104] Chuang, Isaac L.; Vandersypen, Lieven M. K.; Zhou Xinlan; Leung Debbie W.; Lloyd Seth: *Experimental realization of a quantum algorithm*. Nature, 393:143–146, 1998. https://doi.org/10.1038/30181. Citado na página 19.

[105] Schmidt-Kaler, Ferdinand; Häffner, Hartmut; Riebe Mark; Gulde Stephan; Lancaster Gavin P. T.; Deuschle Thomas; Becher Christoph; Roos Christian F.; Eschner Jürgen; Blatt Rainer: *Realization of the Cirac–Zoller controlled-NOT quantum gate*. Nature, 422:411–422, 2003. https://doi.org/10.1038/nature01494. Citado na página 19.

[106] Yamamoto, T.; Pashkin, Yu. A.; Astafiev O.; Nakamura Y.; Tsai J. S.: *Demonstration of conditional gate operation using superconducting charge qubits*. Nature, 425:941–944, 2003. https://doi.org/10.1038/nature02015. Citado na página 19.

[107] Montangero, Simone, Tommaso Calarco e Rosario Fazio: *Robust Optimal Quantum Gates for Josephson Charge Qubits*. Phys. Rev. Lett., 99:170501, Oct 2007. https://link.aps.org/doi/10.1103/PhysRevLett.99.170501. Citado na página 19.

[108] Jelezko, F., T. Gaebel, I. Popa, M. Domhan, A. Gruber e J. Wrachtrup: *Observation of Coherent Oscillation of a Single Nuclear Spin and Realization of a Two-Qubit Conditional Quantum Gate*. Phys. Rev. Lett., 93:130501, Sep 2004. https://link.aps.org/doi/10.1103/PhysRevLett.93.130501. Citado na página 19.

[109] Zu, C.; Wang, W. B.; He L.; Zhang W. G.; Dai C. Y.; Wang F.; Duan L. M.: *Experimental realization of universal geometric quantum gates with solid-state spins*. Nature, 514:72–75, 2014. https://doi.org/10.1038/nature13729. Citado na página 19.

[110] Isenhower, L.; Saffman, M.; Mølmer K.: *Multibit CkNOT quantum gates via Rydberg blockade*. Citado na página 19.

[111] Du, Jiangfeng, Ping Zou e Z. D. Wang: *Experimental implementation of high-fidelity unconventional geometric quantum gates using an NMR interferometer*. Phys. Rev. A, 74:020302, Aug 2006. https://link.aps.org/doi/10.1103/PhysRevA.74.020302. Citado na página 19.

[112] Du, Jiang Feng, Ji Hui Wu, Ming Jun Shi, Liang Han, Xian Yi Zhou, Bang Jiao Ye, Hui Ming Weng e Rong Dian Han: *Implementation of Quantum Logic Gates by Nuclear Magnetic Resonance Spectroscopy*. Chinese Physics Letters, 17(1):64–66, jan 2000. https://iopscience.iop.org/article/10.1088/0256-307X/17/1/022. Citado na página 19.

[113] *Construction and Implementation of NMR Quantum Logic Gates for Two Spin Systems*. Journal of Magnetic Resonance, 140(2):371–378, 1999. Citado na página 19.

[114] O'Brien, J. L.; Pryde, G. J.; withe A. G.; Ralph T. C.; Branning D.;: *Demonstration of an all-optical quantum controlled-NOT gate*. Nature, 426:264–267, 2003. https://doi.org/10.1038/nature02054. Citado na página 19.

[115] Zhao, Zhi, An Ning Zhang, Yu Ao Chen, Han Zhang, Jiang Feng Du, Tao Yang e Jian Wei Pan: *Experimental Demonstration of a Nondestructive Controlled-NOT Quantum Gate for Two Independent Photon Qubits*. Phys. Rev. Lett., 94:030501, Jan 2005. https://link.aps.org/doi/10.1103/PhysRevLett.94.030501. Citado na página 19.

[116] Goodman, Joseph W: *Introduction to Fourier optics*, volume 1. 2005. Citado 2 vezes nas páginas 21 e 22.

[117] Mandel, L. e E. Wolf: *Optical Coherence and Quantum Optics*. Cambridge University Press, 1995, ISBN 9780521417112. https://books.google.com.br/books?id=FeBix14iM70C. Citado 5 vezes nas páginas 21, 27, 50, 59 e 65.

[118] Born, M., E. Wolf, A.B. Bhatia, D. Gabor, A.R. Stokes, A.M. Taylor, P.A. Wayman e W.L. Wilcock: *Principles of Optics: Electromagnetic Theory of Propagation, Interference and Diffraction of Light*. Cambridge University Press, 2000, ISBN 9780521784498. https://books.google.com.br/books?id=oV8OAAAAIAAJ. Citado na página 21.

[119] Baldijão, R. D., G. F. Borges, B. Marques, M. A. Solís-Prosser, L. Neves e S. Pádua: *Proposal for automated transformations on single-photon multipath qudits*. Phys. Rev. A, 96:032329, Sep 2017. https://link.aps.org/doi/10.1103/PhysRevA.96.032329. Citado 11 vezes nas páginas 21, 23, 24, 26, 28, 48, 49, 53, 58, 59 e 70.

[120] Cardoso, A. C., J. G. L. Condé, B. Marques, J. S. Cabral e S. Pádua: *Simulation of a quantum jump in three-level systems using photonic Gaussian modes*. Phys. Rev. A, 103:013722, Jan 2021. https://link.aps.org/doi/10.1103/PhysRevA.103.013722. Citado 5 vezes nas páginas 21, 36, 38, 40 e 48.

[121] Júnior, Gilberto Ferreira Borges: *Realização de operações não diagonais em qutrits de caminho*. Tese de Doutoramento, Universidade Federal de Minas Gerais, 2018. Citado 8 vezes nas páginas 23, 24, 26, 28, 48, 49, 53 e 70.

[122] Baldijão, Roberto Dobal: *Transformação de estados e medições sequenciais: uma proposta experimental*. Tese de Mestrado, Universidade Federal de Minas Gerais, 2016. Citado 10 vezes nas páginas 23, 24, 26, 28, 48, 49, 53, 58, 59 e 70.

[123] Pimenta, W. M., B. Marques, M. A. D. Carvalho, M. R. Barros, J. G. Fonseca, J. Ferraz, M. Terra Cunha e S. Pádua: *Minimal state tomography of spatial qubits using a spatial light modulator*. Opt. Express, 18(24):24423–24433, Nov 2010. http://www.opticsexpress.org/abstract.cfm?URI=oe-18-24-24423. Citado na página 26.

[124] Cardoso, A. C., L. P. Berruezo, D. F. Ávila, G. B. Lemos, W. M. Pimenta, C. H. Monken, P. L. Saldanha e S. Pádua: *Classical imaging with undetected light*. Phys. Rev. A, 97:033827, Mar 2018. https://link.aps.org/doi/10.1103/PhysRevA.97.033827. Citado na página 26.

[125] Z. Zhang, Z. You e D. Chu: *Fundamentals of phase-only liquid crystal on silicon (LCOS) devices*. Light: Science & Applications, 3, 2014. Citado na página 26.

[126] Griffiths, D.J.: *Introduction to Quantum Mechanics*. Pearson Education, 2005, ISBN 9788177582307. https://books.google.com.br/books?id=9sqIaRGx_EoC. Citado na página 27.

[127] Ballentine, L.E.: *Quantum Mechanics: A Modern Development*. World Scientific, 1998, ISBN 9789810241056. https://books.google.com.br/books?id=sHJRFHz1rYsC. Citado 4 vezes nas páginas 27, 29, 30 e 42.

[128] Cohen-Tannoudji, C., B. Diu e F. Laloe: *Quantum Mechanics*. Número v. 1 em *Quantum Mechanics*. Wiley, 1991, ISBN 9780471164333. https://books.google.com.br/books?id=iHcpAQAAMAAJ. Citado 3 vezes nas páginas 27, 29 e 30.

[129] Zurek, W. H.: *Environment-induced superselection rules*. Phys. Rev. D, 26:1862–1880, Oct 1982. https://link.aps.org/doi/10.1103/PhysRevD.26.1862. Citado 2 vezes nas páginas 29 e 36.

[130] Asorey, M, A Kossakowski, G Marmo e E C G Sudarshan: *Dynamical maps and density matrices*. Journal of Physics: Conference Series, 196:012023, nov 2009. https://doi.org/10.1088/1742-6596/196/1/012023. Citado na página 33.

[131] Lindblad, G.: *On the generators of quantum dynamical semigroups*. Communications in Mathematical Physics, 48:119–130, Jun 1976. Citado na página 35.

[132] Kraus, K., A. Böhm, J.D. Dollard e W.H. Wootters: *States, effects, and operations: fundamental notions of quantum theory : lectures in mathematical physics at the University of Texas at Austin*. Lecture notes in physics. Springer-Verlag, 1983, ISBN 9780387127323. https://books.google.com.br/books?id=fRBBAQAAIAAJ. Citado na página 37.

[133] Williams, Colin P.: *Explorations in Quantum Computing*. Springer-Verlag London, 2ª edição, 2011, ISBN 978-1-84628-887-6. https://link.springer.com/book/10.1007/978-1-84628-887-6. Citado na página 43.

[134] Greentree, Andrew D., S. G. Schirmer, F. Green, Lloyd C. L. Hollenberg, A. R. Hamilton e R. G. Clark: *Maximizing the Hilbert Space for a Finite Number of Distinguishable Quantum States*. Phys. Rev. Lett., 92:097901, Mar 2004. https://link.aps.org/doi/10.1103/PhysRevLett.92.097901. Citado na página 45.

[135] Tamir, Boaz: *Quantum query complexity for qutrits*. Phys. Rev. A, 77:022326, Feb 2008. https://link.aps.org/doi/10.1103/PhysRevA.77.022326. Citado na página 45.

[136] Bartlett, Stephen D., Hubert de Guise e Barry C. Sanders: *Quantum encodings in spin systems and harmonic oscillators*. Phys. Rev. A, 65:052316, May 2002. https://link.aps.org/doi/10.1103/PhysRevA.65.052316. Citado 2 vezes nas páginas 45 e 46.

[137] Gottesman, Daniel: *Fault-Tolerant Quantum Computation with Higher-Dimensional Systems*. Em Williams, Colin P. (editor): *Quantum Computing and Quantum Communications*, páginas 302–313, Berlin, Heidelberg, 1999. Springer Berlin Heidelberg, ISBN 978-3-540-49208-5. Citado na página 45.

[138] Bechmann-Pasquinucci, Helle e Asher Peres: *Quantum Cryptography with 3-State Systems*. Phys. Rev. Lett., 85:3313–3316, Oct 2000. https://link.aps.org/doi/10.1103/PhysRevLett.85.3313. Citado na página 45.

[139] Bregman, I., D. Aharonov, M. Ben-Or e H. S. Eisenberg: *Simple and secure quantum key distribution with biphotons*. Phys. Rev. A, 77:050301, May 2008. https://link.aps.org/doi/10.1103/PhysRevA.77.050301. Citado na página 45.

[140] Zhou, D. L., B. Zeng, Z. Xu e C. P. Sun: *Quantum computation based on d-level cluster state*. Phys. Rev. A, 68:062303, Dec 2003. https://link.aps.org/doi/10.1103/PhysRevA.68.062303. Citado na página 45.

[141] Khan, Faisal Shah e Marek Perkowski: *Synthesis of multi-qudit hybrid and d-valued quantum logic circuits by decomposition*. Theoretical Computer Science, 367(3):336 – 346, 2006, ISSN 0304-3975. http://www.sciencedirect.com/science/article/pii/S0304397506006049. Citado 2 vezes nas páginas 45 e 46.

[142] Jie, Zhang, Di Yao-Min e Wei Hai-Rui: *Realization of Two-Qutrit Quantum Gates with Control Pulses*. Communications in Theoretical Physics, 51(4):653–658, apr 2009. https://doi.org/10.1088/0253-6102/51/4/15. Citado na página 45.

[143] Brylinski, Jean Luc e Ranee Brylinski: *Universal quantum gates*. arXiv e-prints, páginas quant–ph/0108062, Aug 2001. https://ui.adsabs.harvard.edu/#abs/2001quant.ph..8062B. Citado na página 45.

[144] Di, Yao Min e Hai Rui Wei: *Elementary gates for ternary quantum logic circuit*. arXiv e-prints, página arXiv:1105.5485, May 2011. https://ui.adsabs.harvard.edu/#abs/2011arXiv1105.5485D. Citado na página 45.

[145] Patera, J. e H. Zassenhaus: *The Pauli matrices in n dimensions and finest gradings of simple Lie algebras of type An-1*. Journal of Mathematical Physics, 29(3):665–673, 1988. https://doi.org/10.1063/1.528006. Citado na página 45.

[146] Muthukrishnan, Ashok e C. R. Stroud: *Multivalued logic gates for quantum computation*. Phys. Rev. A, 62:052309, Oct 2000. https://link.aps.org/doi/10.1103/PhysRevA.62.052309. Citado na página 46.

[147] Daboul, Jamil, Xiaoguang Wang e Barry C Sanders: *Quantum gates on hybrid qudits*. Journal of Physics A: Mathematical and General, 36(10):2525–2536, feb 2003. https://doi.org/10.1088/0305-4470/36/10/312. Citado na página 46.

[148] Abouraddy, Ayman F., Bahaa E. A. Saleh, Alexander V. Sergienko e Malvin C. Teich: *Role of Entanglement in Two-Photon Imaging*. Phys. Rev. Lett., 87:123602, Aug 2001. https://link.aps.org/doi/10.1103/PhysRevLett.87.123602. Citado na página 50.

[149] Paul, Tania e Tabish Qureshi: *Measuring quantum coherence in multislit interference*. Phys. Rev. A, 95:042110, Apr 2017. https://link.aps.org/doi/10.1103/PhysRevA.95.042110. Citado na página 65.

[150] Machado, Paula e S. Pádua: *Quantum coherence of spatial photonic qudits: experimental measurement and path-marker analysis*. Journal of Optics, 22:065201, Apr 2020. Citado na página 65.